

ARRAKIS: atlas of resonance rings as known in the S⁴G^{★,★★}

S. Comerón^{1,2,3}, H. Salo¹, E. Laurikainen^{1,2}, J. H. Knapen^{4,5}, R. J. Buta⁶, M. Herrera-Endoqui¹, J. Laine¹,
B. W. Holwerda⁷, K. Sheth⁸, M. W. Regan⁹, J. L. Hinz¹⁰, J. C. Muñoz-Mateos¹¹, A. Gil de Paz¹²,
K. Menéndez-Delmestre¹³, M. Seibert¹⁴, T. Mizusawa^{8,15}, T. Kim^{8,11,14,16}, S. Erroz-Ferrer^{4,5}, D. A. Gadotti¹⁰,
E. Athanassoula¹⁷, A. Bosma¹⁷, and L. C. Ho^{14,18}

¹ University of Oulu, Astronomy Division, Department of Physics, P.O. Box 3000, FIN-90014, Finland
e-mail: seb.comeron@gmail.com

² Finnish Centre of Astronomy with ESO (FINCA), University of Turku, Väisälantie 20, FI-21500, Piikkiö, Finland

³ Korea Astronomy and Space Science Institute, 776, Daedeokdae-ro, Yuseong-gu, Daejeon 305-348, Republic of Korea

⁴ Instituto de Astrofísica de Canarias, E-38205 La Laguna, Tenerife, Spain

⁵ Departamento de Astrofísica, Universidad de La Laguna, E-38200, La Laguna, Tenerife, Spain

⁶ Department of Physics and Astronomy, University of Alabama, Box 870324, Tuscaloosa, AL 35487

⁷ European Space Agency, ESTEC, Keplerlaan 1, 2200 AG, Noordwijk, the Netherlands

⁸ National Radio Astronomy Observatory/NAASC, 520 Edgemont Road, Charlottesville, VA 22903, USA

⁹ Space Telescope Science Institute, 3700 San Antonio Drive, Baltimore, MD 21218, USA

¹⁰ European Southern Observatory, Casilla 19001, Santiago 19, Chile

¹¹ MMTO, University of Arizona, 933 North Cherry Avenue, Tucson, AZ 85721, USA

¹² Departamento de Astrofísica, Universidad Complutense de Madrid, Madrid 28040, Spain

¹³ Universidade Federal do Rio de Janeiro, Observatório do Valongo, Ladeira Pedro Antônio, 43, CEP 20080-090, Rio de Janeiro, Brazil

¹⁴ The Observatories of the Carnegie Institution for Science, 813, Santa Barbara Street, Pasadena, CA 91101, USA

¹⁵ Florida Institute of Technology, Melbourne, FL 32901, USA

¹⁶ Astronomy Program, Department of Physics and Astronomy, Seoul National University, Seoul 151-742, Republic of Korea

¹⁷ Aix Marseille Université, CNRS, LAM (Laboratoire d'Astrophysique de Marseille) UMR 7326, 13388, Marseille, France

¹⁸ Kavli Institute for Astronomy and Astrophysics, Peking University, Beijing 100871, China

Preprint online version: September 28, 2018

ABSTRACT

Context. Resonance rings and pseudorings (here collectively called rings) are thought to be related to the gathering of material near dynamical resonances caused by non-axisymmetries in galaxy discs. This means that they are the result of secular evolution processes that redistribute material and angular momentum in discs. Studying them may give clues on the formation and growth of bars and other disc non-axisymmetries.

Aims. Our aims are to produce a catalogue and an atlas of the rings detected in the Spitzer Survey of Stellar Structure in Galaxies (S⁴G) and to conduct a statistical study of the data in the catalogue.

Methods. We traced the contours of rings previously identified and fitted them with ellipses. We found the orientation of bars by studying the galaxy ellipse fits from the S⁴G pipeline 4. We used the galaxy orientation data obtained by the S⁴G pipeline 4 to obtain intrinsic ellipticities and orientations of rings and the bars.

Results. ARRAKIS contains data on 724 ringed galaxies in the S⁴G. The frequency of resonance rings in the S⁴G is of $16 \pm 1\%$ and $35 \pm 1\%$ for outer and inner features, respectively. Outer rings are mostly found in Hubble stages $-1 \leq T \leq 4$. Inner rings are found in a broad distribution that covers the range $-1 \leq T \leq 7$. We confirm that outer rings have two preferred orientations, namely parallel and perpendicular to the bar. We confirm a tendency for inner rings to be oriented parallel to the bar, but we report the existence of a significant fraction (maybe as large as 50%) of inner features that have random orientations with respect to the bar. These misaligned inner rings are mostly found in late-type galaxies ($T \geq 4$). We find that the fraction of barred galaxies hosting outer (inner) rings is ~ 1.7 times (~ 1.3 times) that in unbarred galaxies.

Conclusions. We confirm several results from previous surveys as well as predictions from simulations of resonant rings and/or from manifold flux tube theory. We report that a significant fraction of inner rings in late-type galaxies have a random orientation with respect to the bar. This may be caused by spiral modes that are decoupled from the bar and dominate the Fourier amplitude spectrum at the radius of the inner ring. The fact that rings are only mildly favoured by bars suggests that those in unbarred galaxies either formed because of weak departures from the axisymmetry of the galactic potential or that they are born because of bars that were destroyed after the ring formation.

Key words. Astronomical databases: Atlases – Astronomical databases: Catalogues – Galaxies: statistics – Galaxies: structure

* Appendices A, B, and C are available in electronic form at <http://www.aanda.org>

** Tables A1 and A2 are only available in electronic form at the CDS via anonymous ftp to cdsarc.u-strasbg.fr (130.79.128.5) or via <http://cdsweb.u-strasbg.fr/cgi-bin/qcat?J/A+A/>

1. Introduction

Galaxies are constantly evolving. Their properties change because of fast interactions and mergers (Toomre 1977) and also

because of slow secular evolution (e.g., Kormendy & Kennicutt 2004; Athanassoula 2012a). Part of the secular evolution in disc galaxies is driven by non-axisymmetries such as bars and oval distortions. Long-lived non-axisymmetries efficiently redistribute material and angular momentum across the discs in a Hubble-Lemaître time, which makes understanding them crucial to describe present-day galaxies. This slow process is, among many other consequences, responsible for the creation of pseudobulges (Kormendy & Kennicutt 2004), for the radial spread of outer parts of discs (Schwarz 1984; Athanassoula 2012b), and also for building spectacular rings and pseudorings. In this paper we study rings and pseudorings in a representative sample of nearby galaxies.

Rings are beautiful closed structures made of stars and/or gas. Pseudorings are their open counterparts, sometimes incomplete versions of rings and sometimes formed by spiral arms that almost connect. Here we use the word rings to refer to the set that includes both rings and pseudorings. The set of closed features is referred to as closed rings.

Rings often host intense star formation and/or are made of young blue stars (see, e.g., Buta & Crocker 1993; Knapen et al. 1995; Crocker et al. 1996; Buta 2002; Knapen 2005; Buta et al. 2007; Comerón et al. 2010; Grouchy et al. 2010). However, “dead” purely stellar rings exist as well (Buta 1991; Erwin & Sparke 1999, 2002; Comerón 2013).

The majority of rings seen in normal disc galaxies are likely caused by the influence of dynamical orbital resonances on the motions of gas clouds in the plane of the disc. The presence of a rotating bar or oval sets up a pattern speed and probably drives spiral patterns that can, via action of gravity torques, secularly evolve into more closed, ring-like features (Schwarz 1981, 1984). The main evidence in support of this idea has come from observations of ring morphologies, intrinsic ring shapes, and intrinsic bar and ring major axis orientations as well as test-particle and n -body simulations [see review by Buta & Combes (1996) and Rautiainen & Salo (2000)].

There are four major and two secondary dynamical resonances that are believed to be important for ring formation (for detailed reviews of barred galaxy dynamics, see Sellwood & Wilkinson 1993; Athanassoula 2012a). These are defined (in the epicyclic approximation) by the relation between the bar pattern speed, Ω_p , the circular angular speed Ω , and the radial epicyclic frequency κ . The major resonances are the outer Lindblad resonance (OLR, where $\Omega_p = \Omega + \kappa/2$), the corotation resonance (CR, where $\Omega_p = \Omega$), and the two inner Lindblad resonances (ILRs, where $\Omega_p = \Omega - \kappa/2$). The secondary resonances are the inner 4:1 resonance (often called the UHR for ultraharmonic resonance, but which is here referred to as I4R, where $\Omega_p = \Omega - \kappa/4$) and the outer 4:1 resonance (O4R, where $\Omega_p = \Omega + \kappa/4$). Because Ω and κ depend on the rotation curve of a galaxy, resonance locations will be tied to the gravitational potential of the system. For example, depending on the bar pattern speed and the central mass concentration, one or both ILRs may be absent. Typically, the OLR is located at a radius of roughly twice the bar length, the CR is located slightly outside the end of the bar, and the ILRs are well inside the bar.

Between the outermost ILR and the CR, the main family of orbits, called x_1 orbits, is parallel to the bar. In the framework of the epicyclic approximation, each time a main resonance is crossed, the orbits change their orientation by 90° . Because of this, orbits that are slightly inside a resonance will intersect with those slightly outside it. Graphic depictions of this can be found, for instance, in Figure 11 in Knapen et al. (1995) and Figure 2 in Elmhaier & Gerhard (1997). Growing bars redis-

tribute the angular momentum in a galaxy. Gas outside CR tends to be moved to the OLR radius (Lynden-Bell & Kalnajs 1972; Sellwood 1981; Schwarz 1981). Gas inside CR tends to move inwards and is collected either close to the I4R and/or close to the ILRs (Schwarz 1984). Thus, orbits near resonances are fed with gas by the bar angular momentum redistribution. Because of the high gas densities reached there and because of the collisions of gas clumps moving in intersecting orbits, star formation starts and resonance rings are created. Although strictly speaking the epicyclic approximation is no longer valid for strongly perturbed potentials such as those affected by a strong bar (for a good example of that see Salo et al. 1999), the picture described here remains qualitatively valid.

Rings in barred galaxies are classified according to their size compared to that of the bar. The precise location of a resonance cannot be determined unless the rotation curve of the galaxy and the pattern speed of the bar are known. Thus the resonance interpretations come from a confrontation between theory and observation:

- Outer rings are found at a radius roughly twice as large as that of the bar and are thought to be typically related to the OLR. Occasionally, some outer rings may be linked to the O4R as in the case of the dimpled ones in Byrd et al. (1998), those in simulations by Rautiainen & Salo (2000), and in the modelling of NGC 1433 by Treuthardt et al. (2008). The first outer feature that has been described is that in NGC 1291 (Perrine 1922).
- Inner rings are found slightly outside the bar and are thought to be related to the I4R. They have been observed since R. J. Mitchell’s observations of NGC 4725 in 1858 (Parsons 1880). They were first described by Curtis (1918).
- Nuclear rings are found well inside the bar and are generally thought to be related to the ILRs (but see Kim et al. 2012, where nuclear rings are suggested to be caused by the centrifugal barrier encountered by gas migrating to the inner regions of the galaxy). They were first seen in NGC 4321 by Keeler (1908) and described in NGC 3351 by Curtis (1918). Nuclear rings are especially bright and correlate with the presence of sigma-drops (sigma-drops are nuclear regions in the centre of galaxies where the stellar velocity dispersion is measured to be lower than in the surroundings; Comerón et al. 2008b).

We caution about the naming conventions and note that inner rings in barred galaxies are not thought to be related to the inner Lindblad resonances, but to the I4R.

Based on data from the Third Reference Catalogue of Bright Galaxies (RC3; de Vaucouleurs et al. 1991), Buta & Combes (1996) found that roughly 10% of disc galaxies host outer rings and that 45% of disc galaxies host inner rings. Comerón et al. (2010) found that the fraction of nuclear rings is roughly 20% for galaxies with Hubble stages between $T = -3$ and $T = 7$.

Rings have been associated to resonances since the pioneering works by Marochnik et al. (1972) and Schommer & Sullivan (1976). Subsequently, this connection has been made in simulations by, among others, Schwarz (1981, 1984), Byrd et al. (1994), and Knapen et al. (1995). Because of that, outer, inner, and nuclear rings have historically been called resonance rings.

A complementary theory explains the formation of at least some rings. This theory, called manifold theory, shows in a single framework the creation of outer spirals and outer and inner rings. It proposes that they are made of particles trapped in invariant manifolds (tubes of orbits) that start and end in one of the two unstable Lagrangian points at the end of the bar, L_1 and L_2

(Romero-Gómez et al. 2006, 2007; Athanassoula et al. 2009b,a, 2010; Athanassoula 2012b). This theory predicts the existence of inner rings and that they are mainly oriented along the bar. It also predicts the existence of the outer R_1 , R_2 , and R_1R_2 rings and their orientation with respect to the bar (for a description of outer ring morphologies see Section 3.1). It also predicts the locations and axial ratios of rings. In fact, there is no prediction of the resonance ring simulations that the flux tube manifold theory does not predict as well, while the manifold shapes reproduce well that of rings in the response simulations mentioned above. The latter is possible because the values of the radii of the L_1 , L_2 , L_3 , and L_4 Lagrangian points in barred galaxies are so close to that of the corotation radius that for observed galaxies they can be considered as equal. In this way it is possible to overcome the approximation of a resonant radius that is only valid in the linear and epicyclic approximations, that is, not in realistic barred galaxies. In the following we write manifold theory instead of flux tube manifold theory, and we use the generic name resonant rings for resonant and flux tube manifold rings.

Rings are also observed in galaxies that do not host a bar (see, e.g., Figures. 3e and 3f in Buta 1995). Comerón et al. (2010) claimed that the frequency of rings with sizes comparable with those of nuclear rings in unbarred galaxies ($19 \pm 4\%$) is similar to the frequency of unbarred disc galaxies. One possibility to explain the existence of such rings is that they are remnants left after the bar dissolved (for possible bar dissolution mechanisms, see e.g., Raha et al. 1991; Friedli & Benz 1993; Bournaud & Combes 2002; Bournaud et al. 2005) or were destroyed in interactions with other galaxies (Athanassoula 1996; Berentzen et al. 2003). However, the possibility of bar dissolution has to be taken with caution because many simulations showed that bars cannot be easily erased without interactions (see, e.g., Martínez-Valpuesta & Shlosman 2004; Debattista et al. 2004, 2006; Berentzen et al. 2007; Athanassoula et al. 2013). Alternatively, these rings that apparently do not fit in the resonance theory might be explained by resonances caused by weak oval distortions, strong spiral patterns (Jungwiert & Palous 1996; Rautiainen & Salo 2000), or by the gravitational potential distortions induced during minor mergers and/or interactions. This last possibility has been suggested by Knapen et al. (2004) for the pseudoring in NGC 278 and by some numerical experiments (Tutukov & Fedorova 2006).

Another kind of interesting morphological feature in disc galaxies are the lenses. Lenses are typically found in early-type disc galaxies, they have flat luminosity profiles and fairly sharp edges. Lenses, like rings, can be classified as outer, inner, or nuclear, based on their sizes. They have been studied in detail in the Near-Infrared atlas of S0-Sa galaxy Survey (NIRS0S; Laurikainen et al. 2011). Some features, called ring-lenses and first reported by Kormendy (1979), have properties between those of rings and lenses; they are lens-like features with a significant enhancement of luminosity close to their edges. In this paper we included ring-lenses together with classical rings.

Rings can be responsible for a significant fraction of the light emitted by a galaxy. For example, the exceptionally bright nuclear ring in NGC 1097 emits $\sim 10\%$ of the light of the galaxy at $3.6\mu\text{m}$ (Sheth et al. 2010). This can be considered as an estimate of the upper limit of the fraction of light coming from rings in present-day galaxies. However, since rings are often regions of intense star formation with a low mass-to-light ratio even in the mid-infrared, the fraction of the galaxy baryonic mass found in them is smaller than that.

Non-resonant mechanisms also produce rings, but they often have an appearance fairly different from that of resonance rings. A ring can be formed at the largest non-looping orbit whose major axis is parallel to the major axis of the bar. Such a ring is called an x_1 -ring (Regan & Teuben 2004). Collisional rings occur when a disc galaxy collides head-on with a satellite (Lynds & Toomre 1976; Theys & Spiegel 1977). Polar rings occur when part of the mass of a satellite is accreted in an orbit perpendicular to the disc plane of the main galaxy (Schweizer et al. 1983). These three types of rings are rarer than resonance rings.

Moreover, some of the smallest nuclear rings (also called ultra-compact nuclear rings; Comerón et al. 2008a,c) might be related to the interaction of an AGN with the surrounding interstellar medium (Comerón et al. 2010).

Some rings that are coplanar with the galaxy disc may be related to polar rings. In a few galaxies, in-plane rings are found to be made of counterrotating material postulated to come from a recent minor merger. This could be the case, for instance, for the outer ring in IC 2006 (Schweizer et al. 1989; Bettoni et al. 2001), the inner ring in NGC 3593 (Corsini et al. 1998), the inner ring in NGC 4138 (Jore et al. 1996; Thakar et al. 1997), and the innermost ring in NGC 7742 (Sil'chenko & Moiseev 2006; Mazzuca et al. 2006).

In this paper we present a catalogue (Appendix A) and an atlas (Appendix B) of the rings identified in the Spitzer Survey of Stellar Structure in Galaxies (S^4G ; Sheth et al. 2010). The focus is on resonance rings, hence the title ARRAKIS: atlas of resonance rings as known in the S^4G . In the catalogue section, we present data on the projected and intrinsic ring major and minor axes and orientations. We also present the projected and intrinsic highest bar ellipticities, which can be used as a rough estimate of the bar strength, and the bar orientations. The atlas presents images of all the galaxies with rings. We overlay the measured contour of the rings on these images.

The paper is structured as follows: in Section 2 we briefly describe the S^4G and the ring identification process, in Section 3 we describe the types of rings detected in the S^4G , and in Section 4 we describe the production process of the catalogue. We compare our measured ring properties with those in previous studies in Section 5, we present some statistical results on the ring fraction, their intrinsic axis ratio, their position angle (PA) offset with bars and sizes in Section 6, and we discuss some of these points in Section 7. We summarise our results and conclusions in Section 8. The Catalogue is presented in Appendix A and the atlas of rings is presented in Appendix B. Appendix C contains a list of galaxies in the catalogue with a duplicated NGC/IC identification.

2. Identification of rings and pseudorings in the S^4G

2.1. The S^4G

The rings in this paper are identified and described using S^4G images. The S^4G is a mid-infrared survey that has observed a sample of galaxies representative of the local Universe using the InfraRed Array Camera (IRAC; Fazio et al. 2004) of the *Spitzer* Space Telescope (Werner et al. 2004). The goal of the S^4G is to describe the stellar mass distribution in the local Universe. The mid-infrared is the ideal band to do so because it has little dust absorption. The selection criteria of the sample are the following:

- Radio radial heliocentric velocity $v_{\text{radio}} < 3000 \text{ km s}^{-1}$, which is equivalent to a distance of $D < 41 \text{ Mpc}$ when using a Hubble-Lemaître constant of $H_0 = 73 \text{ km s}^{-1} \text{ Mpc}^{-1}$.
- Integrated blue magnitude $m_{B,\text{corr}} < 15.5 \text{ mag}$. The magnitude considered here is that corrected for Galactic extinction, inclination, and K -correction.
- Angular diameter $D_{25} > 1'$.
- Galactic latitude $|b| > 30^\circ$ to avoid the observations to be overly affected by foreground stars and other Galactic emission.

All these parameters were taken from HyperLeda (Paturel et al. 2003). One of the reasons why the sample is representative and not volume-limited is that the galaxies in the sample are limited in diameter and in brightness. Another source of incompleteness is that one of the main inputs of HyperLeda is the RC3, which is only reasonably complete at $m_B < 15.5 \text{ mag}$ (this time the blue magnitude is uncorrected). An additional reason is that some galaxies, especially those of earlier types, did not have a radial velocity in radio in HyperLeda at the time when the sample was defined. The final S⁴G sample size is 2352 galaxies.

The images were taken to map the galaxies at least up to $1.5 \times D_{25}$ and mosaics were produced when needed. The galaxies were observed in the 3.6 and 4.5 μm filters of IRAC with a total integration time of four minutes, obtaining images with a surface brightness sensitivity of $\mu(\text{AB})_{3.6\mu\text{m}} \sim 27 \text{ mag arcsec}^{-2}$. Such deep images are unprecedented for a large survey of galaxies in the mid-infrared.

Because the distances used here are redshift-independent or Hubble-Lemaître flow-corrected, some of the galaxy distances listed in the table in Appendix A exceed 41 Mpc, as explained in Section 6.5.

The S⁴G data is now public and can be downloaded from the NASA/IPAC Infrared Science Archive (IRSA) website¹.

Some galaxies in the S⁴G have two identifications in the NGC and IC catalogues (Dreyer 1888, 1895). To facilitate the comparison of the data presented here with other samples, Appendix C presents a list of the galaxies with a double identification that have been included in ARRAKIS. This list has been made by using mostly data from The Historically Corrected New General Catalogue², but also from NED and HyperLeda.

2.2. Morphological classification of S⁴G galaxies

Buta et al. (in preparation) classified most of the galaxies in the S⁴G using the criteria described in Buta et al. (2010) and Laurikainen et al. (2011). In brief, the galaxies were classified using the de Vaucouleurs revised Hubble-Sandage system (de Vaucouleurs 1959) and its revision (de Vaucouleurs 1963), which has three dimensions, namely the stage (E, E⁺, S0⁻, S0^o, S0⁺, S0/a, Sa, Sab, Sb, Sbc, Sc, Scd, Sd, Sdm, Sm, Im), the family (SA, SAB, SAB, SAB, SB), and the variety (r, rs, rs, rs, s). Additional dimensions were added to the classification by indicating which galaxies are highly inclined (spindle or sp), which galaxies are double-staged, which galaxies have shells, lenses, nuclear bars, nuclear discs, triaxial bulges, ansæ, X-shaped bars, tidal debris, pseudobulges, and other peculiarities. Most important for this work, they also classified which galaxies host outer and nuclear rings. For an extensive review of this matter see Buta (2013).

The galaxies were classified using the S⁴G 3.6 μm band and interpreting the images as if they were blue light. The classifications in both bands are in general very similar and only differ in galaxies with stages between S0/a and Sc, for which the classification in 3.6 μm is on average one stage earlier than in the B band (Buta et al. 2010). This one-stage shift should be taken into account when comparing ARRAKIS results with those in previous studies based on B -band imaging.

A problem may appear when, assuming that rings are related to resonances, those in unbarred galaxies are classified as outer, inner, and nuclear rings. In that case, they were classified comparing the ring size with the galaxy radius and/or the location where they appear in relation to spiral arms. This approach may cause some rings to be misclassified, as discussed in Buta (1995) and Comerón et al. (2010).

A few of the classified galaxies have two or even three features that fit in the outer, inner, or nuclear categories. For example, NGC 5055 is an SA(rs,rl)bc galaxy and has two inner features. In this case, the feature that appears first in the classification (rs) is the outermost feature. The only exceptions for this rule are R₁R'₂ and R'₁R'₂ combinations, for which the order is reversed because of historical reasons.

Because of the limited amount of dust obscuration it suffers, the 3.6 μm band presents an advantage over optical wavelengths at detecting and describing rings that otherwise could remain hidden. This, combined with the angular resolution of the images in the S⁴G (0''.75 pixel size and a full width at half maximum of $\sim 2''$), allowed us to identify rings with diameters down to $\sim 10''$ in low-inclination galaxies. We here considered low-inclination galaxies to be those with $i \leq 60^\circ$. This value is based on our ability to measure bar properties as explained in Sections 4.5 and 4.6. The ring identification becomes increasingly difficult for higher disc inclinations due to higher optical depth and ring foreshortening (see, e.g., Tables IV and V in Buta & Combes 1996). A diameter of 10'' corresponds to 1.0 kpc at a distance 20 Mpc, and to 2.4 kpc at a distance of 50 Mpc, below which 98% of ARRAKIS galaxies are found.

The completeness regarding outer rings is hard to assess; some outer rings are known to be exceedingly faint and some may have surface brightnesses below the sensitivity level of the S⁴G. Additionally, in some cases, outer features are better seen in blue light: for example, the outer ring in NGC 7743, which is distinguishable in the B -band image in Buta et al. (2007), is not seen in the mid-infrared. Moreover, in at least one case (NGC 4151) an outer ring has not been detected here because it is larger than the region covered by the S⁴G frame.

The completeness in the detection of inner rings is very high. When looking at galaxies with $D < 20 \text{ Mpc}$, we find that only 5% of inner rings have a diameter smaller than 2.4 kpc and therefore could not be detected for galaxies at $D = 50 \text{ Mpc}$. We therefore expect to be missing less than 5% of the inner rings due to spacial resolution problems.

Regarding nuclear features, we cannot expect to be as complete as we are at finding inner rings: at a distance $D = 20 \text{ Mpc}$, 5'' correspond to a ring radius of $r = 500 \text{ pc}$, which is similar to the average size of the nuclear rings detected in Comerón et al. (2010). Therefore, any statistics based on the nuclear rings in ARRAKIS must be considered uncertain and only representative of the behaviour of the largest nuclear rings.

A total of 2347 S⁴G galaxies have been classified in Buta et al. (2013, in preparation). One of these galaxies, NGC 7204 (also named PGC 68061), is a pair composed of NGC 7204A and NGC 7204B, leading the count of S⁴G classified galaxies to 2348. Four S⁴G galaxies could not be classified because they ap-

¹ <http://irsa.ipac.caltech.edu/>

² <http://www.ngcicproject.org>

Table 1. Glossary with some notation used in galaxy classification

Notation	Feature
R	Outer closed ring
R ₁	Outer closed ring with Type 1 morphology
R ₂	Outer closed ring with Type 2 morphology
<u>RL</u> , RL, <u>RL</u>	Outer closed ring-lenses
L	Outer lens
R'	Outer pseudoring
R' ₁	Outer pseudoring with Type 1 morphology
R' ₂	Outer pseudoring with Type 2 morphology
<u>R'L</u> , R'L, R' <u>L</u>	Outer pseudoring-lenses
r	Inner closed ring
<u>rl</u> , rl, <u>rl</u>	Inner closed ring-lenses
l	Inner lens
<u>r's</u> , <u>rs</u> , <u>rs</u> , <u>rs</u>	Inner pseudorings
<u>r'l</u> , r'l, r' <u>l</u>	Inner pseudoring-lenses
nr	Nuclear closed ring
nl	Nuclear lens
nrl	Nuclear closed ring-lens
nr'	Nuclear pseudoring
nr'l	Nuclear pseudoring-lens
x ₁ r	x ₁ -ring
RG	Ring galaxy (collisional ring)
PRG	Polar ring galaxy

pear close to very bright saturated stars which makes the galaxy morphology hard to describe. In addition, 70 galaxies were classified that not belong to the S⁴G sample, but appear in the S⁴G frames. Most of these galaxies are satellites of galaxies in the S⁴G sample or background galaxies. Thus, we have data of a total of 2418 galaxies for which there is a classification that considers the presence of rings.

The total number of galaxies that appear in S⁴G frames and have been classified to host rings is 735. Of these, 724 galaxies are included in the original S⁴G sample. These 724 galaxies have 295 outer rings, 609 inner rings, 47 nuclear rings, 4 x₁-rings, 4 collisional rings, and 7 polar rings.

To ensure the reliability of the ring statistics we considered only the galaxies in the S⁴G sample, which, as said before, is representative of the local Universe. However, for the sake of completeness, in the appendices we also included the data and the images corresponding to rings in galaxies not included in the original S⁴G sample.

3. Ring morphologies

The types of rings studied here are described below. A schematic description of the different ring categories can be found in Figure 1. A glossary of some common morphological features is presented in Table 1. For more information on ring classification and morphology see, for example, Buta et al. (2007) and Buta (2013).

3.1. Outer rings

In barred galaxies, outer rings are those with roughly twice the size of the bar. They are thought to be related to the OLR or, occasionally, to the O4R. Since the work from de Vaucouleurs (1959), outer features have been divided into closed rings (R) and pseudorings (R'), depending on whether the feature is closed/complete or not.

Additional subdivisions have been made later based on the morphology of the outer features in the simulations of Schwarz

(1981, 1984) (see Figure 2 in Buta 1986a). R₁ closed rings and R'₁ pseudorings consist of arms that start at one end of the bar and end after a 180° bend in the other end of the bar. These rings typically have a dimpling in the region of the end of the bar and thus are 8-shaped. R₂ closed rings and R'₂ pseudorings consist of two spiral arms, each starting at one of the ends of the bar and intersecting with each other at a position roughly perpendicular to the main axis of the bar after a 270° bend. ARRAKIS includes some R'₂ pseudorings, but no R₂ rings. According to the simulations from Schwarz (1981, 1984), R₁ features are expected to be elongated and perpendicular to the major axis of the bar, and R₂ features are expected to be elongated and parallel to the major axis of the bar. Sometimes galaxies host an R'₁R'₂ or an R₁R'₂ combination.

When an outer feature could not be unambiguously classified in the R₁ and R₂ categories (for example in unbarred galaxies), it was classified as R in the case of closed rings and as R' in the case of pseudorings.

Some outer features have properties intermediate between rings and lenses and were classified as outer ring-lenses. They are indicated by adding an L to the morphological classifications, for instance, RL and R'₁L. Subtler degrees of ringness of outer ring-lenses are sometimes described by underlines, forming the sequence R, RL, RL, RL, L.

A selection of galaxies showing a variety of outer rings observed in the S⁴G is presented in Figure 2.

3.2. Inner rings

In barred galaxies, inner rings are those that are roughly the size of the bar or slightly larger than the bar. They are thought to be related to the I4R. They are classified in a sequence of openness of the spiral arms that curve to form the ring. This sequence ranges from completely closed inner rings to spirals in the following order, r, rs, rs, rs, s (de Vaucouleurs 1963). Underlines indicate transitions between the r, rs, and s varieties. Intermediate varieties between r and s may also indicate rings that are not complete. Features classified as inner pseudorings (rs, rs, rs) are sometime denoted as r' in the literature.

Inner features can also be ring-lenses. Closed inner ring-lenses are indicated as rl and inner pseudoring-lenses are indicated as r'l. Subtler degrees of ringness of inner ring-lenses are sometimes described by underlines, forming the sequence r, rl, rl, rl, l.

A selection of galaxies showing a variety of inner rings observed in the S⁴G is presented in Figure 3.

3.3. Nuclear rings

Although generally small, several nuclear features are visible in the S⁴G images. In barred galaxies, nuclear rings are found inside bars. They are thought to be related to the ILRs (but see Kim et al. 2012). They are expected to be located between the outer and the inner ILR when both are present and inside the ILR when the galaxy has only one of them (see, e.g., Shlosman 1999; Sheth et al. 2000). Nuclear rings have been studied in detail in the atlas of images of nuclear rings (AINUR; Comerón et al. 2010).

Nuclear features are classified into the closed nuclear ring (nr) and nuclear pseudoring (nr') subtypes depending on whether the feature appears completely closed or not. Closed nuclear ring-lenses and pseudoring-lenses are denoted as nrl and nr'l, respectively.

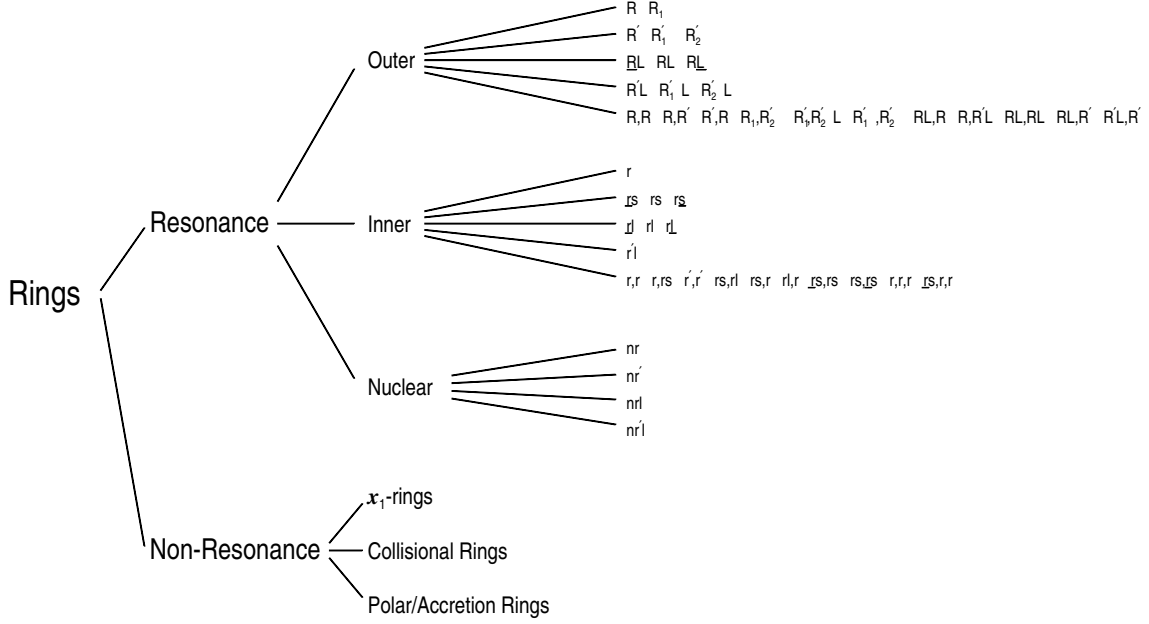


Fig. 1. Schematic classification of the ring types found in ARRAKIS. Multiple ring combinations are also included.

A selection of galaxies showing a variety of nuclear rings observed in the S^4G is presented in Figure 4.

3.4. x_1 , collisional, polar, and accretion rings

Although the rings discussed in this subsection have a non-resonant origin, they have been included in ARRAKIS for the sake of completeness.

x_1 -rings, indicated as x_1r in the morphological classification, are very elongated and parallel to bars. Collisional rings, indicated as RG, are in general as large as outer rings, but their centres are typically significantly offset from the galaxy nucleus. They often appear to be intrinsically elliptical (see, e.g., Appleton & Struck-Marcell 1996). Finally, polar rings, indicated as PRG, are typically seen as needle-like features roughly perpendicular to the major axis of the galaxy, although they can be at other angles, like in the case of NGC 660, which is shown in Figure 5 (Whitmore et al. 1990; van Driel et al. 1995).

Accretion rings are thought to be similar to polar rings, but in their case the material has been accreted at a small angle compared to the galaxy main plane. Since accretion rings are indistinguishable from resonance rings unless kinematic data are available, we included them in the statistics together with resonance rings. To our knowledge, the only rings in this paper that belong to this category are the inner ring in NGC 3593 (Corsini et al. 1998), the inner ring in NGC 4138 (Jore et al. 1996; Thakar et al. 1997), and the innermost ring in NGC 7742 (Sil'chenko & Moiseev 2006; Mazzuca et al. 2006).

A selection of images showing galaxies with x_1 , collisional, and polar rings observed in the S^4G is presented in Figure 5.

4. Preparation of the catalogue

4.1. Description of the projected shapes of rings

To describe the shapes of rings, we assumed that they are intrinsically circular or elliptical, as was done in other statistical ring studies (de Vaucouleurs & Buta 1980; Buta

1986a; Buta & Crocker 1993; Buta 1995; Knapen et al. 2002; Comerón et al. 2010; Grouchy et al. 2010; Laurikainen et al. 2011). Because an ellipse in projection is also an ellipse, the geometrical description of a projected ring in these studies was done by giving the sizes of its major and minor axes (D_r and d_r) or by giving its major axis and its axial ratio ($q_r = d_r/D_r$). To fully characterize the ring geometrical properties, its projected major axis position angle, PA_r , is sometimes given as well.

Although the original S^4G frames have been used for the identification of the rings in Buta et al. (in preparation), working with these images is not always optimal when describing their shape because the contrast between rings and the rest of the galaxy is sometimes very low. A way to overcome this problem is to model the emission of the main components of the galaxy (bulge, bar, disc, etc.) and subtract this model from the original image. This results in the so-called residual image where the disc substructure, such as rings and spiral arms, appears contrast-enhanced. This procedure was preferred to other methods to enhance rings such as unsharp masking because the galaxies were modelled by the S^4G pipeline 4 (P4; Salo et al. in preparation). In short, P4 models were made by fitting the S^4G images with up to four components (nucleus, bulges, discs, and/or bars) using version 3.0 of GALFIT (Peng et al. 2002, 2010). When fitting the model, the disc ellipticity ($\epsilon_d = 1 - q_d$) and position angle (PA_d) were fixed to the values corresponding to deep outer-disc isophotes obtained with an ellipse-fitting routine. A model galaxy image and a residual image were obtained as an output of P4. For the few ARRAKIS galaxies not included in the S^4G sample, additional ellipse fits and decompositions were made using the P4 software.

We examined the original and residual images of the galaxies and decided for each ring in which image, original or residual, it was better defined, and thus in which image its shape was easier to measure. Although a priori this should always be the residual image (see, e.g., the example in Figure 6), because of the galaxies with complicated morphologies and/or because P4 models were intentionally kept simple, some residual images have artefacts that hinder defining the outline of a ring. This occurs more

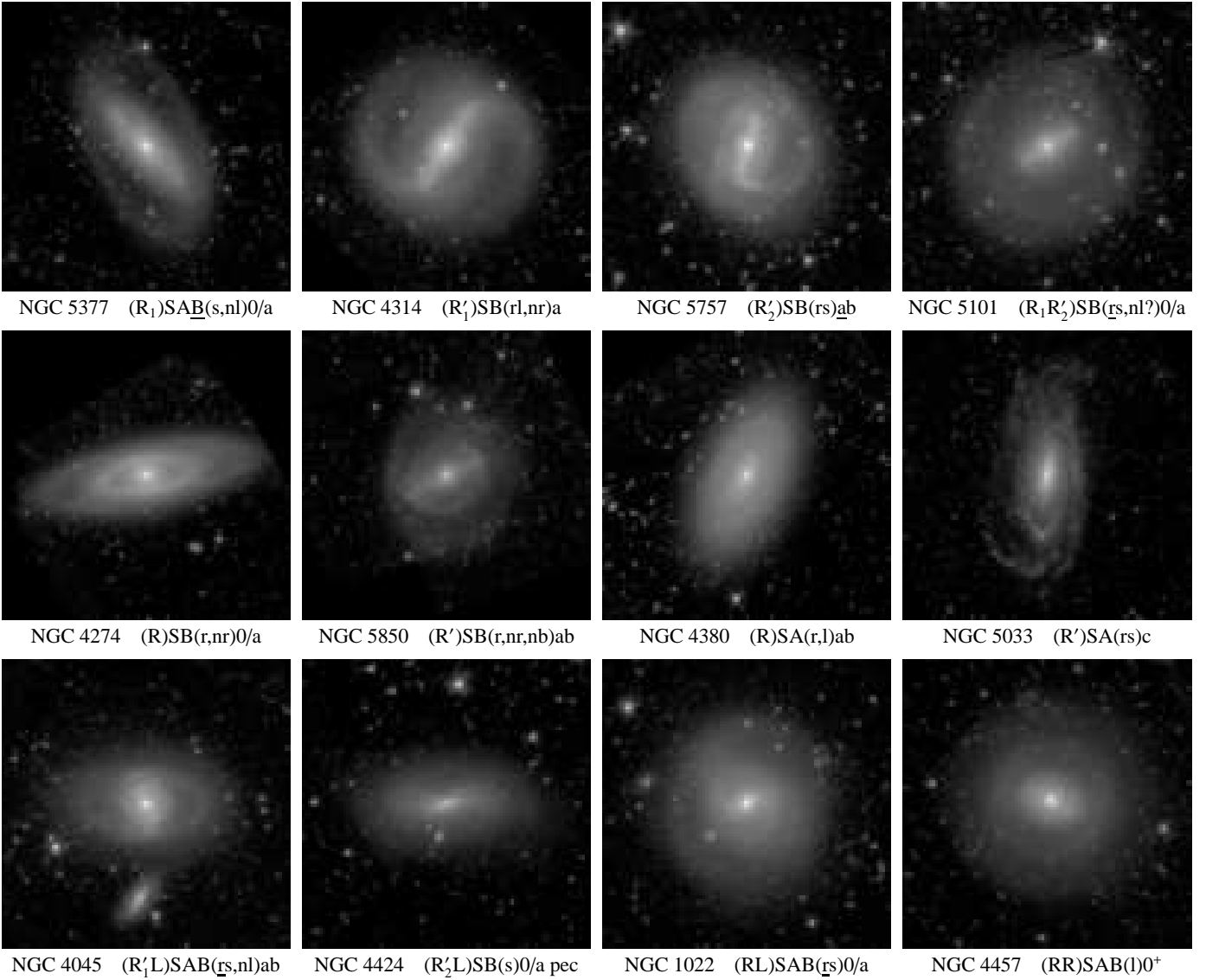


Fig. 2. Selection of S⁴G galaxies hosting a variety of outer rings. The images are in the 3.6 μm band, have a size twice that of the $\mu_{3.6\mu\text{m}} = 25.5 \text{ mag arcsec}^{-2}$ diameter isophote and are oriented with north up and east left. The top row shows galaxies with outer features compatible with the R₁ and R₂ ring morphologies seen in simulations by Schwarz (1981, 1984) and defined by Buta (1986a). The second row shows outer rings that cannot be easily recognised to belong to these categories in either barred or unbarred galaxies. The third row has three example of ring-lenses and a rare example of a galaxy with two outer rings. The names of the galaxies and their morphological classification (from Buta et al. in preparation) can be found below each image.

often when looking at the inner features in galaxies with strong bars.

After selecting the image in which the rings were better defined, we used IRAF's³ (Tody 1986, 1993) TVMARK task to describe them. When used in interactive mode, TVMARK allows marking points in an image displayed in DS9 (Joye & Mandel 2003). This was used to characterise the shape of rings by marking by hand bright star-forming patches belonging to the feature or stellar emission that probably belonged to the ring, as was done in Grouchy et al. (2010). All the ring features were measured by the same person (S. Comerón). This procedure was re-

peated twice for each ring, typically with several days to a few months between the two measurements.

The points marking the outline of the rings for each of the two sets of measurements were fitted with an ellipse using a least-squares fitting algorithm. The output of the fits was the ring diameter in the major axis direction D_r , the diameter along the minor axis direction d_r , and the major axis PA (PA_r). The data used for the statistics in this paper are presented in Appendix A and were obtained by averaging the D_r , d_r , and PA_r values obtained from the fits to the two sets of measurements for each ring. Ellipses made from these averaged values are overlaid on the atlas images and in the example shown in Figure 7.

4.2. Accuracy of the measured projected ring properties

To study the accuracy of the D_r , d_r , and PA_r measurements, we examined the residuals between the values of these parameters

³ IRAF is distributed by the National Optical Astronomy Observatories, which are operated by the Association of Universities for Research in Astronomy, Inc., under cooperative agreement with the National Science Foundation.

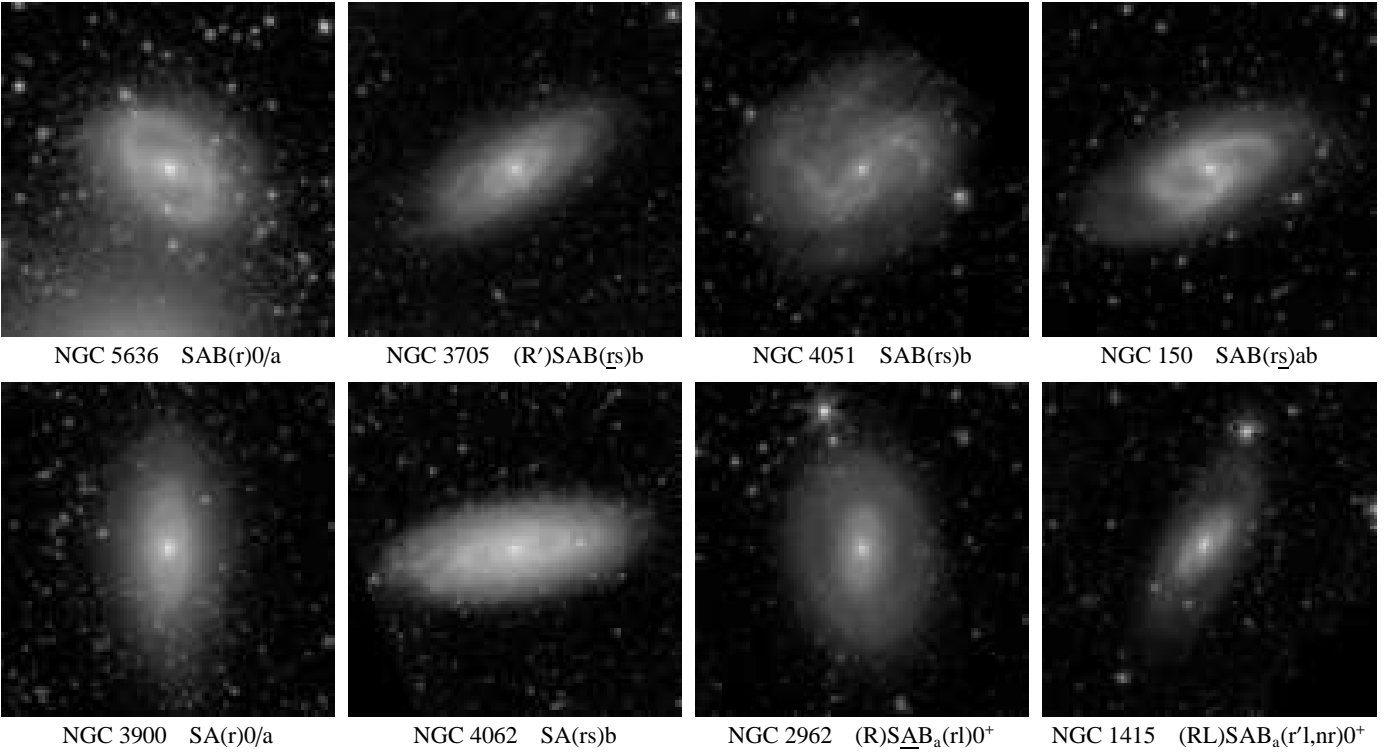


Fig. 3. Selection of S⁴G galaxies hosting a variety of inner rings presented in the same way as those in Figure 2. The top row presents a succession of increasingly more spiral-like inner features in a series of SAB or moderately barred galaxies. The second line shows example of inner rings in unbarred galaxies and two examples of ring-lenses in early-type disc galaxies.

obtained for each of the two fits and the averaged values, that is, $d_r, D_r - \langle d_r, D_r \rangle$ and $PA_r - \langle PA_r \rangle$. These residuals can be considered as a rough estimate of internal errors caused by the observer's judgement (Figure 8). However, we warn that these error estimates do not include those associated with the use of a given method when measuring ring properties. A different ring measurement method may yield values differing from those presented here by many times the error estimate that we discuss.

The top-left panel in Figure 8 shows how the error in the major and minor diameters tends to grow with ring radii: for small diameters, the $d_r, D_r - \langle d_r, D_r \rangle$ never exceeds 0.2, but for larger diameters, it can increase up to 0.6. The four points with larger $d_r, D_r - \langle d_r, D_r \rangle$ correspond, from left to right, to the major axis diameters of the outer features of NGC 4736 and NGC 4258. The outer ring of NGC 4736 appears to be double in its south-eastern side. Our choice in selecting the outline of the ring changed between the two measurements, which explains the large error. NGC 4258 is a galaxy for which the S⁴G frame does not fully cover the disc, thus a significant fraction of the outer ring lies outside the frame and cannot be studied, causing a large uncertainty in the D_r measurement. The range of $d_r, D_r - \langle d_r, D_r \rangle$ values is similar to that found in the catalog of southern ringed galaxies (CSRG; Figure 5a in Buta 1995).

The errors in the measured ring axis ratios are presented in the top-right panel of Figure 8. We found that the average error is $|\Delta q_r| = 0.02$.

The PA_r uncertainty is larger for smaller and/or rounder rings, as seen in the bottom panels of Figure 8; this is natural since for a round ring PA_r is undefined. The range of $PA_r - \langle PA_r \rangle$ in our study and its behaviour as a function of D and $\langle q_r \rangle = 1 - \epsilon_r = \langle d_r \rangle / \langle D_r \rangle$ is qualitatively similar to that in Figures 5c,d of the CSRG.

Because the CSRG is the largest ring catalogue with an internal error estimate, it can be compared with our results. The CSRG data come from analogically measuring diameters and PAs in photographic plates, but here we present data measured by digital means, which may yield significantly different accuracies.

The CSRG presents two internal error functions that we reproduce here with S⁴G data. The internal error function for the diameter residuals was obtained by sorting the residuals according to their mean diameter and then calculating the standard deviation for groups of 200 residuals, $\sigma(d_r, D_r)$ (top panel in Figure 9). As in the CSRG, we linearly fitted the points and obtained

$$\sigma(d_r, D_r) = 0.009 + 0.023 \langle d_r, D_r \rangle. \quad (1)$$

Since in ARRAKIS the error grows slower with increasing d_r, D_r , our accuracy is slightly better than that obtained in the CSRG ($\sigma(d_r, D_r) = 0.009 + 0.029 \langle d_r, D_r \rangle$). The 95% confidence bands in Figure 9 were calculated with the assumption that the errors are normally distributed. The statistics for the confidence bands corresponding to the CSRG were obtained by measuring the position of the data points in a magnified version of Figure 5e in the CSRG.

The internal errors for the ring orientations were calculated by sorting the PA_r residuals according to their q_r and then calculating the standard deviation for groups of 100 residuals (bottom panel in Figure 9). As in the CSRG, we produced a fit that scales inversely with the fitted ellipticity

$$\sigma(PA_r) = -0.87 + 1.35/(1 - q_r), \quad (2)$$

and thus our PA_r determinations are better than those in the CSRG for $q_r < 0.83$ [in the CSRG $\sigma(PA_r) = 2.29 + 0.81/(1 - q_r)$].

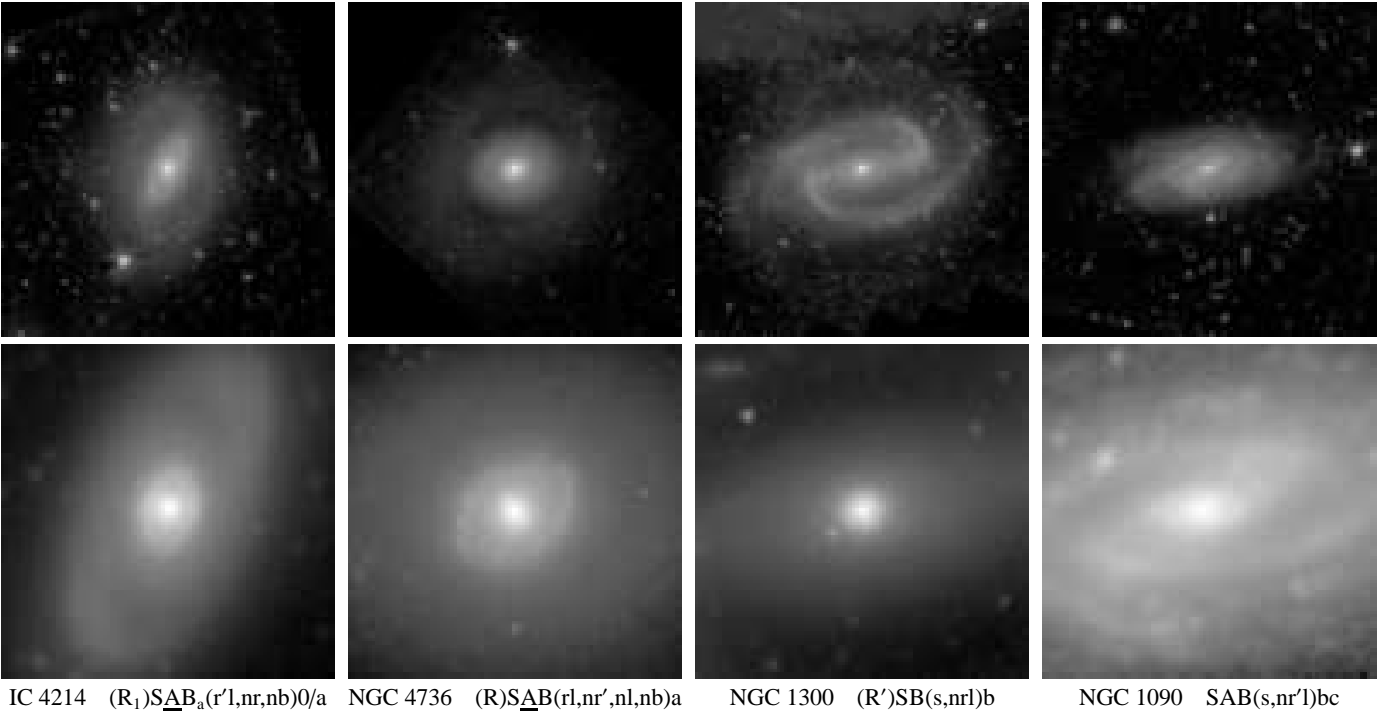


Fig. 4. Selection of S^4G galaxies hosting a variety of nuclear features. The images in the top row are presented in the same way as those in Figure 2. The bottom panels are zoomed by a factor of five compared with those in the top row. The frames show galaxies hosting a ring, a pseudoring, a ring-lens, and a pseudoring-lens, respectively.

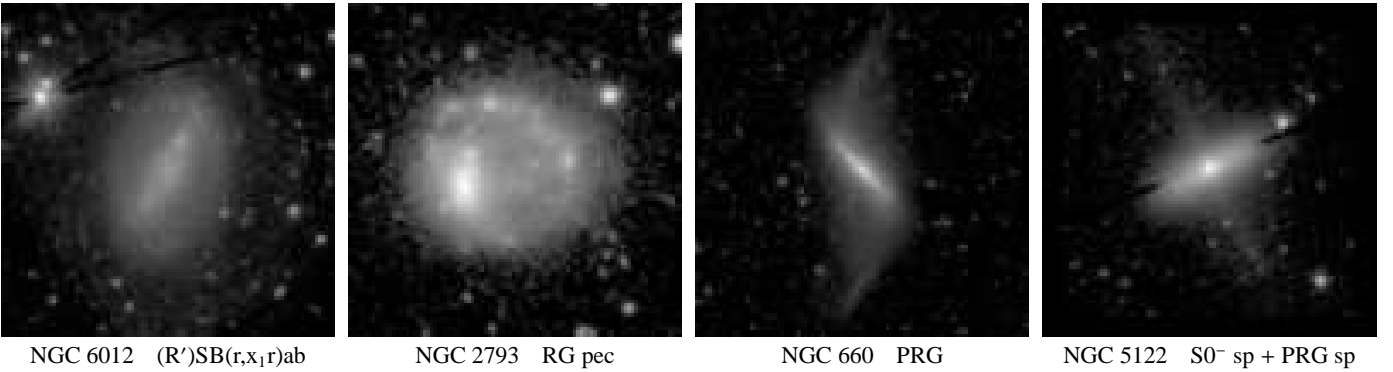


Fig. 5. Selection of S^4G galaxies hosting a variety of non-resonance rings presented in the same way as those in Figure 2. The first frame shows a galaxy with an x_1 -ring, the second one a galaxy with a collisional one, and the last two show galaxies with polar rings.

Our PA_r measurements are at least twice as precise than those in the CSRG for $q_r < 0.53$. However, perhaps surprisingly, the manual PA_r determination in the CSRG seems to have fewer internal errors than ARRAKIS for rings that are nearly round ($q_r > 0.83$). This is no problem because PA_r becomes meaningless for almost round rings. We calculated the confidence bands for this fit in the same way as for the top panel. For the CSRG fit, we made the statistics based on the information on CSRG's Figure 5f.

We can thus conclude that the internal errors in ARRAKIS are the smallest for such a large dataset of rings so far and that this can be attributed to the use of digital deep images.

4.3. Obtaining the projected bar parameters

Simulations by Schwarz (1981, 1984) and the flux tube manifold orbital calculations (Athanasoula et al. 2009b,a) predict R_1

rings to be elongated and perpendicular to bars, R_2 rings to be elongated and parallel to bars, and inner rings to be elongated and parallel to bars. It is thus interesting to know the bar PA in galaxies with rings. We also measured the highest bar ellipticity $\epsilon_b = 1 - q_b = 1 - d_b/D_b$ (D_b and d_b are the bar major and minor diameters and q_b is the bar axis ratio). ϵ_b roughly scales with more sophisticated bar strength indicators such as the bar torque (Block et al. 2001; Laurikainen et al. 2002).

The bar data were obtained by studying the ellipticity fits from S^4G 's P4. We searched for the peak ellipticity within the radius of the bar, regardless of how big the drop in the ellipticity after the maximum was or how the PA varied with radius. We considered the PA at that radius to be representative of the bar orientation. Moreover, the maximum ellipticity radius is typically a lower estimate of the bar length (Erwin 2005), except in galaxies in which the bar merges with rings and/or spiral arms. In the catalogue of Appendix A, we present the diameters along

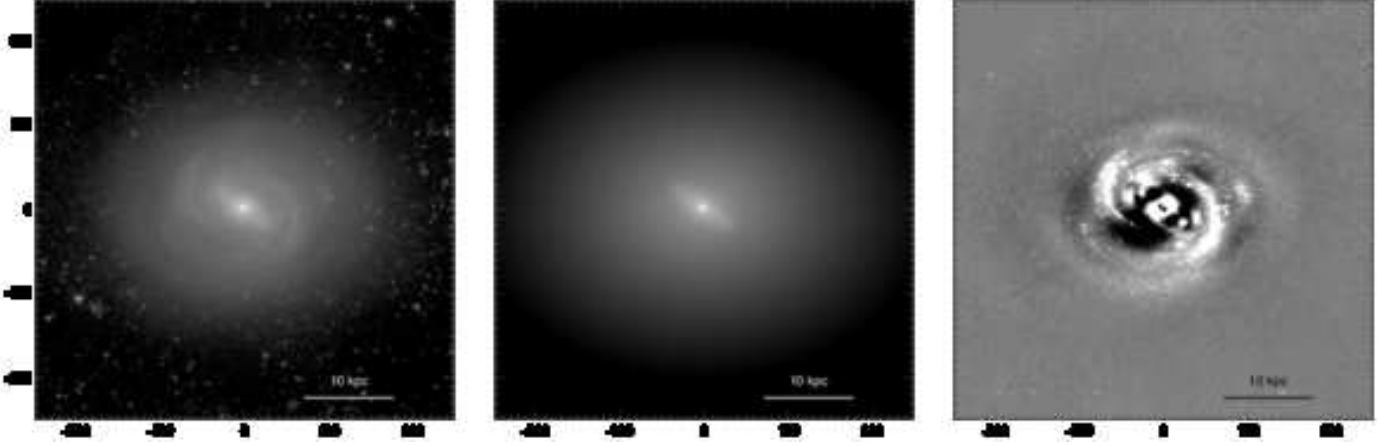


Fig. 6. Original image, P4 model, and model-subtracted image of NGC 4579. The model has three components, namely a bulge, a bar, and a disc. NGC 4579 is a galaxy classified as (RL,R')SB(rs)a by Buta et al. (in preparation). NGC 4579 has an exceedingly diffuse outer ring as seen in the first frame. The ring becomes more obvious in the model-subtracted image. The axis units are arcseconds.

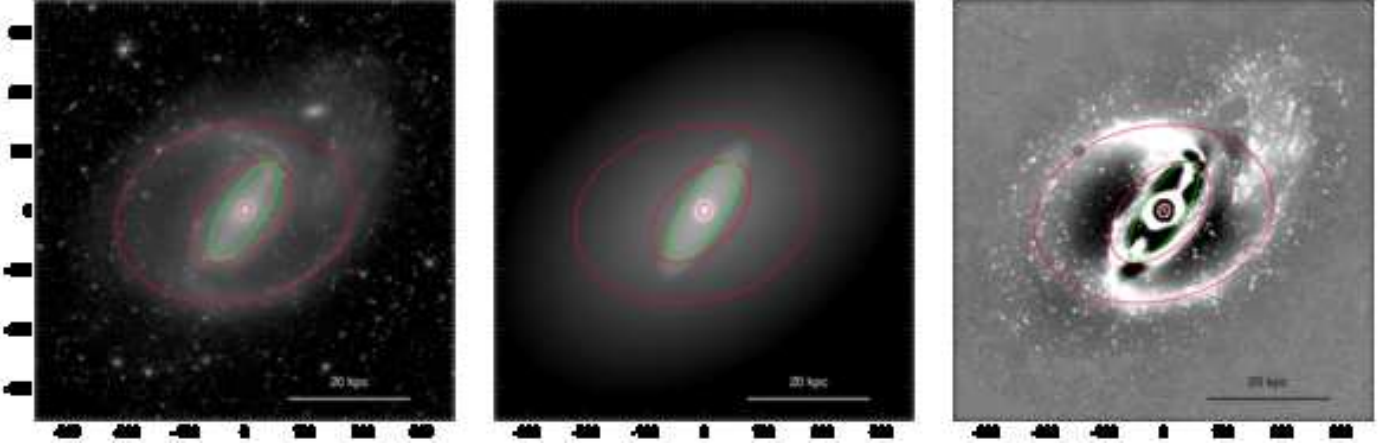


Fig. 7. Original image, P4 model, and model-subtracted image of NGC 1097, which is classified as an (R')SB(rs,nr)ab pec galaxy in Buta et al. (in preparation). The red ellipses indicate in an outside-in order the average of the two ellipse fits made to the outer, the inner, and the nuclear rings. The green ellipses are the result of an ellipse fit at the radius of the highest bar ellipticity. The red crosses indicate the centre of the galaxy. The axis units are arcseconds.

the major and minor axes of the ellipse fits at the position of the bar maximum ellipticity (D_b and d_b) and the bar PA at the same position, (PA_b). We checked that each individual PA_b roughly corresponds to what would be expected from visual inspection. If it did not, we labelled it as unsuitable for bar analysis, as discussed at the end of Section 4.5.

4.4. Obtaining the intrinsic ring and bar shape and orientation

ARRAKIS is the first large ring catalogue that provides intrinsic ring shapes and orientations. The reason is that deprojecting rings requires knowing, within a few percent, the disc orientation parameters, that is, the ellipticity, $\epsilon_d = 1 - q_d$, and the position angle, PA_d . Under the assumption of discs being intrinsically circular, one needs very deep images to measure ϵ_d and PA_d in the outer disc, a region where the effect of perturbing non-axisymmetries such as bars is most likely weak. This was not possible for the CSRG because it was produced using

photographic plates, but was performed in Knapen et al. (2002), Comerón et al. (2010), and Grouchy et al. (2010).

The S⁴G P4 makes use of deprojection parameters obtained from isophote fits at low surface brightness (for more details see Salo et al. in preparation). These are the deprojection parameters that we used here for obtaining intrinsic ring and bar shapes ($q_{r,0}$ and $q_{b,0}$) except for the few ARRAKIS galaxies not in the S⁴G sample (but appearing in S⁴G frames) and NGC 4698. For this last galaxy our interpretation of the deprojection parameters is very different from that in P4. P4 deprojection parameters were also used to calculate the counter-clockwise angular distance between the line of nodes and the ring and bar major axis (θ_r and θ_b), under the assumptions that the outer parts of discs are circular and that rings and bars are roughly elliptical. The equations that we used for deprojection can be found in Appendix A of Gadotti et al. (2007). The deprojected D and d values for both rings and bars are presented in the catalogue of Appendix A. The angle difference between the deprojected major axis and the line of nodes of the deprojection is also indicated. The only rings for which we have not included deprojected parameters are the

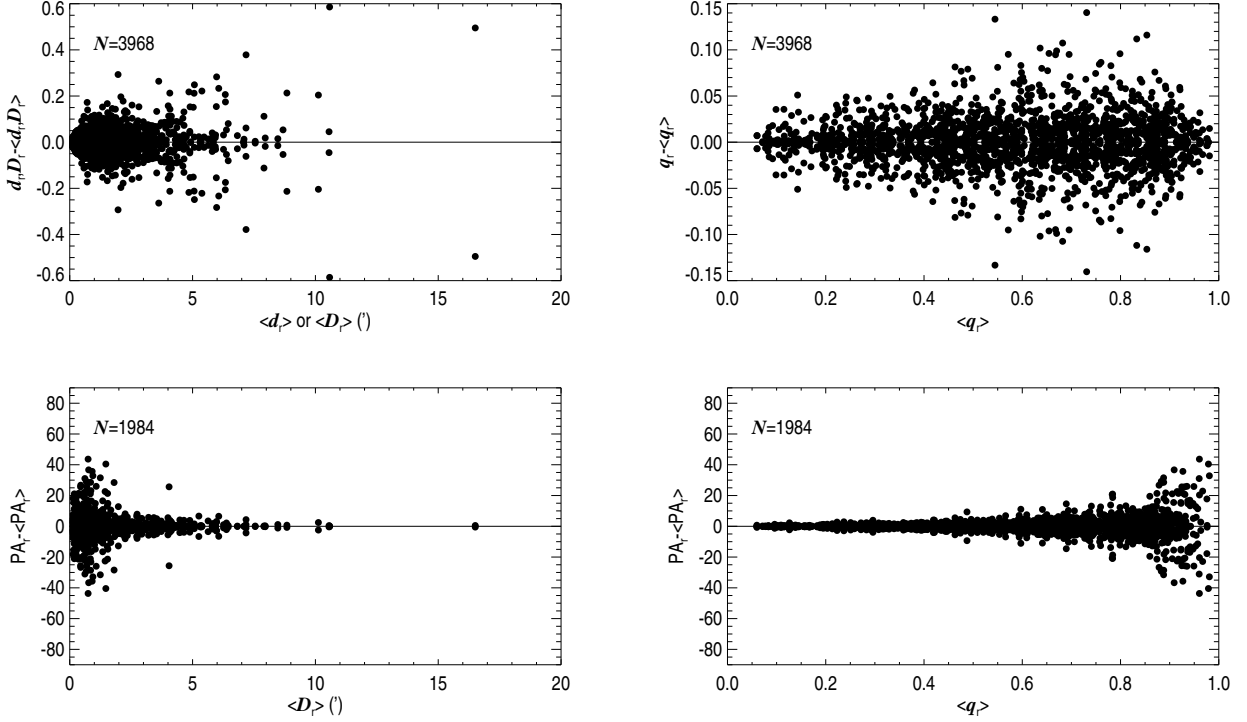


Fig. 8. Top-left panel: residuals of the ring diameters along the major and minor axes as a function of the averaged diameters, $\langle d_r, D_r \rangle$. Top-right panel: residuals of the ring axis ratios, $q_r = d_r/D_r$, as a function of the mean axis ratios $\langle q_r \rangle = \langle d_r \rangle / \langle D_r \rangle$. Bottom-left panel: residuals of the ring position angles as a function of the averaged ring major axis $\langle D_r \rangle$. Bottom-right panel: residuals of the ring position angles as a function of the mean ring axis ratios. N refers to the number of points in each plot.

Table 2. Parameters of the model galaxies used to study the reliability of the bar deprojected parameters

Model	$\rho_{\text{bulge},0}$	a	b	c	Bulge/ Total	Bar/ Total
Model 1	5	30	10	3	11%	3%
Model 2	10	30	10	3	20%	2%
Model 3	5	50	15	4	11%	8%
Model 4	10	50	15	4	19%	7%

Notes. Bulge/Total stands for the bulge-to-total mass ratio and Bar/Total stands for the bar-to-total mass ratio.

polar rings, because they are known not to lie in the galaxy disc plane.

4.5. Reliability of the deprojected bar parameters

The presence of a bar can be recognised in very inclined galaxies and sometimes also in edge-on galaxies (see, e.g., how box/peanut bulges are related to bars in Kuijken & Merrifield 1995). However, obtaining their orientation and ellipticity from ellipse fits can be very difficult. Indeed, the ellipse deprojection would give precise bar parameters for isolated infinitely thin bars. But real bars have some amount of vertical thickening and are embedded in galaxies with discs and bulges. As a natural consequence of that, the more inclined a galaxy, the harder it is to obtain accurate bar intrinsic parameters.

To estimate how precise our bar measurements are, we prepared a set of four toy model galaxies with an exponential disc, a classical spherical bulge, and a Ferrers bar (Ferrers 1877).

Assuming that the centre of the galaxy is located at $x = 0$, $y = 0$, and $z = 0$ and that the disc lies in the $x - y$ plane, this simplified disc can be described as

$$\rho_d(R, z) = \rho_{d,0} e^{-R/h_R} e^{-|z|/h_z}, \quad (3)$$

where R is the radius in the plane of the galaxy ($R = \sqrt{x^2 + y^2}$), $\rho_{d,0}$ stands for the disc central mass density, h_R for the disc scale-length, and h_z for the disc scale-height.

To describe the bulge we used a Jaffe profile (Jaffe 1983) which, when projected onto a plane, results approximately in a de Vaucouleurs profile (de Vaucouleurs 1948):

$$\rho_{\text{bulge}}(r) = \rho_{\text{bulge},0} \left(\frac{r}{r_0} \right)^{-2} \left(1 + \frac{r}{r_0} \right)^{-2}, \quad (4)$$

where r is the 3D radius ($r = \sqrt{x^2 + y^2 + z^2}$), $\rho_{\text{bulge},0}$ controls the bulge mass, and r_0 controls its size.

Finally, the bar was described as

$$\rho_{\text{bar}}(m) = \rho_{b,0} (1 - m^2) \text{ for } m \leq 1, \rho_b = 0 \text{ for } m > 1, \quad (5)$$

where $\rho_{b,0}$ is the central bar mass density and

$$m^2(x, y, z) = \frac{x^2}{a^2} + \frac{y^2}{b^2} + \frac{z^2}{c^2}. \quad (6)$$

Here, a is the major axis, b is the minor axis, and c is the vertical axis of the bar.

The four model galaxies had (in arbitrary units) $\rho_{d,0} = 1$, $\rho_{b,0} = 1$, $h_R = 30$, $h_z = 5$, and $r_0 = 5$. The other parameters were model-dependent and are listed in Table 2. Table 2 also presents the fraction of mass in the bulge and in the bar for each

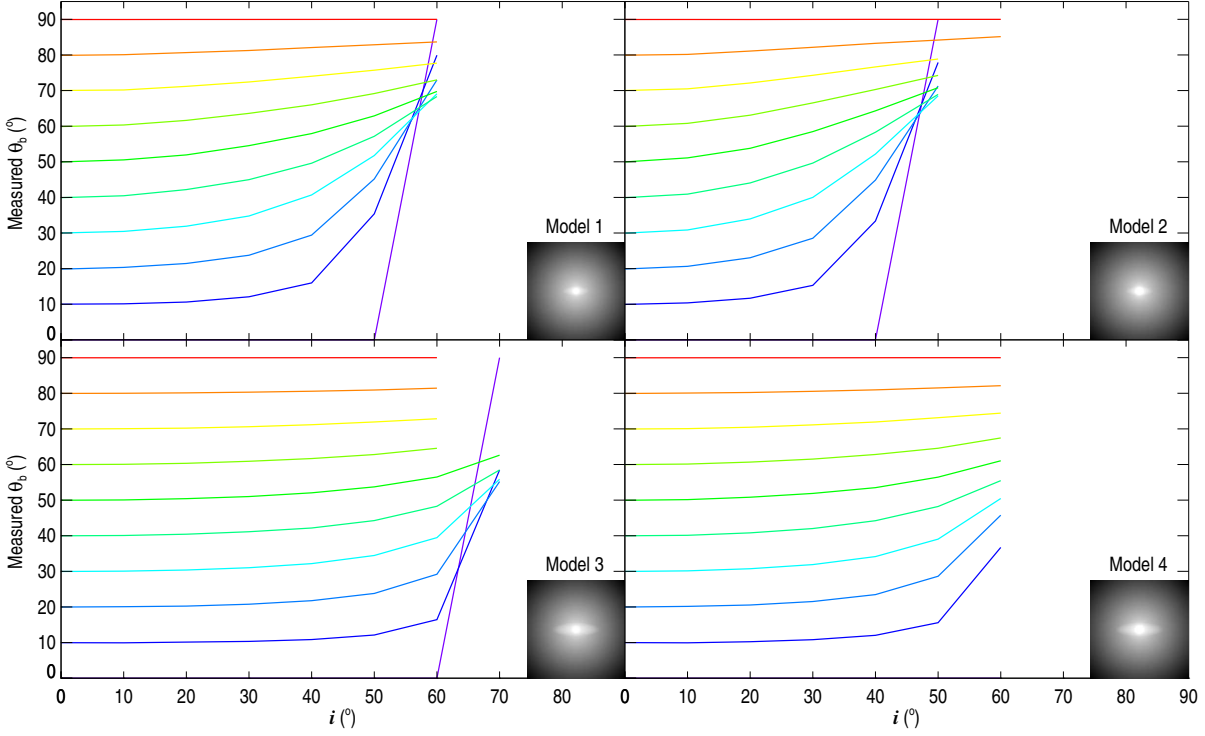


Fig. 10. Measured orientation of the bar with respect to the line of nodes of the galaxy (θ_b) as a function of the galaxy inclination (i) for each of our four galaxy models described in the text and Table 2. Each coloured line represents a single real θ_b value, which is the one corresponding to the position at which the line crosses the $i = 0^\circ$ axis, that is, from purple to red (bottom to top), $\theta_b = 0^\circ$, $\theta_b = 10^\circ$, $\theta_b = 20^\circ$, $\theta_b = 30^\circ$, $\theta_b = 40^\circ$, $\theta_b = 50^\circ$, $\theta_b = 60^\circ$, $\theta_b = 70^\circ$, $\theta_b = 80^\circ$, and $\theta_b = 90^\circ$. The images at the bottom-right corner of each panel represent the corresponding galaxy when $\theta_b = 0^\circ$ and $i = 0^\circ$.

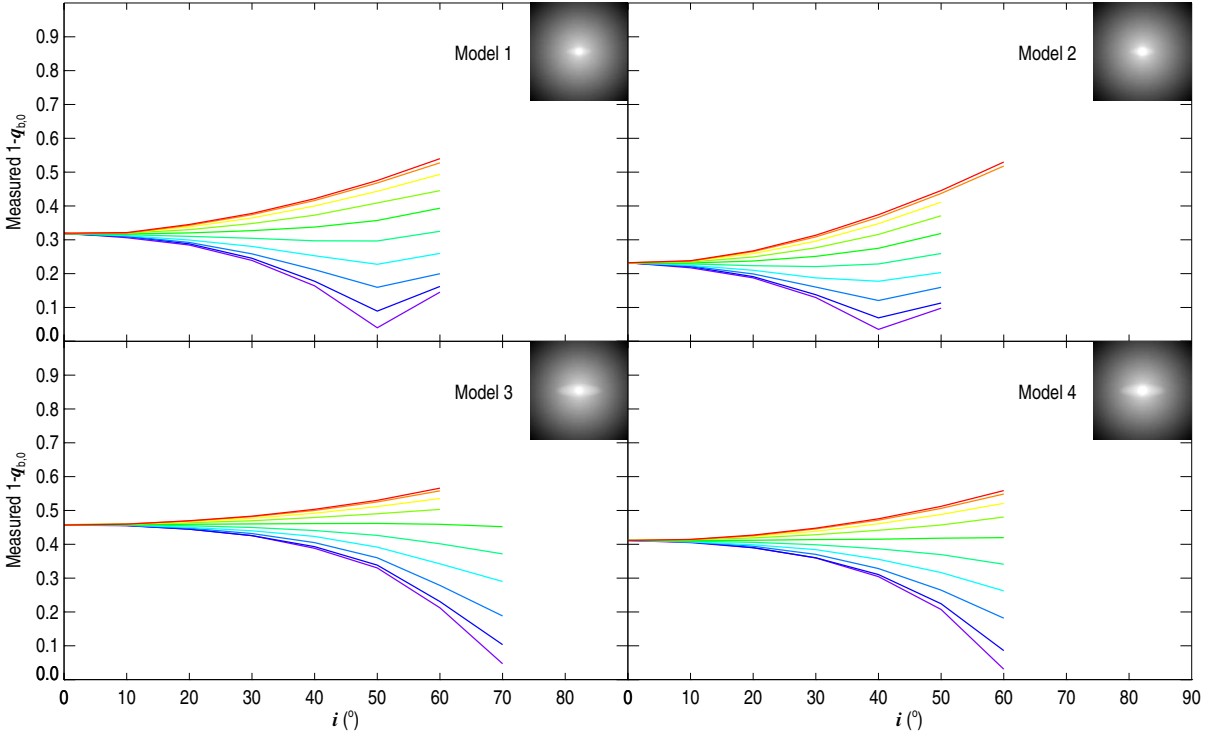


Fig. 11. Measured bar ellipticity (measured $1 - q_{b,0}$) as a function of the galaxy inclination (i) for each of our four galaxy models. Each coloured line represents a single θ_b value colour-coded in the same way as in Figure 10 (also ordered here from bottom to top). The intrinsic $1 - q_{b,0}$ value is that corresponding to $i = 0^\circ$. The images at the top-right corner of each panel represent the corresponding galaxy when $\theta_b = 0^\circ$ and $i = 0^\circ$.

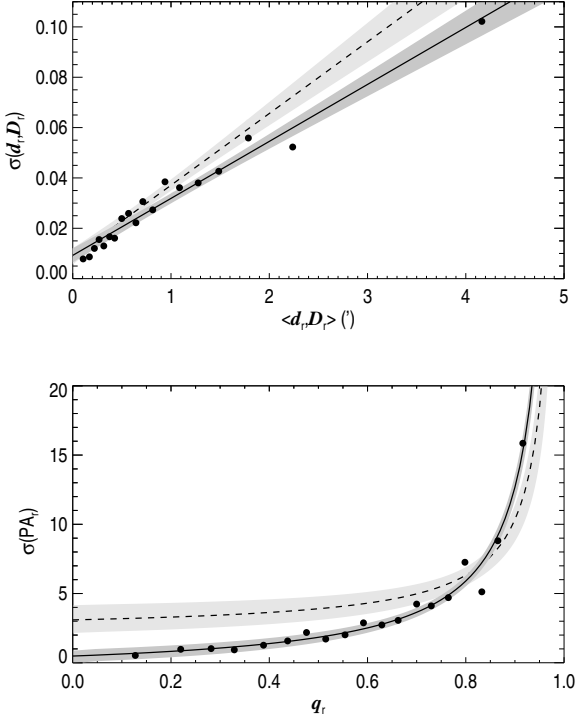


Fig. 9. Top panel: internal errors of d_r, D_r as a function of $\langle d_r, D_r \rangle$. Bottom panel: internal errors of PA_f as a function of q_r . The solid lines represent the fits described in Equations 1 and 2 and the dashed lines correspond to the same expressions as presented in the CSR. Darker grey areas indicate the 95% confidence interval of the fit for ARRAKIS and lighter grey indicates the same for the CSR.

model. As seen there, the fraction of mass in bars is rather low and thus our fit to models is a worst-case study.

We decided that the x axis would be the line of nodes of our rotation. We first rotated the bar by a given angle θ_b with respect to the line of nodes and then inclined the galaxy by an angle i . We defined θ_b to vary from $\theta_b = 0^\circ$ to $\theta_b = 90^\circ$ in steps of 10° . We explored the space of galaxy inclinations from $i = 0^\circ$ to $i = 80^\circ$ in steps of 10° . The rotated and inclined galaxies were then projected onto 2D fits images. We used these images to measure the bar properties by fitting ellipticity profiles. We considered that a bar ellipticity and PA could be measured when a peak in ellipticity with prominence larger than 0.01 occurred within the bar radius. We used the ellipticity fit at the maximum ellipticity peak to obtain the deprojected bar parameters, as was done for observed bars in Section 4.4. The results on the recovery of the original bar PA with respect to the line of nodes, θ_b , and the original bar ellipticity, $\epsilon_{b,0} = 1 - q_{b,0}$, are presented in Figures 10 and 11. In several cases in highly inclined galaxies, no clear maximum in ellipticity was found, therefore no deprojection of the bar properties was obtained.

The angle θ_b is typically well recovered for galaxies with $i \leq 40^\circ$ when the bar is small compared to the bulge size (models 1 and 2 in Figure 10). For galaxies with longer bars (models 3 and 4), θ_b is well recovered for $i \leq 60^\circ$. The reason for this is that the bulge, which is intrinsically spherical, and to some extent also the disc, soften the isophotes, which makes them less elliptical. In some cases, for low real θ_b values and high disc inclinations, this effect is so strong that the measured projected el-

lipticity becomes lower than the ellipticity of the projected disc, causing the measured θ_b to shift by some 90° from the real value.

The measured intrinsic bar ellipticity $\epsilon_{b,0} = 1 - q_{b,0}$ is highly dependent on the real θ_b . When the bar is parallel to the line of nodes (real $\theta_b \sim 0^\circ$), $1 - q_{b,0}$ becomes increasingly underestimated for increasing i . For bars oriented perpendicular to the line of nodes (real $\theta_b \sim 90^\circ$), the effect is reversed.

Because the S⁴G sample is under-abundant in early-type galaxies, bulges are in general not expected to play a significant role when producing ellipticity profiles. Therefore, we considered the parameters of the bars in galaxies with $i \leq 60^\circ$ (corresponding to a disc ellipticity $\epsilon_d = 1 - q_d \leq 0.5$) to be reliably measured. The properties of bars in such discs almost always appear in the catalogue in Appendix A and the ellipse fit to the highest bar ellipticity is overlaid on the images of the atlas in Appendix B.

However, even for galaxies with $i \leq 60^\circ$ six bar fits were found to be unreliable and were excluded from the appendices. The reason for this is that the bar fit is obviously wrong in galaxies with bars with a low contrast (NGC 2552) or that are influenced by surrounding bright regions such as a ring (NGC 2967, NGC 4351, NGC 5595, NGC 5744, and NGC 6923). For five additional galaxies with $\epsilon_d \leq 0.5$ classified as barred by Buta et al. (in preparation), ESO 443-80, NGC 2460, NGC 5633, NGC 6278, and UGC 5814, we were unable to distinguish a peak corresponding to a bar in the ellipticity profiles. Finally, the centre of NGC 4108B is affected by an image artefact that made impossible to measure the bar properties. For galaxies with $i > 60^\circ$, we did not include the bar properties in the appendices even for those that are obviously barred.

Moreover, even though inner rings are defined to be surrounding the bar, for 73 galaxies the maximum in ellipticity that we fitted as an estimate for the bar radius is slightly larger than the inner ring radius in projection and/or in deprojection. This is caused by our very simple approach at describing bars. In most of these cases the bar merges with the ring and the junction points have strong star-forming regions, ansæ, and/or the beginning of spiral arms, which affect the ellipticity fits in such a way as to move the ellipticity maximum outwards. In other cases, the reason that the bar is larger than the fitted ring diameter may be that some rings slightly deviate from an elliptical shape in such a way that the bar fits within them. These deviations are not captured by our simple ring-fitting approach. In none of the cases considered for the statistics in this paper would this change the bar orientation by more than a few degrees from what would be measured visually.

4.6. Reliability of the deprojected ellipse parameters in discs with a finite thickness

The reliability of the deprojected ring parameters depends on the quality of the P4 measured disc deprojection parameters. One source of error when deprojecting is the assumption that discs are infinitely thin. Indeed, the thicker a galaxy disc, the more the measured galaxy inclination, i , will differ from the real inclination, i' .

The thickness of discs has been studied by de Grijs (1998). He found that the ratio between the disc scale-height and the disc scale-length (h_z and h_R , respectively) decrease monotonically with Hubble stage. The average h_z/h_R is around 1/3 for S0 galaxies and decreases to 1/9 for Sd galaxies. However, for a given stage the scatter in h_z/h_R is large, so the relationship described by de Grijs (1998) cannot be used for correcting the finite thickness effects in deprojected parameters without adding

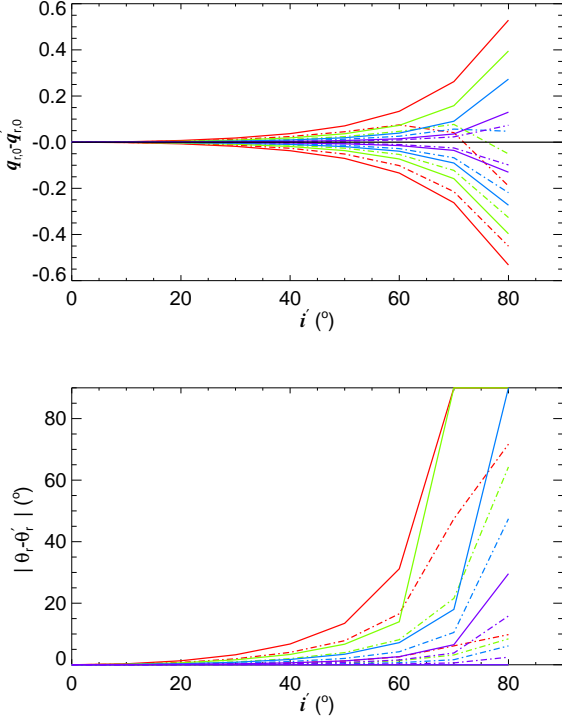


Fig. 12. Top panel: difference between the measured intrinsic axis ratio of a ring, $q_{r,0}$, and the real one, $q'_{r,0}$, as a function of the real galaxy inclination, i' , for four disc scale-height to scale-length ratios. The colour code corresponds in an outside-in order to $h_z/h_R = 1/3$ (red), $h_z/h_R = 1/5$ (green), $h_z/h_R = 1/7$ (blue), and $h_z/h_R = 1/10$ (purple). Bottom panel: difference of the measured angle difference between the orientation of the major axis of a ring with respect to the line of nodes, θ_r , with respect to the real one, θ'_r , as a function of the real galaxy inclination. In both panels, the solid lines indicate the maximum and the minimum $q_{r,0} - q'_{r,0}$ ($|\theta_r - \theta'_r|$) for a given i' colour-coded as in the top panel. The dashed lines indicate the limits of the region enclosing 68.2% of $q_{r,0} - q'_{r,0}$ ($|\theta_r - \theta'_r|$) values at a given i' .

a substantial error. Instead, in this section we adopt the approach of quantifying possible biases in the deprojected parameters.

Hubble (1926) described the formalism for finding inclination of an oblate ellipsoid,

$$\cos^2 i' = \frac{q_d^2 - q_z^2}{1 - q_z^2}, \quad (7)$$

where q_d is the observed galaxy disc axis ratio and q_z is the galaxy flattening, that is, h_z/h_R . From this, and knowing that $\cos i = q_d$, we can derive the formula for calculating the i corresponding to a given i' :

$$i = \arccos\left(\sqrt{q_z^2 + (1 - q_z^2) \cos^2 i'}\right). \quad (8)$$

From this expression we can deduce that the maximum bias at finding a disc inclination comes from the galaxies with thicker discs, namely S0s with $h_z/h_R \sim 1/3$. Most of our results in Section 6 are based on galaxies with $i \leq 60^\circ$. For an S0 galaxy with $i' = 60^\circ$ $\Delta i = i' - i \sim 5^\circ$. Accordingly, for most of the galaxies with $i \leq 60^\circ$, $i \sim i'$.

To examine how the biased i values calculated from Equation 8 would affect our ring deprojection values, we created four model galaxies with $h_z/h_R = 1/3$, $h_z/h_R = 1/5$, $h_z/h_R = 1/7$, and $h_z/h_R = 1/10$. We then inclined each of them with angles in the range $i' = 0^\circ$ to $i' = 80^\circ$ with 10° intervals.

We checked how the underestimated inclination measurements would affect the measured intrinsic ring ellipticities, $q_{r,0}$, and the angle between their major axes and the lines of nodes of the deprojection, θ_r . To do this, we considered a population of rings with a Gaussian distribution of intrinsic axis ratios, $q'_{r,0}$, with the centre of the Gaussian at $q'_{r,0} = 0.8$ and a dispersion of $\sigma' = 0.13$. These values are representative of the measured axis ratio distribution of inner rings as seen in Section 6.3. For each galaxy model with a given h_z/h_R and for each of the studied inclinations, we obtained 1000 random ring axis ratios. The intrinsic axis ratio of each of these rings was recovered after projecting it using the real galaxy inclination, i' , and deprojecting it using the measured galaxy inclination, i . This was repeated for 19 angle differences between the ring major axis and the line of nodes used for inclining the model galaxy. These angles ranged from $\theta'_r = 0^\circ$ to $\theta'_r = 90^\circ$ in steps of 5° .

In the top panel in Figure 12 we study the accuracy of the measured ring axis ratios. If, as in our results section, we focus on galaxies with $i' \leq 60^\circ$, the errors at measuring $q_{r,0}$ are always below $|\Delta q_{r,0}| = 0.05$ except for galaxies with $h_z/h_R = 1/3$ and a few cases with $h_z/h_R = 1/5$. Except in exceptional cases for $h_z/h_R = 1/3$, $|\Delta q_{r,0}| \leq 0.10$. For $i' \leq 40^\circ$, the uncertainties in q_0 due to the finite thickness of discs are always rather small and in the order of the uncertainty in the measurement of q_r ($|\Delta q_r| = 0.02$) as measured in Section 4.2.

In the bottom panel in Figure 12 we study the accuracy of the measured ring intrinsic orientation. We find that for galaxies with $i' \leq 60^\circ$, the maximum $|\theta_r - \theta'_r|$ is always below 10° except, again, for galaxies with $h_z/h_R = 1/3$ and in a few cases in those with $h_z/h_R = 1/5$.

We conclude this section by saying that as found for bars in Section 4.5, results from deprojected parameters seem in general reliable for galaxies with $i \leq 60^\circ$. The exception are the moderately inclined galaxies ($i = 40 - 60^\circ$) with a larger disc thickness relative to the scale-length (S0 galaxies), whose deprojected ring parameters are in some cases not very accurate.

5. Comparison of ring properties in ARRAKIS with the data in the literature

In this section we compare the measured properties of rings with those reported in a set of significant papers in the literature that have samples in common with ours.

In several cases, significant discrepancies have been found between the ring diameters in ARRAKIS and those in the literature. In most of them, we found that this is because the features are classified in a different way in ARRAKIS and in the literature. For example, the feature with an ARRAKIS major diameter of 1.48 in NGC 4736 was classified as an inner ring by de Vaucouleurs & Buta (1980). Here, this feature is considered as a nuclear ring because it is found inside a very broad bar/oval that was unnoticed by de Vaucouleurs & Buta (1980). The broad bar in NGC 4736 is here recognized as being surrounded by a subtle ring-lens 4.48 in major diameter that was considered to be an outer lens in de Vaucouleurs & Buta (1980). Therefore, when comparing the inner ring in de Vaucouleurs & Buta (1980) with that in ARRAKIS, we are actually comparing two different features. Such features with a wrong classification appear as outliers

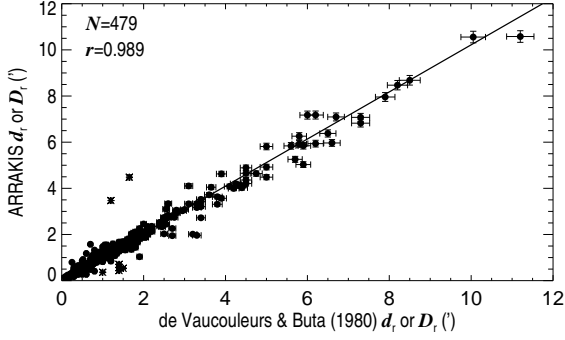


Fig. 13. Comparison of the angular diameters of ARRAKIS rings with those in VB80. The line corresponds to a linear fit to the data points in the plot. The outliers due to the wrong identification of the resonance to which a ring is linked in VB80 are marked with asterisks and are excluded from the fit. The numbers in the top-left corner indicate the number of points considered in the fit and their correlation coefficient.

in Figures 13–17 and have not been considered for the statistics in this section.

5.1. ARRAKIS and de Vaucouleurs & Buta (1980)

De Vaucouleurs & Buta (1980; hereafter VB80) compiled a catalogue that includes the diameter of outer and inner rings in 532 bright galaxies. The S⁴G and the VB80 samples have 303 galaxies in common.

We compared the sizes of the rings listed both in ARRAKIS and VB80. For this, we performed a linear least-squares fit of the major and minor axis diameter measurements in the two surveys. The fit takes into account the errors both in the ARRAKIS and the VB80 measurements. The ARRAKIS diameter errors were considered to follow the internal error function in Equation 1. VB80 did not quantify their errors. Since their data are collected from photographic plates, we considered that their errors are probably similar to those in the CSRG, and therefore we used the CSRG internal error function for their diameters.

The fit we obtained is

$$d_r, D_r(\text{ARRAKIS}) = 0'013 \pm 0'006 + (1.021 \pm 0.003)(d_r, D_r)(\text{VB80}) \quad (9)$$

with a correlation factor $r = 0.989$. This means that the agreement between the measurements in ARRAKIS and in VB80 is very good.

5.2. ARRAKIS and Buta & Crocker (1993)

Buta & Crocker (1993, hereafter BC93) studied galaxies with nuclear components, mostly nuclear rings, but also lenses and spirals. In BC93, galaxies with nuclear features also had their inner and outer features classified. The BC3 catalogue lists 64 galaxies, 37 of which are included in the S⁴G. Figure 14 compares the sizes of the features measured in ARRAKIS with those in BC93.

As with the VB80 data, we performed a least-squares fit to compare the BC93 data with ours. Again, the CSRG internal error function was used to describe the errors in the diameters in BC3. The fit gives

$$d_r, D_r(\text{ARRAKIS}) =$$

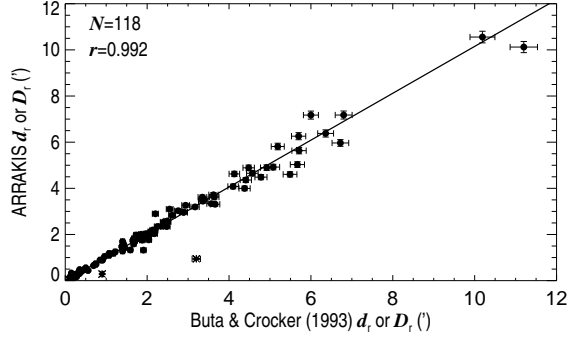


Fig. 14. As in Figure 13, but with data from BC93.

$$-0'008 \pm 0'016 + (1.016 \pm 0.006)(d_r, D_r)(\text{BC93}) \quad (10)$$

with a correlation factor $r = 0.992$.

5.3. ARRAKIS and the CSRG

The CSRG includes 3692 galaxies that host outer and inner rings and lenses south of declination $\delta = -17^\circ$. The CSRG has 120 galaxies in common with the S⁴G.

In the top-left panel of Figure 15 we compare the size of a feature when it is identified in both the CSRG and ARRAKIS. A linear fit to the data accounting for the ARRAKIS and CSRG internal error functions at measuring diameters yields

$$d_r, D_r(\text{ARRAKIS}) = -0'018 \pm 0'011 + (0.994 \pm 0.005)(d_r, D_r)(\text{CSRG}), \quad (11)$$

and a correlation factor $r = 0.992$, again indicating excellent agreement.

The CSRG describes the projected ring orientation as the PA offset between the bar and the ring major axis. ARRAKIS has such data only for galaxies with $q_d > 0.5$ because we considered more inclined galaxies to have unreliable bar axis ratio determinations (Section 4.5). The correlation between the ring orientation values for the CSRG and ARRAKIS is not as tight as it is for the angular sizes (top-right panel in Figure 15). This is probably due to the analogue procedure used for building the CSRG. Indeed, it is conceivable to obtain accurate results on ring diameters using a magnifying device, but the determination of the major axis of bars and especially rings is doomed to be much more subjective.

The difference between the CSRG $\text{PA}_r - \text{PA}_b$ values and ours is plotted in the bottom-left and bottom-right panels of Figure 15 as a function of the ring size and the ring axis ratio. The differences in $\text{PA}_r - \text{PA}_b$ are larger than our internal error for PA_r , which is generally below 10° for rings with $D_r > 3'$ and/or $q_r < 0.7$ (Figure 8).

5.4. ARRAKIS and AINUR

AINUR contains the most complete catalogue of nuclear rings to date, mostly relying on *Hubble Space Telescope* images that in some cases have an angular resolution as high as $\sim 0'.1$. Because of that, it contains detailed information of angularly small rings that cannot be expected to be described this thoroughly in ARRAKIS. Sixty out of 107 galaxies in AINUR are in the S⁴G sample. Of these 60 galaxies 26 are reported here to have a nuclear ring.

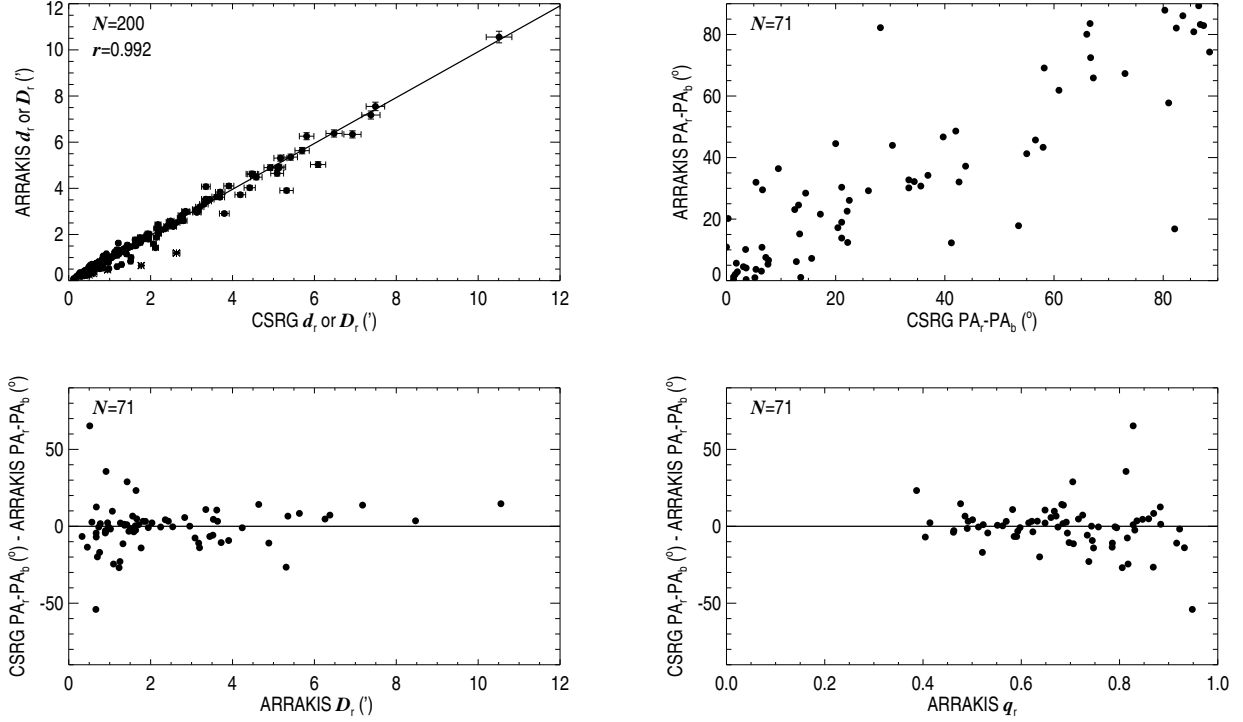


Fig. 15. Top-left panel: As in Figure 13, but with data from the CSRG. Top-right panel: comparison of the PA offset between the major axis of bars and that of rings in the CSRG and ARRAKIS. Bottom panels: difference in the PA offsets between the bar and the ring major axis as a function of the ring size and of the ring axis ratio. In the three last panels, only points for barred galaxies with $\epsilon_d \leq 0.5$ are presented.

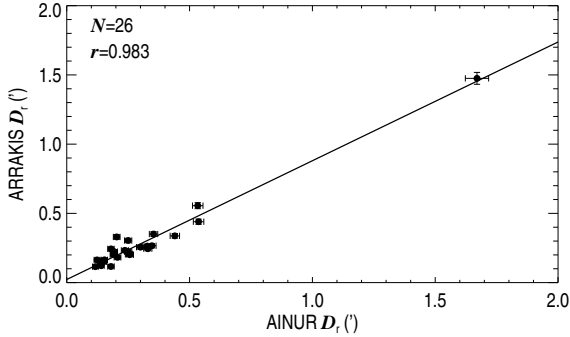


Fig. 16. As in Figure 13, but with data from AINUR.

When comparing the major axis diameter of features classified as nuclear rings both in AINUR and ARRAKIS, we obtain

$$d_r, D_r(\text{ARRAKIS}) = 0.022 \pm 0.010 + (0.858 \pm 0.029)(d_r, D_r)(\text{AINUR}), \quad (12)$$

with a correlation factor $r = 0.983$. Here, the internal error functions for the diameters are those in Equation 1 both for AINUR and ARRAKIS. We chose this error function for AINUR because, as for ARRAKIS, the ring measurements were made on digital images. This fit is much poorer than those found for VAU80, BU93, CSRG, and NIRS0S. This is probably because of the difficulty found in measuring the properties of features that are often barely resolved in the S⁴G. The difference may also reflect that the procedures used to measure the ring properties in the two works are different.

5.5. ARRAKIS and NIRS0S

NIRS0S is a ground-based survey of 206 nearby early-type disc galaxies with a sample dominated by S0s. The survey was produced using the K_s band. NIRS0S does not reach as deep as the S⁴G but has a better angular resolution (typical pixel resolution of 0.3 and typical seeing around 1''). NIRS0S and the S⁴G have 93 galaxies in common.

The ring sizes measured in NIRS0S agree very well with ours (Figure 17). When comparing the ring diameters from ARRAKIS and NIRS0S (in both cases we use the internal error function from Equation 1 because in both cases the rings are measured on digital images), we obtain the following excellent linear fit

$$d_r, D_r(\text{ARRAKIS}) = 0.006 \pm 0.009 + (0.993 \pm 0.005)(d_r, D_r)(\text{NIRS0S}), \quad (13)$$

and the correlation factor is $r = 0.988$.

Figure 17 also shows that the agreement in the measured position angle of the ring major axis is very good and much better than when comparing this paper with the CSRG. One possible reason is that NIRS0S is a digital survey where PA_r can be measured more easily. The second reason is that in the CSRG the position angle difference between the ring and the bar major axis was measured. This measurement includes two errors: that related to the orientation of the ring, and that related to the orientation of the bar, and thus causes larger discrepancies than those found when comparing NIRS0S with this paper. As we found when we compared ARRAKIS with the CSRG and from our internal errors, the uncertainty in the orientation measurement increases for smaller and/or rounder rings.

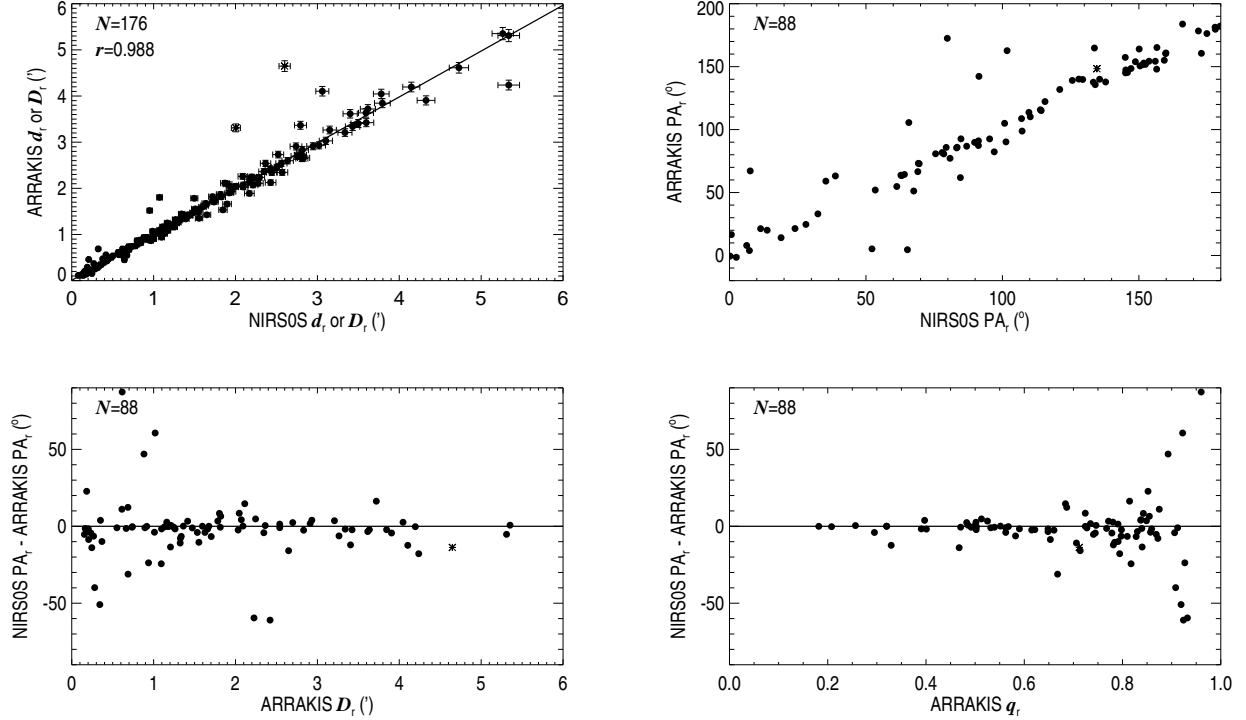


Fig. 17. As in Figure 15, but with data from NIRSOS.

6. Results

We recall that in this paper rings refers to the set including both open pseudorings and closed features. Here, the set including only closed features is referred to as closed rings.

6.1. Fraction of rings as a function of the Hubble stage

Stage classification is commonly described by a numerical code ranging from -5 to 10 corresponding to the sequence going from E to I galaxies. However, in some cases, a more detailed classification can be made and is then denoted with intermediate stages such as S_{bc} or S_{cd} , which in turn are codified as $T = 4.5$ and $T = 5.5$. In the few particular cases for which such a classification is provided, we rounded up the stage so that, for example, S_{bc} becomes S_c ($T = 5$) and S_{cd} becomes S_{cd} ($T = 6$).

Some galaxies in Buta et al. (in preparation) have not been classified into categories that fit in the traditional Hubble fork. Indeed, based on the van den Bergh (1976) hypothesis that S0 galaxies form a sequence from early to late galaxies just like normal disc galaxies do, some galaxies have been classified as S_{0b} , S_{0bc} , S_{0c} , S_{0cd} , S_{0d} , and S_{0m} . This is true for 36 S^4G galaxies, three of which host rings. These galaxies were included in the bin corresponding to their counterpart in the traditional sequence (e.g., S_{0b} galaxies were grouped together with S_b galaxies).

A few galaxies (12) have a double stage (for details on double-stage galaxies see Buta et al. 2010), five of which are ringed. These galaxies were not included in the stage statistics. We also excluded the dwarf elliptical galaxies from the results in this subsection (34 galaxies, none of which is ringed). Finally, we also excluded 12 S^4G galaxies that are so difficult to classify that there were assigned no stage. None of these galaxies is ringed

The distribution of resonant features varies greatly with the stage of the galaxies, as seen in Figure 18. The bottom-row panels in that figure have $1 - \sigma$ (68%) confidence levels calculated using binomial distribution statistics,

$$\Delta(p) = \sqrt{\frac{p(1-p)}{n}}, \quad (14)$$

where p is the probability of a galaxy in a given stage bin to have a specific type of ring and n the total number of galaxies in that stage bin. All the uncertainties given in this section were calculated using this expression. When the data in this section are quantitatively compared with the data in other papers, we verified that the uncertainties in those papers were computed in the same way as we did.

Inclination has to be taken into account before discussing in detail the stage distributions statistics. Indeed, it is more likely for inclined galaxies to have unidentified or misinterpreted rings. We found that of the whole sample of galaxies, 31% have some resonant feature, but that this fraction is increased to 41% for the subsample with $\epsilon_d \leq 0.5$. These numbers indicate that as much as $\sim 50\%$ of the resonant features are missed in inclined galaxies. This effect is especially pronounced for inner features, most likely because they are found in regions of galaxies that are hard to interpret because of bars, spiral arms, and/or intense star formation regions.

6.1.1. Outer rings

The stage distribution of outer rings based on the S^4G subsample with $\epsilon_d \leq 0.5$ indicates the following (see also continuous blue lines in Figure 18):

- They are found in $16 \pm 1\%$ of S^4G galaxies.

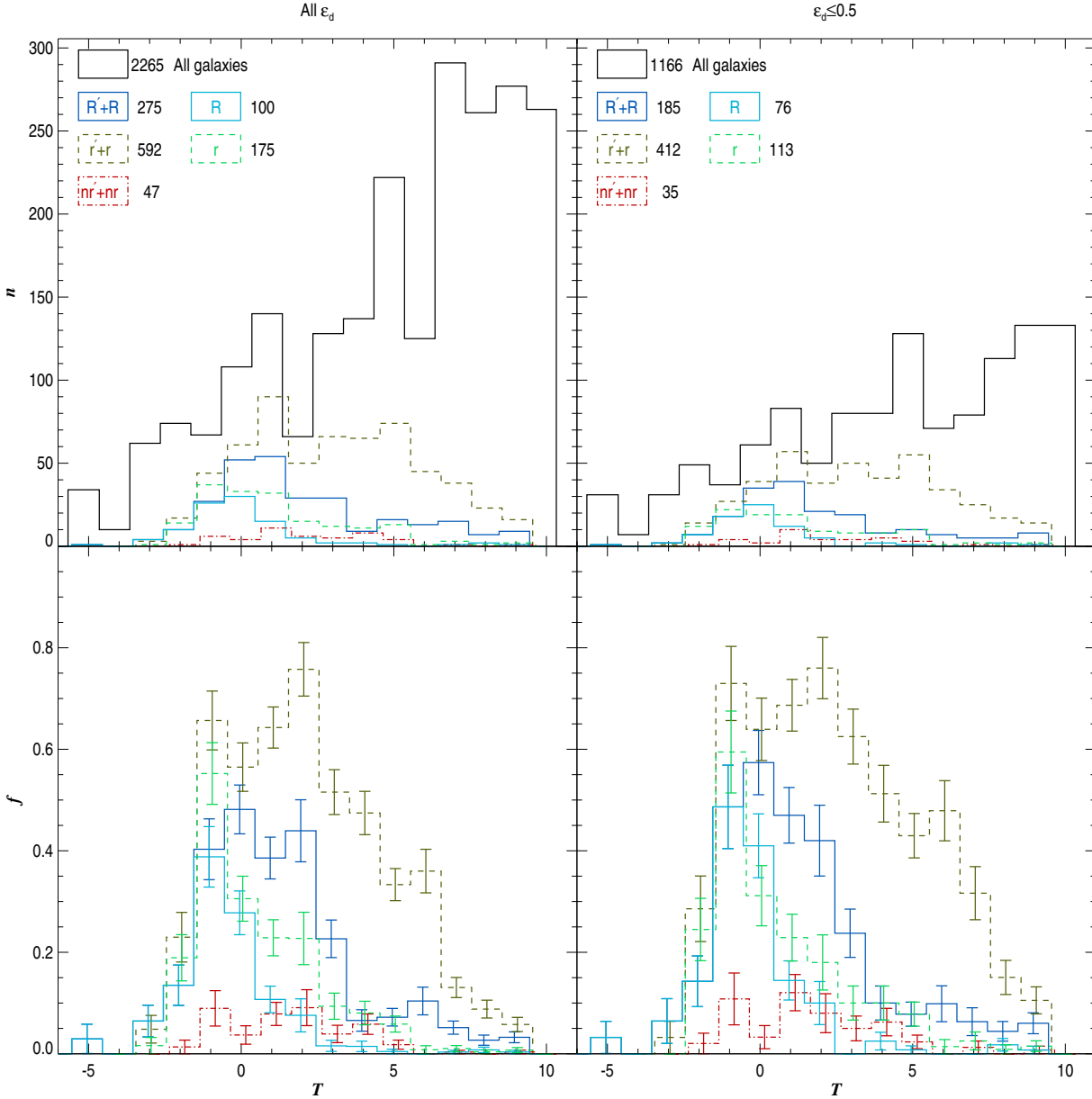


Fig. 18. Top panels: stage distribution of the S⁴G sample (black line), of galaxies hosting outer rings (continuous darker blue line), inner rings (dashed darker green line), and nuclear rings (dash-point red line). Lighter blue and green lines indicate histograms considering only galaxies hosting closed outer and closed inner rings, respectively. Bottom panels: fraction of galaxies with resonant features for a given stage colour-coded as in the two top panels. Left panels are for the whole sample and right panels for galaxies with a disc ellipticity $\epsilon_d \leq 0.5$. The numbers in the top panels indicate the number of galaxies included in the histograms that corresponds to the colour and line pattern of the adjacent box.

- They are mostly found at $-1 \leq T \leq 2$ where they appear in over 40% of galaxies. This number is similar to the $53 \pm 5\%$ fraction of outer features found in NIRS0S for stages $-1 \leq T \leq 1$ (Laurikainen et al. 2011).
- For $T \geq 4$ they are quite rare, and their frequency drops below 10%.
- Outer closed rings (continuous light blue lines) are most frequent for $T \leq 0$, with a peak frequency of $\sim 50\%$ at $T = -1$. Above $T = 0$ their frequency drops fast with increasing stage. This behaviour is also seen in NIRS0S.
- Outer closed rings and closed ring-lenses account for 100% of the outer features for $T \leq -1$. This is a difference with NIRS0S: the fraction of pseudorings for $T \leq 1$ NIRS0S

galaxies is non-zero, though still rather small, $19 \pm 7\%$. Of the five NIRS0S galaxies with $T \leq -1$ and with an outer pseudoring, two are included in the S⁴G sample. These two galaxies have been classified with the same stage in NIRS0S and Buta et al. (in preparation), which means that the difference between NIRS0S and ARRAKIS probably caused by the different appearance of outer features at different wavelengths and not by problems in the stage classification.

Buta & Combes (1996) found qualitatively similar results using RC3 data. Using data from VB80, Elmegreen et al. (1992) also found that earlier-type galaxies are more likely to have outer rings.

6.1.2. Inner rings

The stage distribution of inner rings based on the S⁴G subsample with $\epsilon_d \leq 0.5$ indicates the following (see also dashed green lines in Figure 18):

- They are found in $35 \pm 1\%$ of S⁴G galaxies.
- They have a frequency of over 40% for stages $-1 \leq T \leq 6$. The distribution is not very peaked and has its maximum for $-1 \leq T \leq 3$ (more than 60% of these galaxies have inner features).
- Their frequency drops below 20% for galaxies with $T \leq -3$ and $T \geq 8$. They are therefore very frequent in most disc galaxy stages.
- The peak in the inner closed ring frequency is found at $T = -1$ (light green lines) as also found in NIRSOS. The inner closed ring frequency distribution is shifted towards earlier types than that of the inner ring distribution.
- Inner closed rings are more frequent than inner pseudorings for $T \leq 1$. This agrees very well with the results in NIRSOS. There the fraction of inner features that are inner closed rings in galaxies with $-3 \leq T \leq -1$ is $75 \pm 7\%$, we found $81 \pm 6\%$. For galaxies with types $0 \leq T \leq 1$ NIRSOS reports a fraction of inner closed rings among inner features of $38 \pm 8\%$, we found $40 \pm 5\%$.

These results differ from those presented in Buta & Combes (1996), which were based on RC3 data. These authors found the inner closed ring fraction to be roughly constant for all types of disc galaxies with $T \leq 5$ (here the distribution is peaked at $T = -1$) and also that they are more frequent than pseudorings for $T \leq 3$ (here, this only occurs for $T \leq -1$). These differences are too large to be a consequence of the one stage shift caused by classifying galaxies in 3.6 μ m instead of the B band.

The stage distribution of outer and inner rings is quite different. While the outer ring distribution drops between types $T = 3$ and $T = 4$, the inner rings distribution does so between types $T = 7$ and $T = 8$.

6.1.3. Nuclear rings

Nuclear rings (dash-point red lines in Figure 18) are found in galaxies with $-1 \leq T \leq 6$, which is similar to that obtained in AINUR ($-3 \leq T \leq 7$). However, the peak in the distribution ($T = 2$) does not coincide with those in AINUR ($T = -1$ and $T = 4$). These differences are probably not significant, because the number of nuclear rings here is a factor of three smaller than in AINUR.

In AINUR nuclear rings were found in $\sim 20\%$ of galaxies with stages $-3 \leq T \leq 7$. A similar fraction was given by Knapen (2005). However, the fraction of low inclination ($\epsilon_d \leq 0.5$) S⁴G galaxies that host nuclear rings is $5 \pm 1\%$ in the same range of stages. The reason for the discrepancy is that, because of angular resolution problems, many of the smaller rings are undetected or are classified as nuclear lenses in the S⁴G.

6.2. Fraction of rings as a function of the galaxy family

Of the 2348 S⁴G galaxies that have been classified in Buta et al. (in preparation), 1725 are disc galaxies ($-3 \leq T \leq 9$) to which a family has been assigned (SA, SAB, SAB, SAB, SB). Some disc galaxies (233) have no assigned family and are mostly close to edge-on galaxies without obvious signatures of edge-on bars such as boxy inner isophotes. The ring distribution with family is shown in Figure 19.

6.2.1. Outer rings

The fraction of galaxies with $\epsilon_d \leq 0.5$ that host outer rings (blue continuous lines in Figure 19) increases steadily from SA ($15 \pm 2\%$) to SAB ($32 \pm 7\%$). For stronger bars (SB), it drops to $20 \pm 2\%$.

The distribution of outer closed rings (light blue continuous lines) is qualitatively similar: the fraction of galaxies that host closed rings rises from $7 \pm 2\%$ to $20 \pm 6\%$ between SA and SAB and then drops down to $5 \pm 1\%$ for the SB family.

6.2.2. Inner rings

The inner ring family distribution is quite different from that for the outer rings (green dashed lines in Figure 19). The fraction of galaxies that host inner rings remains roughly constant from SA to SAB at a level of $\sim 40\%$ and then suddenly increases to $64 \pm 7\%$ for SAB galaxies. The fraction of SB galaxies that host inner rings is similar to that in SA to SAB galaxies.

We also find that galaxies with no bars or weak bars (SA and SAB) have a higher fraction of inner closed rings (light green dashed lines) than galaxies with stronger bars.

6.2.3. Nuclear rings

The number of nuclear rings in ARRAKIS is small and thus the validity of the statistics is uncertain. However, we can see that the nuclear feature fraction increases from families SA to SAB and then remains roughly constant (dash-point red lines in Figure 19).

6.3. Ring shapes

6.3.1. Projected ring shapes

The top-left panel in Figure 20 shows the projected axis ratio of resonance rings, under the assumption that they can be described by an ellipse coplanar with the disc of the galaxy. It is qualitatively similar to that found in the CSRG (top panels of its Figure 7): the distribution grows gently from zero and has a maximum for quite round rings ($0.8 < q_r \leq 0.9$ for inner and outer rings here and $0.7 < q_r \leq 0.8$ in the CSRG). It then drops abruptly for even rounder rings.

The statistical expectation is that if rings were intrinsically circular and sitting in perfectly circular discs, with their rotation axis with random orientations, the projected ring axis ratio probability density function would be uniform. As explained in the CSRG, the reason to justify the lack of rings with a low apparent axis ratio is that they become increasingly harder to identify in inclined galaxies. It is interesting to see that just like in the CSRG, for the axis ratios close to $q_r = 0$, outer rings show a behaviour closer to the statistical expectation than inner rings. This is because they are found in outer parts of the galaxy that are less messy and easier to interpret than inner regions when seen close to edge-on. We do not observe the distribution to be uniform near $q_r = 1$ because there is a dip in the observed distribution of rings. The reason why we do not see more rings that appear nearly round in projection is that they are not intrinsically circular, as described in the next subsection.

6.3.2. Deprojected ring shapes

One of the improvements of this study over the largest systematic study of rings conducted so far, the CSRG, is that the S⁴G

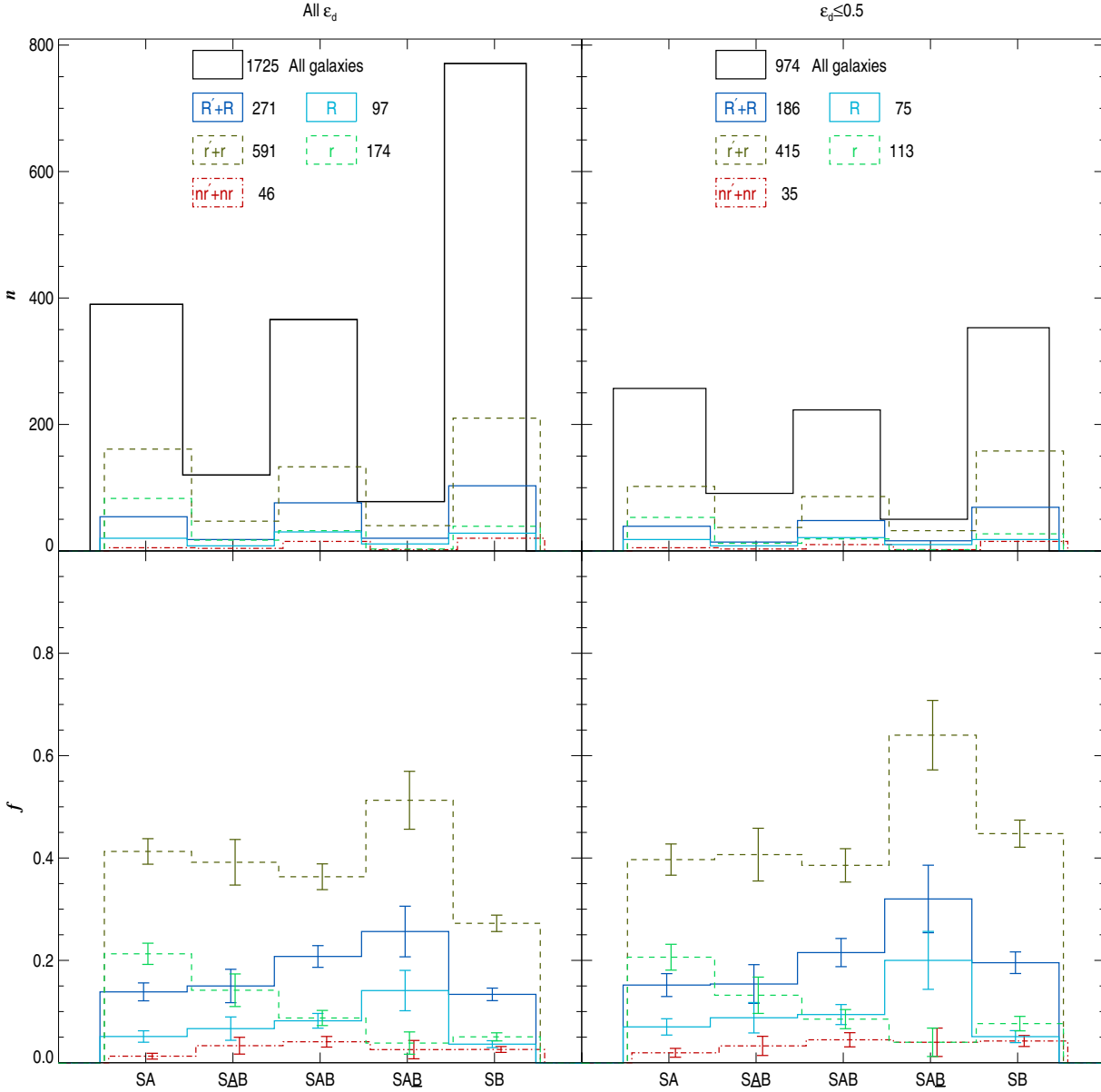


Fig. 19. Top panels: family distribution of the S⁴G sample and ringed galaxies colour- and line-coded as in Figure 18. Bottom panels: fraction of galaxies with rings for a given family colour- and line-coded as in the two top panels. Left panels are for the whole sample and right panels for galaxies with a disc ellipticity $\epsilon_d \leq 0.5$. The numbers in the top panels indicate the number of galaxies included in the histogram that corresponds to the colour- and line pattern of the adjacent box.

P4 provides us with reliable orientations of the galaxies. This allows us to obtain intrinsic ring shapes and orientations, as explained in Section 4.4.

In the CSRG, the deprojected ring axis ratio distribution was studied under several assumptions and using a statistical treatment. One of the assumptions was that the actual shape of the deprojected axis ratio distribution is Gaussian, with a peak at $\langle q_{r,0} \rangle$ and a dispersion σ . With our deprojected data we do not need this assumption.

The deprojected ring distribution is shown in the bottom panels of Figure 20. We overlay Gaussian fits to show how well the Gaussian distribution hypothesis works. The parameters of the Gaussian fits in this section can be found in Table 3. Although the fitted Gaussians are nearly the same when fitting rings in all galaxies and when fitting them only for galaxies with $\epsilon_d \leq 0.5$,

the distributions are slightly different in the low- q_r wing; indeed, when considering all galaxies, the left wing for outer and inner rings extends farther than when considering only galaxies with $\epsilon_d \leq 0.5$. This is because for close to edge-on galaxies deprojections based on the shape of outer isophotes of discs become unreliable due to the non-zero thickness of discs (see Section 4.6) and/or the presence of extended bulges and haloes. Thus, for some galaxies, the obtained deprojection parameters can be considered to be tentative at best and may cause the calculated deprojected ring shapes to be unrealistically stretched. A notorious case is NGC 4594 (the Sombrero galaxy), where outer isophotes have an ellipticity of about $\epsilon_d = 0.58$ even though the real figure is probably closer to $\epsilon_d = 0.83$ (see, e.g., Jardel et al. 2011). All but one ring with deprojected axis ratio $q_{r,0} \leq 0.4$ are found in galaxies with fitted disc ellipticity $\epsilon_d > 0.5$ (IC 5264, NGC 4594,

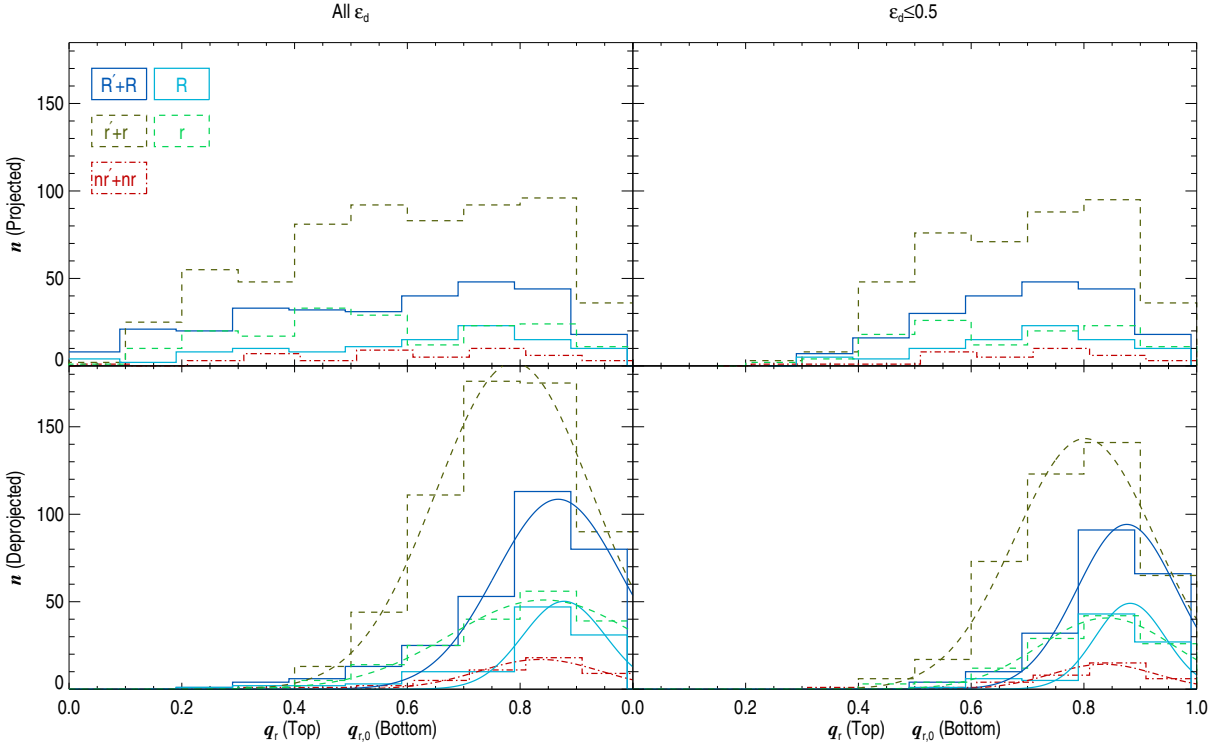


Fig. 20. Distribution of the resonance ring axis ratios colour- and line-coded as in Figure 18. The left-hand plots are for the whole ARRAKIS sample and the right-hand plots correspond to rings in host galaxies with $\epsilon_d \leq 0.5$. The top-row plots show the distribution of projected axis ratios, the bottom row shows the distribution of deprojected ones.

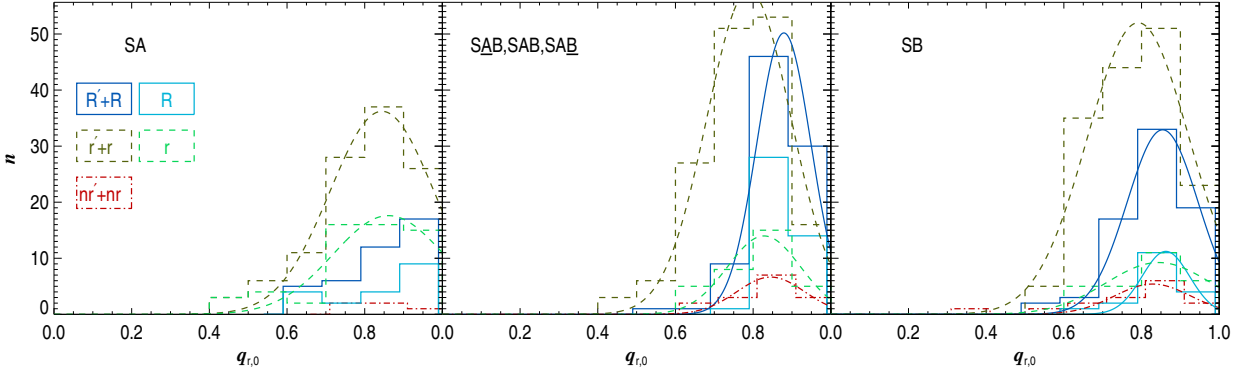


Fig. 21. Distribution of the resonance ring deprojected axis ratios colour- and line-coded as in Figure 18 for different galaxy families and for $\epsilon_d \leq 0.5$. The left panel shows SA galaxies, the middle one SAB to SAB galaxies, the right panel SB galaxies.

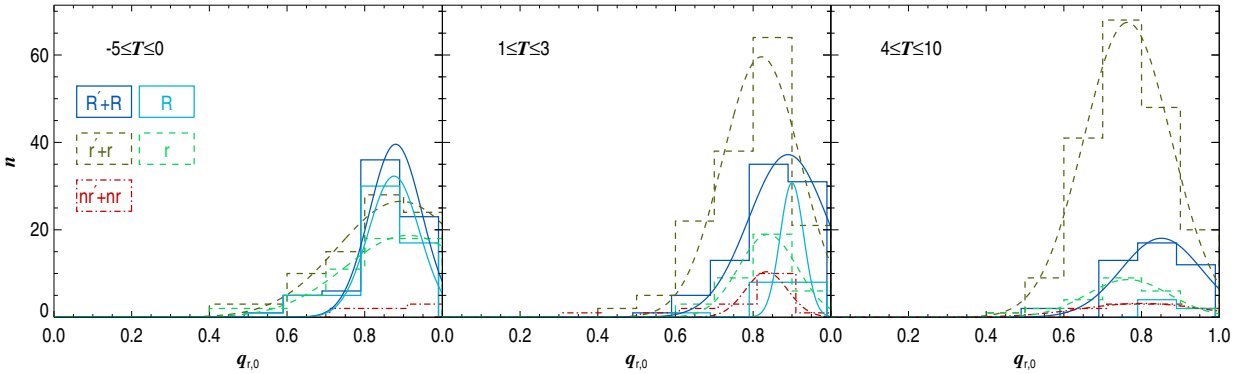


Fig. 22. Distribution of the resonance ring deprojected axis ratios colour- and line-coded as in Figure 18 for different galaxy stage ranges and for $\epsilon_d \leq 0.5$. The left panel represents galaxies with $-5 \leq T \leq 0$, the middle panel galaxies with $1 \leq T \leq 3$, the right panel galaxies with $4 \leq T \leq 10$.

Table 3. Number of galaxies in the histograms in Figures 20, 21, and 22 and parameters of the Gaussian fits to the $q_{r,0}$ distributions

Galaxy subsample	Feature type	n	$\langle q_{r,0} \rangle$	σ
All galaxies	Outer rings	295	0.87 (0.01)	0.11 (0.01)
	Inner rings	610	0.79 (0.00)	0.14 (0.00)
	Nuclear rings	47	0.84 (0.01)	0.11 (0.01)
	Outer closed rings	106	0.88 (0.01)	0.07 (0.01)
	Inner closed rings	180	0.84 (0.02)	0.17 (0.02)
$\epsilon_d \leq 0.5$	Outer rings	203	0.88 (0.01)	0.09 (0.01)
	Inner rings	425	0.80 (0.01)	0.12 (0.01)
	Nuclear rings	35	0.84 (0.01)	0.09 (0.01)
	Outer closed rings	82	0.88 (0.01)	0.06 (0.01)
	Inner closed rings	116	0.84 (0.01)	0.12 (0.01)
$\epsilon_d \leq 0.5$	Outer rings	40	–	–
	Inner rings	111	0.84 (0.01)	0.13 (0.01)
	Nuclear rings	5	–	–
SA	Outer closed rings	19	–	–
	Inner closed rings	56	0.86 (0.04)	0.14 (0.04)
	Outer rings	87	0.88 (0.00)	0.07 (0.00)
$\epsilon_d \leq 0.5$	Inner rings	156	0.79 (0.01)	0.11 (0.01)
	Nuclear rings	15	0.85 (0.03)	0.09 (0.03)
	Outer closed rings	43	–	–
<u>SAB,SAB,SAB</u>	Inner closed rings	33	0.83 (0.03)	0.09 (0.03)
	Outer rings	74	0.85 (0.00)	0.09 (0.00)
$\epsilon_d \leq 0.5$	Inner rings	158	0.79 (0.02)	0.13 (0.02)
	Nuclear rings	15	0.83 (0.02)	0.10 (0.02)
	Outer closed rings	18	0.86 (0.01)	0.06 (0.01)
SB	Inner closed rings	27	0.84 (0.06)	0.14 (0.07)
	Outer rings	71	0.88 (0.01)	0.07 (0.01)
$\epsilon_d \leq 0.5$	Inner rings	83	0.89 (0.03)	0.16 (0.03)
	Nuclear rings	7	–	–
	Outer closed rings	58	0.88 (0.01)	0.07 (0.01)
$-5 \leq T \leq 0$	Inner closed rings	56	0.91 (0.02)	0.16 (0.02)
	Outer rings	85	0.89 (0.01)	0.10 (0.01)
	Inner rings	152	0.82 (0.02)	0.10 (0.02)
$1 \leq T \leq 3$	Nuclear rings	18	0.83 (0.01)	0.05 (0.01)
	Outer closed rings	17	0.90 (0.00)	0.03 (2.97)
	Inner closed rings	37	0.84 (0.01)	0.08 (0.01)
$\epsilon_d \leq 0.5$	Outer rings	44	0.85 (0.02)	0.10 (0.02)
	Inner rings	187	0.76 (0.00)	0.11 (0.00)
	Nuclear rings	10	0.80 (0.00)	0.16 (0.00)
$4 \leq T \leq 10$	Outer closed rings	6	–	–
	Inner closed rings	24	0.77 (0.01)	0.11 (0.01)

Notes. $\langle q_{r,0} \rangle$ stands for the fitted centre of the Gaussian distribution and σ for its width. The numbers in brackets indicate 1-sigma errors of the fits.

NGC 5078, NGC 5746, NGC 5777, and NGC 5900). The exception is NGC 986, a galaxy with $\epsilon_d = 0.1$ and a peculiar elongated nuclear ring. Because this effect may also occur (although in a less obvious way) in other inclined galaxies, we continue our analysis of intrinsic ring shapes based only on galaxies with $\epsilon_d \leq 0.5$.

Based on the fitted $\langle q_{r,0} \rangle$, we find that outer rings are generally rounder than the inner ones. More specifically, for the ARRAKIS sample we find $\langle q_{r,0}(\text{O}) \rangle = 0.88$ and $\langle q_{r,0}(\text{I}) \rangle = 0.80$, respectively. Outer closed rings have the same average $\langle q_{r,0}(\text{O}) \rangle$ as outer features in general, but inner closed rings are on average slightly rounder than the average for inner features.

Rings become systematically more elliptical when moving along the family sequence from SA to SB (Figure 21). However, the dispersion in each of the Gaussian distributions is always wide enough to allow very round rings to exist, even for SB galaxies. Fits for outer rings in SA galaxies are not shown because they yield that the centre of the Gaussian would be located at $\langle q_{r,0}(\text{O}) \rangle > 1$.

Inner rings tend to become more elliptical with increasing galaxy stage. This trend is not found for the outer features, although this might be explained by the low number of them found at stages $T \geq 4$.

6.4. Ring orientations

In this subsection we describe the orientations of the rings with respect to bars. We focus only on barred galaxies for which we are able to accurately measure their orientation (that is, most of those in galaxies with $\epsilon_d \leq 0.5$). We compared the PA of the major axis of the ring, PA_r , and the bar, PA_b . We denote the difference between those major axis as $\text{PA}_r - \text{PA}_b$. However, because we define it to be in the first quadrant, it should be formally written as $\text{minimum}(|\text{PA}_r - \text{PA}_b|, |\text{PA}_b - \text{PA}_r|)$. Since PA_r is ill-defined for rings that are almost round in projection, we only studied features with a projected axis ratio $q_r \leq 0.85$.

Because for deprojected rings and bars the concept of PA is no longer applicable, we defined the deprojected orientation of a ring or a bar to be the counter-clockwise difference in angle

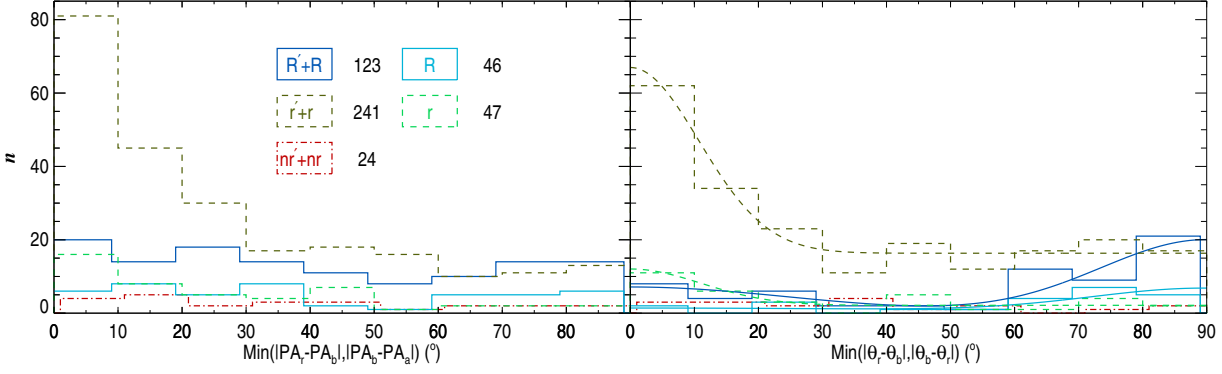


Fig. 23. Distribution of the projected resonance ring PA differences with respect to the bar (left panel) and ring orientation with respect to the bar in the deprojected galaxies (right panel). The histograms are colour- and line-coded as in Figure 18. The plots only include rings with $q_r \leq 0.85$ (left panel) and $q_{r,0} \leq 0.85$ (right panel) and in host galaxies with $\epsilon_d \leq 0.5$. The numbers in the top-left panel indicate the number of galaxies included in the histogram corresponding to the colour of the adjacent box.

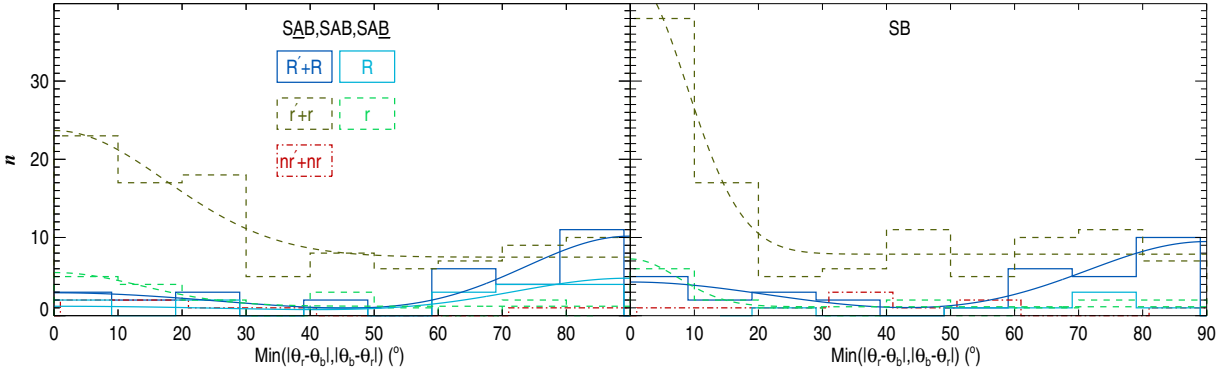


Fig. 24. Distribution of the resonance ring deprojected major axis angle difference with the bar colour- and line-coded as in Figure 18 for different galaxy families and for $\epsilon_d \leq 0.5$. The left panel is for SAB to SAB galaxies, the right panel for SB galaxies. The plots only include rings with $q_{r,0} \leq 0.85$.

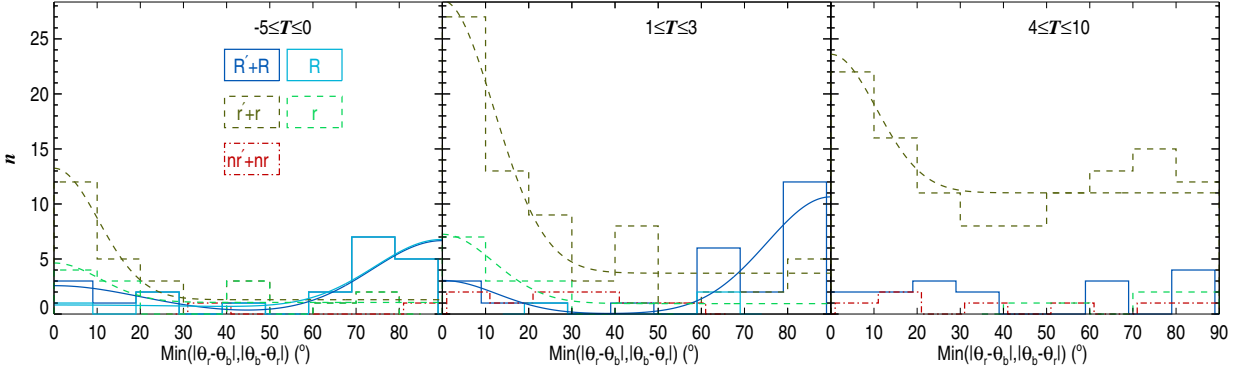


Fig. 25. Distribution of the resonance ring deprojected major axis angle difference with the bar colour- and line-coded as in Figure 18 for different galaxy stage ranges and for $\epsilon_d \leq 0.5$. The left panel represents galaxies with $-5 \leq T \leq 0$, the middle panel galaxies with $1 \leq T \leq 3$, the right panel galaxies with $4 \leq T \leq 10$. The plots only include rings with $q_{r,0} \leq 0.85$.

between the orientation of its major axis and the line of nodes, θ_r and θ_b . Thus, for deprojected galaxies we denote the orientation difference between a ring and the bar as $\theta_r - \theta_b$ [although it is defined as minimum $(|\theta_r - \theta_b|, |\theta_b - \theta_r|)$]. Because θ_r is ill-defined for rings that are almost round in deprojection, we only studied features with a deprojected axis ratio $q_{r,0} \leq 0.85$. In Figure 23 we present the distributions of $\text{PA}_r - \text{PA}_b$ and $\theta_r - \theta_b$.

For the outer rings $\text{PA}_r(\text{O}) - \text{PA}_b$ there is some hint that the distribution has two mild peaks at $\text{PA}_r(\text{O}) - \text{PA}_b = 0^\circ$ and

$\text{PA}_r(\text{O}) - \text{PA}_b = 90^\circ$ divided by a shallow valley. This behaviour is similar to that found in the CSRG, although there the peak at $\text{PA}_r(\text{O}) - \text{PA}_b = 0^\circ$ has more contrast; this may be due to our relatively low number of outer features (our plot has five times fewer objects than Figure 7g in the CSRG).

The distribution for inner rings has a large peak at $\text{PA}_r(\text{I}) - \text{PA}_b = 0^\circ$ and the distribution drops until it stabilises between $\text{PA}_r(\text{I}) - \text{PA}_b = 50^\circ$ and $\text{PA}_r(\text{I}) - \text{PA}_b = 90^\circ$.

Table 4. Number of galaxies in the histograms in Figures 23, 24, and 25 and parameters of the Gaussian fits to the $q_{r,0}$ distributions

Galaxy subsample	Feature type	n	σ_{0° ($^\circ$)	w_{0°	σ_{90° ($^\circ$)	w_{90°	w_c
$\epsilon_d \leq 0.5$	Outer rings	65	25 (3)	0.35 (0.18)	17 (2)	0.65 (0.39)	–
	Inner rings	215	11 (1)	0.48 (0.12)	–	–	0.52 (0.10)
	Nuclear rings	18	–	–	–	–	–
Barred	Outer closed rings	23	53 (4)	0.39 (0.11)	18 (1)	0.61 (0.20)	–
	Inner closed rings	33	11 (1)	0.59 (0.18)	–	–	0.41 (0.16)
$\epsilon_d \leq 0.5$	Outer rings	31	27 (2)	0.32 (0.08)	16 (1)	0.68 (0.19)	–
	Inner rings	103	17 (1)	0.51 (0.11)	–	–	0.49 (0.09)
	Nuclear rings	8	–	–	–	–	–
<u>SAB,SAB,SAB</u>	Outer closed rings	16	37 (8)	0.34 (0.27)	18 (1)	0.66 (0.59)	–
	Inner closed rings	17	14 (1)	0.58 (0.27)	–	–	0.42 (0.30)
$\epsilon_d \leq 0.5$	Outer rings	34	22 (2)	0.35 (0.17)	19 (1)	0.65 (0.44)	–
	Inner rings	110	9 (1)	0.53 (0.18)	–	–	0.47 (0.15)
	Nuclear rings	10	–	–	–	–	–
SB	Outer closed rings	7	–	–	–	–	–
	Inner closed rings	16	7 (1)	0.53 (0.17)	–	–	0.47 (0.22)
$\epsilon_d \leq 0.5$	Outer rings	21	20 (1)	0.32 (0.11)	16 (0)	0.68 (0.36)	–
	Inner rings	26	10 (1)	0.72 (0.41)	–	–	0.28 (0.28)
	Nuclear rings	2	–	–	–	–	–
$-5 \leq T \leq 0$	Outer closed rings	18	60 (8)	0.33 (0.15)	16 (1)	0.67 (0.31)	–
	Inner closed rings	13	11 (2)	0.50 (0.35)	–	–	0.50 (0.50)
$\epsilon_d \leq 0.5$	Outer rings	26	13 (0)	0.19 (0.03)	15 (0)	0.81 (0.21)	–
	Inner rings	70	12 (2)	0.69 (0.33)	–	–	0.31 (0.20)
	Nuclear rings	9	–	–	–	–	–
$1 \leq T \leq 3$	Outer closed rings	3	–	–	–	–	–
	Inner closed rings	14	12 (1)	0.69 (0.18)	–	–	0.31 (0.16)
$\epsilon_d \leq 0.5$	Outer rings	16	–	–	–	–	–
	Inner rings	116	11 (1)	0.25 (0.06)	–	–	0.75 (0.10)
	Nuclear rings	7	–	–	–	–	–
$4 \leq T \leq 10$	Outer closed rings	0	–	–	–	–	–
	Inner closed rings	6	–	–	–	–	–

Notes. σ_{0° and σ_{90° stand for the fitted widths of the Gaussian components set to be centred at $\theta_r - \theta_b = 0^\circ$ and $\theta_r - \theta_b = 90^\circ$. w_{0° , w_{90° , and w_c stand for the fitted fraction of rings found to be in one of the two Gaussian components and that in the component of rings randomly orientated with respect to the bar. The numbers in brackets indicate 1-sigma errors of the fit.

In deprojected galaxies, the outer rings have two preferred orientations, namely parallel and perpendicular to bars [$\theta_r(O) - \theta_b = 0^\circ$ and $\theta_r(O) - \theta_b = 90^\circ$], which can be associated with the R_2 and R_1 ring types in the simulations of Schwarz (1981, 1984) as well as with the predictions from non-deprojected data in the CSRG.

The intrinsic inner ring orientation distribution has a clear peak parallel to the bar [$\theta_r(I) - \theta_b = 0^\circ$], as was previously hinted at in other works (e.g., the CSRG, de Vaucouleurs et al. 1964; Schwarz 1981, 1984; Buta 1986b; Athanassoula et al. 2009b). However, we also found that a significant fraction of rings have random orientations with respect to the bar, as indicated by the flat distribution for $\theta_r(I) - \theta_b > 30^\circ$. Such a randomly oriented inner ring fraction, although sometimes suspected on the basis of a few individual cases of obvious bar/ring misalignment [ESO 565-11 (Buta et al. 1995), NGC 309 (Buta et al. 2007), NGC 4319 (Sulentic & Arp 1987), and NGC 6300 (Buta 1987)] has never been described before.

We fitted the outer ring $\theta_r(O) - \theta_b$ distribution with the superposition of two Gaussian curves centred at $\theta_r(O) - \theta_b = 0^\circ$ and $\theta_r(O) - \theta_b = 90^\circ$, as assumed in the CSRG. For the inner rings, we fitted the superposition of a Gaussian centred at $\theta_r(I) - \theta_b = 0^\circ$, describing the population of inner features parallel to the bar and a constant distribution representing the population of rings oriented at random with respect to the bar. The fitted parameters and the number of galaxies in each histogram are tabulated in Table 4. The fit also provides the fraction of rings that belong to the components parallel and anti-parallel to the bar for outer

rings (w_{0° and w_{90°) and parallel and oriented at random with respect to the bar for inner rings (w_{0° and w_c). We found that the fraction of outer rings aligned parallel to the bar is $35 \pm 18\%$ and that of features oriented perpendicular to the bar is $65 \pm 39\%$. For inner rings, we found that some $48 \pm 12\%$ are aligned parallel to the bar and the other $52 \pm 10\%$ have random orientations.

The distribution of the intrinsic orientations of outer features does not change much when looking separately at weakly and strongly barred galaxies (Figure 24). The inner ring distribution changes more, since the width of the distribution of galaxies parallel to the bar decreases from $17 \pm 1^\circ$ for galaxies with families SAB to SAB to only $9 \pm 1^\circ$ for SB galaxies.

The outer ring orientation distribution is also independent of the galaxy stage (Figure 25). But again, this is not the case for the inner ring distribution. Indeed, the later the stage, the larger the fraction of inner rings oriented at random with respect to the bar. This fraction increases from $28 \pm 28\%$ ($-5 \leq T \leq 0$) and $31 \pm 20\%$ ($1 \leq T \leq 3$) to $75 \pm 10\%$ for galaxies with $4 \leq T \leq 10$. For inner rings in late-type stages there is even some hint of a preferred orientation perpendicular to the bar (right panel in Figure 25).

6.5. Absolute ring sizes

Absolute ring diameters were obtained using the average of the redshift-independent distances provided by NED as the host galaxy distance. If such a distance measurement was not available, we used the NED Hubble-Lemaître flow distance corrected for the effects of the Virgo cluster, the Great

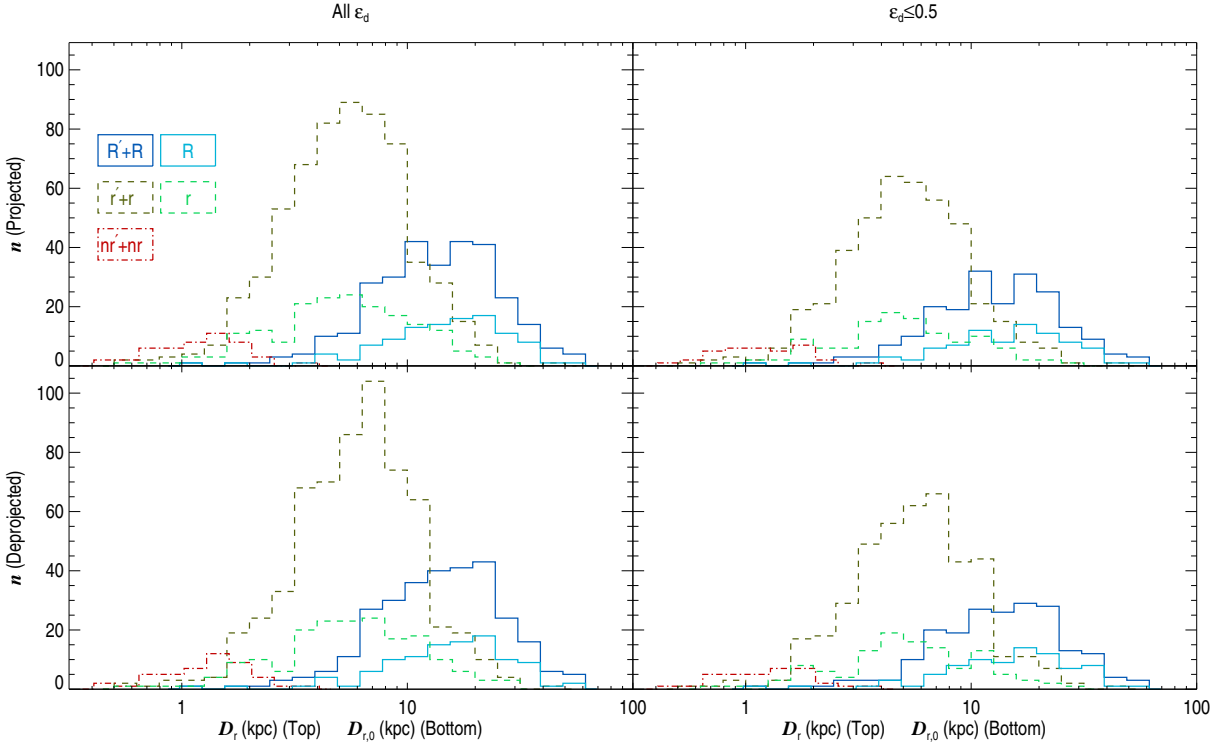


Fig. 26. Distribution of the resonance ring absolute diameters. The top row shows the projected diameters and the bottom row the deprojected ones. The left column shows all galaxies, the right column galaxies with $\epsilon_{dl} \leq 0.5$. The histograms are colour- and line-coded as in Figure 18.

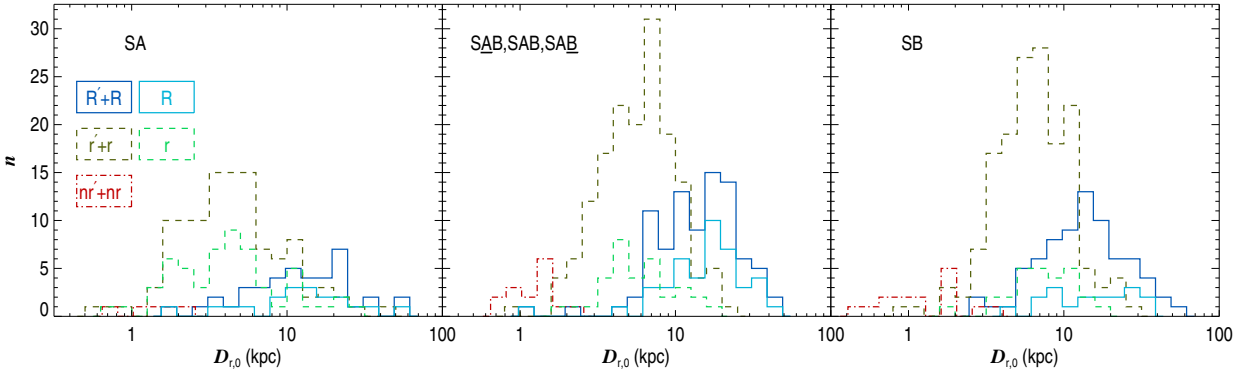


Fig. 27. Distribution of the resonance ring deprojected major axis absolute diameter colour- and line-coded as in Figure 18 for different galaxy families and for $\epsilon_{dl} \leq 0.5$. The left panel shows SA galaxies, the middle one SAB to SAB galaxies, the right panel SB galaxies.

Atractor, and the Shapley cluster (Hubble-Lemaître constant $H_0 = 73 \text{ km s}^{-1} \text{ Mpc}^{-1}$). Because the S^4G sample selection was based on uncorrected flow distances, this means that some of the galaxy distances listed in Appendix A exceed 41 Mpc. Of these galaxies with rings, only six are farther away than 60 Mpc (ESO 576-1, NGC 4722, NGC 5600, PGC 47721, and UGC 5814). Such high distances might indicate either inaccurate redshift-based or redshift-independent distance determinations. However, since these galaxies are only a few, we did not exclude them from the study of absolute ring sizes.

Here, we define the size of a ring to be its major axis diameter. That is, D_r in the projected case and $D_{r,0}$ in the deprojected case. Because rings are in general almost circular, their absolute size distribution does not vary much when comparing the projected and the deprojected sizes (Figure 26). Moreover, because

the ring size is easier to measure than its orientation, the size distribution does not vary much when studying our whole sample or a subsample restricted by disc ellipticity. The averages and the standard deviations of each deprojected distribution in the plots are listed in Table 5.

The average absolute size for each of the three ring flavours is nearly independent of galaxy family (Figure 27 and Table 5). It is noteworthy that the dispersion in the size of inner rings in SA galaxies is higher than that in barred galaxies. This high dispersion can also be seen by examining the smallest and largest rings in the top panel in Figure 27; the smallest resonance feature in SA galaxies is an inner pseudoring. This is also the case for the third-largest feature in this panel. Such a behaviour is not seen in barred galaxies, where the small- and large-size tails are dominated by nuclear and outer rings, respectively. A possible

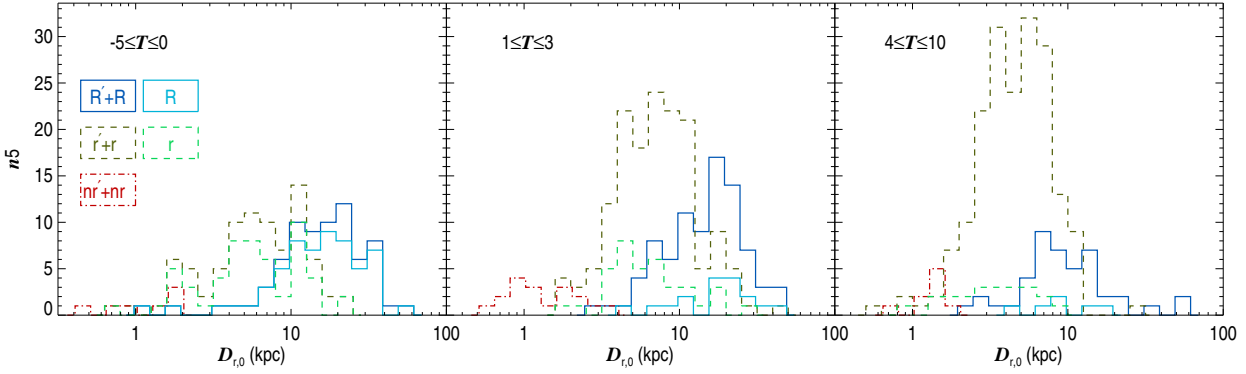


Fig. 28. Distribution of the resonance ring deprojected major axis absolute diameter colour- and line-coded as in Figure 18 for different galaxy stage ranges and for $\epsilon_d \leq 0.5$. The left panel represents galaxies with $-5 \leq T \leq 0$ galaxies, the middle panel galaxies with $1 \leq T \leq 3$, the right panel galaxies with $4 \leq T \leq 10$.

explanation of this high dispersion in the size of inner features found in SA galaxies is that a fraction of outer and nuclear resonant features have been misclassified as inner rings.

Outer and inner rings in galaxies with stages $4 \leq T \leq 10$ are on average much smaller than those found in earlier stages (Figure 28). This effect is not seen for nuclear features, but this may well be because some of them are too small to be resolved in the S⁴G.

6.6. Ring sizes relative to the size of the galaxy

One of the outputs of the S⁴G pipeline 3 (Muñoz-Mateos et al., in preparation) is the diameter at the $\mu_{3.6\mu\text{m}} = 25.5$ mag arcsec⁻² level, $D_{25.5}$. This diameter can be used as an indicator of the size of the disc, although in a few cases it may be overestimating its true size because of the effect of bright extended spheroidal components (an obvious case probably is the Sombrero galaxy). Since $D_{25.5}$ is located in the outskirts of the galaxy, in the region where its orientation is typically measured, it does not need to be deprojected. $D_{25.5}$ is available for all sample galaxies but two, NGC 253 and NGC 4647. For NGC 253 this is because the galaxy is tightly fitted in the S⁴G frame and the $D_{25.5}$ diameter is close to the limits of the frame or even beyond. For NGC 4647 this is because the galaxy isophotes are distorted because of a close galaxy in the same frame.

The distribution of projected and deprojected relative radii of the rings, $D_r/D_{25.5}$ and $D_{r,0}/D_{25.5}$, (Figure 29) shows that these magnitudes are much more useful than D_r and $D_{r,0}$ for separating the three flavours of resonance features. The overlap in radius of the different types of features is much smaller than that found when looking at absolute radii because distributions are much more peaked. Indeed, comparing Table 5 and Table 6 shows that for outer rings in galaxies with $\epsilon_d \leq 0.5$ the ratio between the peak value of the distribution and its dispersion is $[D_{r,0}(\text{O})/D_{25.5}]/\sigma[D_{r,0}(\text{O})/D_{25.5}] = 3.2$, which is almost twice higher than $D_{r,0}(\text{O})/\sigma[D_{r,0}(\text{O})] = 1.6$. For inner rings the values are $[D_{r,0}(\text{I})/D_{25.5}]/\sigma[D_{r,0}(\text{I})/D_{25.5}] = 2.2$ and $D_{r,0}(\text{I})/\sigma[D_{r,0}(\text{I})] = 1.5$.

This effect is not seen for nuclear rings; a reason may be that outer and inner rings are associated to a single resonance or manifold structure that is found at a given radius relative to the bar (with small variations due to the bar pattern speed and the galaxy rotation curve). Instead, nuclear rings are associated to the range of radii between the two ILRs, or to the range of radii between the centre and the ILR, in case of galaxies with

only one such resonance. A complementary explanation is that we are missing all nuclear features below a given angular size. If enough galaxies of a possible $D_{r,0}(\text{N})/D_{25.5}$ peak were smaller than that threshold, the scatter of the nuclear ring absolute size distribution would not be reduced by much when using the ring diameters normalised with $D_{25.5}$.

When segregating galaxies according to their family (Figure 30), we found a large overlap between the range of relative radii occupied by the inner and nuclear rings in SA galaxies. Such a large overlap is not seen in barred galaxies and may indicate, as commented before when looking at the absolute radii of rings, that some nuclear rings may have been classified as inner features in unbarred galaxies. We also found that the peak in the inner ring relative size distribution increases systematically with increasing bar strength. This is probably because of a slight tendency of stronger bars (SB) to be longer on average relative to galaxy size than weaker bars (SAB, SAB, SAB), at least for late-type galaxies. This was originally shown by Erwin (2005), based on the data of Martin (1995). Erwin (2005) used the RC3 R_{25} measurement as the galaxy size.

Finally, we find that the relative ring size distributions are not sensitive to galaxy stage (Figure 31).

6.7. Outer ring sizes relative to those of inner rings

Our sample contains 163 galaxies with both outer and inner features. We calculated the ratio of the major axis of these features, $D_{r,0}(\text{O})/D_{r,0}(\text{I})$. Our sample has 19 galaxies with outer and inner features that also have more than one outer ring and/or more than one inner ring. When that was the case, the average of the major axis diameters of the outer (inner) features was used as the diameter of the outer (inner) feature.

The resulting diameter ratio distribution is represented in Figure 32, colour- and line-coded according to different host galaxy families and stages. One galaxy, NGC 5033, has $D_{r,0}(\text{O})/D_{r,0}(\text{I}) = 17.5$ and is beyond the horizontal limits of the plots. This high ratio may indicate that the innermost resonance feature in this unbarred galaxy is a nuclear and not an inner ring. In fact, this innermost feature in NGC 5033 is classified as a nuclear ring in AINUR.

In Figure 32, the histograms for barred galaxies and those for stages $-5 \leq T \leq 3$ have a shape that can be roughly approximated by a Gaussian, therefore we fitted them with that function. Other histograms (SA galaxies and galaxies with stages $4 \leq T \leq 10$) have too few galaxies to be fitted. The histogram for

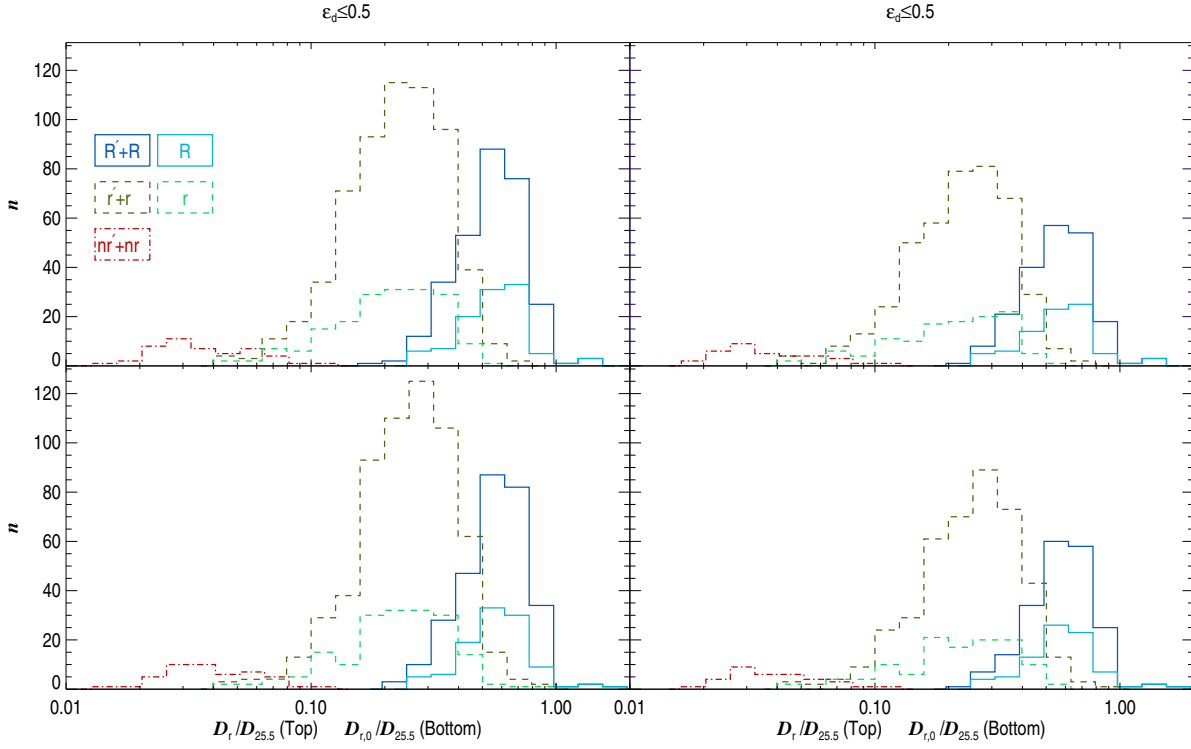


Fig. 29. Distribution of the resonance ring deprojected major axis diameters relative to $D_{25.5}$. The left column shows all galaxies, the right column galaxies with $\epsilon_d \leq 0.5$. The histograms are colour and line-coded as in Figure 18.

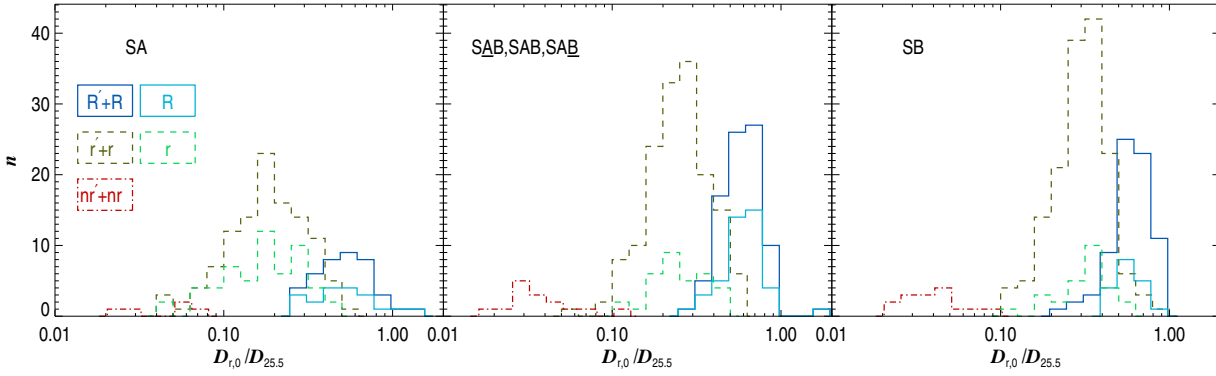


Fig. 30. Distribution of the resonance ring deprojected major axis relative to $D_{25.5}$ colour- and line-coded as in Figure 18 for different galaxy families and for $\epsilon_d \leq 0.5$. The left panel shows SA galaxies, the middle one $\underline{\text{SAB}}$ to $\underline{\text{SAB}}$ galaxies, the right panel SB galaxies.

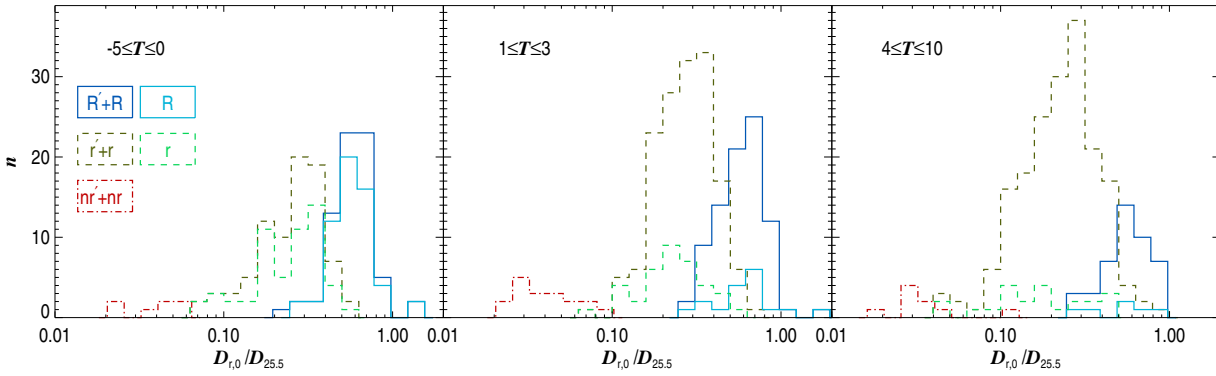


Fig. 31. Distribution of the resonance ring deprojected major axis diameter relative to $D_{25.5}$ colour and line-coded as in Figure 18 for different galaxy stage ranges and for $\epsilon_d \leq 0.5$. The left panel is for $-5 \leq T \leq 0$ galaxies, the middle panel is for $1 \leq T \leq 3$ galaxies, and the right panel is for $4 \leq T \leq 10$ galaxies.

Table 5. Number of galaxies in the histograms in Figures 26, 27, and 28 and average and standard deviation of the absolute ring deprojected diameters for several ARRAKIS subsamples

Galaxy subsample	Feature type	n	$\langle D_{r,0} \rangle$ (kpc)	$\sigma(D_{r,0})$ (kpc)
All galaxies	Outer rings	295	17.0	10.3
	Inner rings	610	7.1	4.7
	Nuclear rings	47	1.4	0.6
	Outer closed rings	106	18.1	10.2
	Inner closed rings	180	7.2	5.3
$\epsilon_d \leq 0.5$	Outer rings	203	16.5	10.3
	Inner rings	425	6.7	4.6
	Nuclear rings	35	1.4	0.6
	Outer closed rings	82	17.8	10.3
	Inner closed rings	116	6.7	4.9
$\epsilon_d \leq 0.5$	Outer rings	40	16.0	12.1
	Inner rings	111	6.0	5.9
	Nuclear rings	5	1.4	0.6
SA	Outer closed rings	19	16.5	12.7
	Inner closed rings	56	5.9	5.8
$\epsilon_d \leq 0.5$	Outer rings	87	16.4	9.1
	Inner rings	156	6.7	3.7
	Nuclear rings	15	1.3	0.4
<u>SAB,SAB,SAB</u>	Outer closed rings	43	18.0	9.4
	Inner closed rings	33	6.7	3.8
$\epsilon_d \leq 0.5$	Outer rings	74	16.5	10.8
	Inner rings	158	7.4	4.3
	Nuclear rings	15	1.4	0.8
SB	Outer closed rings	18	17.8	9.9
	Inner closed rings	27	8.2	3.7
$\epsilon_d \leq 0.5$	Outer rings	71	18.5	10.4
	Inner rings	83	7.3	4.6
	Nuclear rings	7	1.2	0.5
$-5 \leq T \leq 0$	Outer closed rings	58	17.9	10.5
	Inner closed rings	55	7.1	4.7
$\epsilon_d \leq 0.5$	Outer rings	85	17.0	9.4
	Inner rings	152	8.4	5.6
	Nuclear rings	18	1.4	0.8
$1 \leq T \leq 3$	Outer closed rings	17	20.2	10.6
	Inner closed rings	37	7.7	5.7
$\epsilon_d \leq 0.5$	Outer rings	44	12.5	11.2
	Inner rings	184	5.1	2.9
	Nuclear rings	9	1.3	0.3
$4 \leq T \leq 10$	Outer closed rings	6	10.7	5.2
	Inner closed rings	22	3.9	2.2

SA galaxies is very flat and has no distinct peak. The results of the fits and the number of galaxies included in each histogram, are listed in Table 7.

We found that $D_{r,0}(O)/D_{r,0}(I)$ is larger for weaker bars and also for earlier-type galaxies.

The peaks of the fitted distributions in Figure 32 are always about $D_{r,0}(O)/D_{r,0}(I) = 2$, which is consistent with the CSRG, Kormendy (1979), (Athanasoula et al. 1982), and (Buta 1986a).

7. Discussion

7.1. Why is the stage distribution of inner and outer resonance features different?

In Section 6.1 we found that the distribution of stages (morphological type) for inner and outer rings is significantly different. Indeed, the outer ring fraction is high (above 20%) for $-1 \leq T \leq 3$ before dropping at later stages, but the inner ring distribution only drops at $T = 6$ or $T = 7$ (see a schematic view of this in Table 8 where the stages with a frequency of rings one fourth that of the peak for that ring flavour are considered to rarely host rings). For stages below $T = 3$ outer rings are at

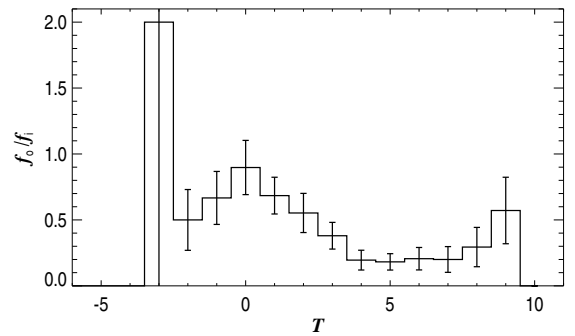


Fig. 33. Fraction of galaxies with $\epsilon_d \leq 0.5$ with outer rings divided by that with inner rings, as a function of the galaxy stage.

least 40% as abundant as inner rings, but this ratio decreases for later stages. Thus, there is a significant under-abundance of outer rings for late-type galaxies (Figure 33).

Table 6. Number of galaxies in the histograms in Figures 29, 30, and 31 and average and standard deviation of the ring deprojected diameters relative to $D_{25.5}$ for several ARRAKIS subsamples.

Galaxy subsample	Feature type	n	$\langle D_{r,0}/D_{25.5} \rangle$	$\sigma(D_{r,0}/D_{25.5})$
All galaxies	Outer rings	295	0.60	0.19
	Inner rings	608	0.27	0.12
	Nuclear rings	47	0.04	0.02
	Outer closed rings	106	0.63	0.22
	Inner closed rings	180	0.25	0.12
$\epsilon_d \leq 0.5$	Outer rings	203	0.62	0.20
	Inner rings	424	0.27	0.12
	Nuclear rings	35	0.04	0.02
	Outer closed rings	82	0.64	0.24
	Inner closed rings	116	0.24	0.11
$\epsilon_d \leq 0.5$	Outer rings	40	0.58	0.24
	Inner rings	111	0.20	0.10
	Nuclear rings	5	0.05	0.02
SA	Outer closed rings	19	0.60	0.30
	Inner closed rings	56	0.19	0.10
$\epsilon_d \leq 0.5$	Outer rings	87	0.63	0.19
	Inner rings	155	0.27	0.11
	Nuclear rings	15	0.04	0.02
	Outer closed rings	43	0.65	0.22
	Inner closed rings	33	0.26	0.09
$\epsilon_d \leq 0.5$	Outer rings	74	0.62	0.16
	Inner rings	158	0.32	0.12
	Nuclear rings	15	0.04	0.02
	Outer closed rings	18	0.60	0.14
	Inner closed rings	27	0.33	0.10
$\epsilon_d \leq 0.5$	Outer rings	71	0.62	0.20
	Inner rings	83	0.27	0.11
	Nuclear rings	7	0.04	0.01
	Outer closed rings	58	0.62	0.20
	Inner closed rings	55	0.26	0.11
$\epsilon_d \leq 0.5$	Outer rings	85	0.63	0.21
	Inner rings	152	0.29	0.11
	Nuclear rings	18	0.04	0.02
	Outer closed rings	17	0.70	0.33
	Inner closed rings	37	0.25	0.10
$\epsilon_d \leq 0.5$	Outer rings	44	0.60	0.18
	Inner rings	183	0.25	0.13
	Nuclear rings	9	0.04	0.02
	Outer closed rings	6	0.59	0.25
	Inner closed rings	22	0.20	0.13

Table 7. Number of galaxies in the histograms in Figure 32 and parameters of the Gaussian fits to the $D_{r,0}(O)/D_{r,0}(I)$ distributions

Galaxy inclinations	Subsample	n	$\langle D_{r,0}(O)/D_{r,0}(I) \rangle$	σ
All ϵ_d	SA	29	–	–
	<u>SAB,SAB,SAB</u>	75	2.22 (0.06)	0.45 (0.06)
	SB	59	1.97 (0.04)	0.37 (0.04)
	$-5 \leq T \leq 0$	52	2.20 (0.03)	0.29 (0.03)
	$1 \leq T \leq 3$	87	2.01 (0.03)	0.40 (0.03)
	$4 \leq T \leq 10$	23	–	–
$\epsilon_d \leq 0.5$	SA	22	–	–
	<u>SAB,SAB,SAB</u>	51	2.19 (0.08)	0.46 (0.08)
	SB	45	1.91 (0.04)	0.40 (0.05)
	$-5 \leq T \leq 0$	36	2.18 (0.05)	0.34 (0.06)
	$1 \leq T \leq 3$	63	1.97 (0.03)	0.36 (0.03)
	$4 \leq T \leq 10$	18	–	–

Notes. $\langle D_{r,0}(O)/D_{r,0}(I) \rangle$ stands for the fitted centre of the Gaussian distribution and σ for its width. The numbers in brackets indicate 1-sigma errors of the fits.

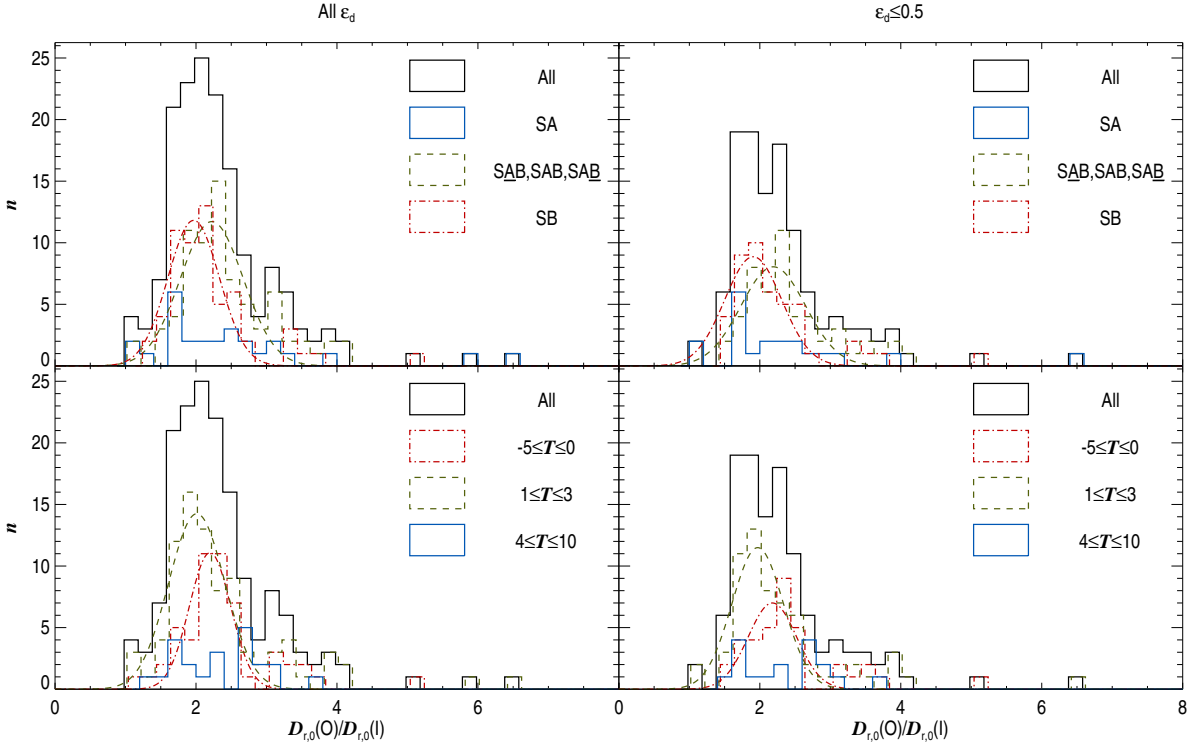


Fig. 32. Distribution of the ratios of the diameters of outer and inner rings. The left column shows all galaxies, the right column galaxies with $\epsilon_d \leq 0.5$. The of histograms are colour- and line-coded according to the host galaxy family (top panels) and stage (bottom panels). One galaxy, NGC 5033, has $D_{r,0}(O)/D_{r,0}(I) = 17.5$ and is beyond the horizontal limits of the plots.

Table 8. Simplified behaviour of the probability of finding outer and inner rings for different galaxy stage ranges

		$-5 \leq T \leq -2$	$-1 \leq T \leq 3$	$4 \leq T \leq 7$	$8 \leq T \leq 10$
Can one frequently find...?	Outer rings	NO	YES	NO	NO
	Inner rings	NO	YES	YES	NO

A possible justification for this effect can be found in the simulations by Combes & Elmegreen (1993), who compared models designed to mimic both early- and late-type spirals distinguished by steeply and slowly rising inner rotation curves, respectively. However, to what extent their galaxy models are realistic is a matter of debate, since their $t = 0$ models were sharply truncated at a radius of only a few disc scale-lengths (as little as 1.5 scale-lengths in some cases). Therefore, any explanation based on these simulations has to be taken with some caution. Combes & Elmegreen (1993) found that for early-type galaxies the CR radius is well inside the optical disc of the galaxy, but for later-type galaxies the CR is moved farther out. As a consequence, for a late-type galaxy, the OLR radius is typically found in a low-density region, and very little material is rearranged into a ring shape. Eventually, an outer feature forms when particles near the CR obtain angular momentum and are moved outwards, but this is a secular process that is even slower in late-type galaxies because regions near the CR have a lower particle density than that in earlier-type galaxies. Our results show that for this particular problem, the transition between an early- and a late-type disc galaxy is at $T = 3$. The connection discussed here between simulations and observational data was previously made by Combes & Elmegreen (1993).

7.2. Why is the family distribution of inner and outer resonance features different?

In Section 6.2 we showed that the outer and inner ring distributions differ in the range of families from SA to SAB. In that range, the fraction of galaxies that host inner rings is constant within the error bars, but that of galaxies that host outer features increases steadily ($15 \pm 2\%$ for SA galaxies, $15 \pm 4\%$ for $\overline{\text{SAB}}$ galaxies, and $22 \pm 3\%$ for SAB galaxies). A straightforward explanation for this effect is that outer rings do not form easily in unbarred galaxies. Indeed, weaker bars are likely to be less effective at redistributing material and angular momentum. It is therefore reasonable to assume that some have not yet had time to bring enough material from the CR region to the OR and, as a consequence, there is not enough material there to build an outer ring.

7.3. Rings in unbarred galaxies

Based on the information in Figure 19 we found that $15 \pm 2\%$ of SA galaxies have an outer ring. This fraction increases to $21 \pm 2\%$ for galaxies with bars ($\overline{\text{SAB}}$, SAB, $\overline{\text{SAB}}$, SB). For inner rings the values are $40 \pm 3\%$ and $44 \pm 2\%$, respectively.

In the range $-1 \leq T \leq 3$, which is where outer features are frequently found according to Table 8, outer rings are found in $29 \pm 5\%$ of the SA galaxies and in $49 \pm 3\%$ of the barred galaxies. In the range $-1 \leq T \leq 7$, where most inner features are found,

the fraction of SA galaxies with inner rings is $46 \pm 4\%$ and that of barred ones hosting them is $59 \pm 2\%$.

These numbers indicate that outer rings are 1.7 times more frequent in the SAB to SB families than in the SA family. For inner rings the fraction in barred galaxies is only larger by a factor of about 1.3 than that in SA galaxies.

Our results are again mostly similar to those that can be obtained from the NIRSOS galaxy classifications (Laurikainen et al. 2011), which include disc galaxies in the range of stages $-3 \leq T \leq 1$. For outer features, we (they) found that the fraction of SA galaxies hosting them is $27 \pm 5\%$ ($15 \pm 5\%$) and that the fraction of barred galaxies hosting them is $49 \pm 4\%$ ($47 \pm 5\%$). For inner features in that range of stages, we (they) found that the fraction of SA galaxies hosting them is $51 \pm 5\%$ ($24 \pm 6\%$) and that the fraction of barred galaxies hosting them is $60 \pm 4\%$ ($56 \pm 5\%$). The NIRSOS statistics were calculated here excluding the galaxies labelled as spindle in Laurikainen et al. (2011) and ours were calculated with galaxies with $\epsilon_d \leq 0.5$.

The fact that outer features are more sensitive to the presence of a bar than inner features fits naturally with a scenario in which the rings in SA galaxies have formed due to broad oval distortions or long-lasting spiral modes (Rautiainen & Salo 2000) or with a model in which bars have been destroyed or dissolved after forming the rings. In the first case, simulations show that outer resonance features take longer to form than their inner counterparts. In the second case, the deficit of outer rings in unbarred galaxies can be explained because they can be destroyed easily by the interaction with companion galaxies (Elmegreen et al. 1992). Alternatively, this effect can be attributed to the fact that a significant fraction of outer rings may have been misclassified as inner rings in unbarred galaxies (Section 6.5).

Quantifying the link between resonance features and ovals or spiral patterns requires studying parameters such as the non-axisymmetric torque, Q . This was defined by Combes & Sanders (1981) and indicates the strength of the non-axisymmetries of the galactic potential. This parameter can be local (Q_r , the local non-axisymmetric torque) or global (Q_g , the maximum of all Q_r). In a study that contained 16 unbarred and 31 barred galaxies, Grouchy et al. (2010) pointed out a correlation between the ring axis ratio and the Q_r at its radius independently of whether the host galaxy is barred or not. This shows that, indeed, not only bars are responsible for shaping the rings, but also other non-axisymmetries in the galactic potential such as those caused by ovals and spiral arms. Further investigation will require analysing larger samples, which may be drawn from the S⁴G.

7.4. Why is the inner ring orientation dependent on the host galaxy stage?

In Section 6.4 we found that inner rings prefer to be aligned in parallel with the bar major axis. However, we also found that a significant fraction of inner rings ($\sim 50\%$) is oriented at random with respect to the bar. The fraction of rings with random orientations is low (20 – 30%) for early-type galaxies, but increases to $\sim 70\%$ for galaxies with $T \geq 4$.

We investigated whether this effect might be related to a high galaxy inclination, which would prevent the accurate measurement of bar and ring orientations. To do this, we divided the galaxies that host inner rings into two groups: those whose inner rings are roughly aligned with the bar ($\theta_r - \theta_b \leq 30^\circ$), and those that are misaligned with it ($\theta_r - \theta_b > 30^\circ$). For each of these groups we plotted the fraction of galaxies that can be found at

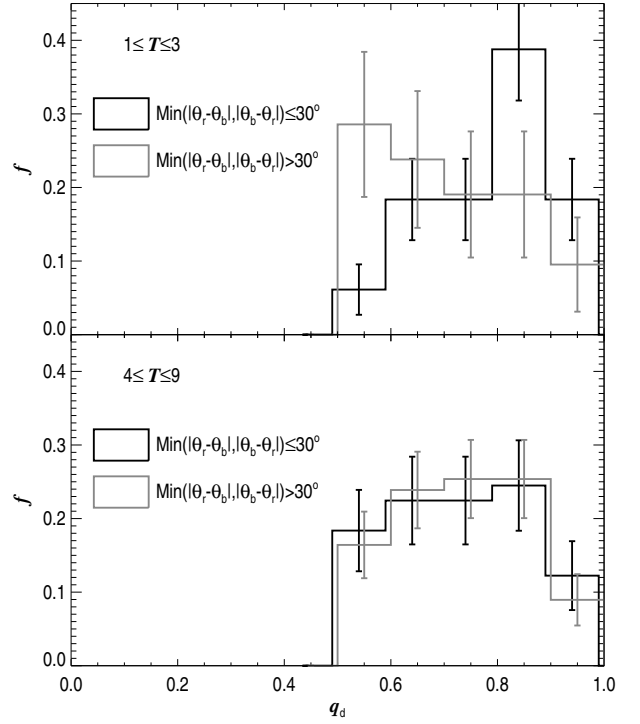


Fig. 34. Fraction of galaxies with inner rings aligned with the bar ($\theta_r - \theta_b \leq 30^\circ$; in black) and inner rings misaligned with the bar ($\theta_r - \theta_b > 30^\circ$; in grey) that have a given disc axis ratio. The top panel shows galaxies with stages $1 \leq T \leq 3$, the bottom panel galaxies with stages $4 \leq T \leq 10$. Only galaxies with deprojected ring axis ratios $q_{r,0}(I) < 0.85$ and disc axis ratios $q_d \leq 0.5$ are included. The error bars are calculated using binomial statistics.

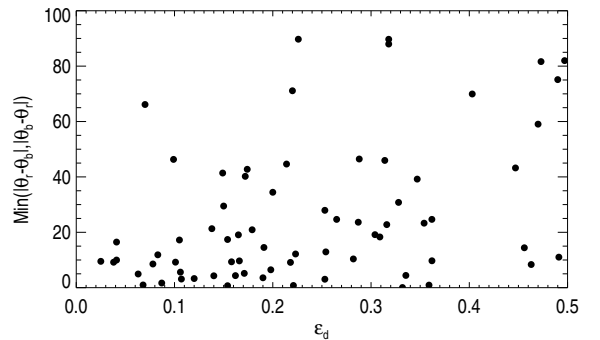


Fig. 35. Ring deprojected major axis angle difference with the bar as a function of the galaxy disc ellipticity for $\epsilon \leq 0.5$.

a given disc axis ratio, restricting ourselves to $\epsilon \leq 0.5$. The expectation for circular discs with their rotation axis pointing at random is that the distribution is uniform. We calculated this for galaxies with $1 \leq T \leq 3$ and $4 \leq T \leq 10$ (top and bottom panels in Figure 34 respectively). Earlier-type galaxies have nearly no misaligned inner rings.

The top panel in Figure 34 suggests that misaligned rings tend to be found more frequently in the bins with more highly inclined galaxies, and the reversed trend is seen for galaxies

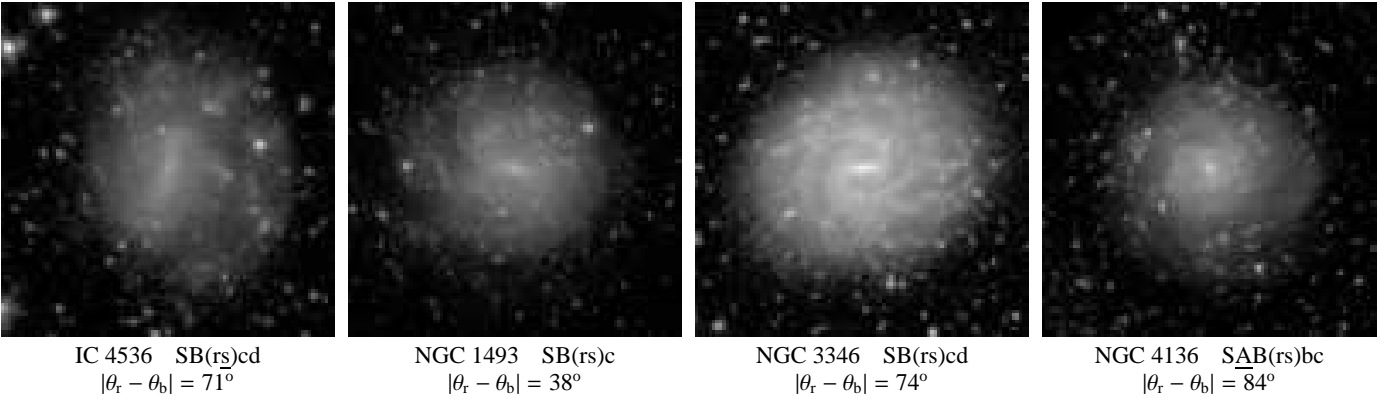


Fig. 36. Selection of close to face-on S⁴G galaxies with stages $4 \leq T \leq 10$ that host inner pseudorings misaligned with the bar. The images have the same properties as those in Figure 2. The name of the galaxies, their morphological classification, and the bar-pseudoring intrinsic misalignment can be found below each image.

oriented parallel with the ring (if we except the bin centred at $q_d = 0.95$). To verify whether this trend is statistically significant, we plotted in Figure 35 the intrinsic ring/bar misalignments as a function of the disc ellipticity for all galaxies in the top panel of Figure 34. We can see that misaligned rings have a preference for inclined galaxies. We calculated the Spearman coefficient of the data in Figure 35 and found that $\rho = 0.37$ and that the probability of the variables in the two axes to be uncorrelated is $p = 0.002$. It is therefore very likely that at least some of the misalignments are caused by incorrect deprojections. We see no such effect for galaxies with $4 \leq T \leq 10$ (bottom panel in Figure 34), which suggests that these deprojection problems might be related to the thickness of the discs. Indeed, as discussed in Section 4.6, earlier-type galaxies have thicker discs.

For late-type discs, the distributions in Figure 34 differ from the uniform expectation in the sense that the bin for rounder discs is less populated than the others. This effect is well known for disc galaxies in general and has been attributed to genuine disc deviations from circularity of the order of $b/a = 0.9$ or to the presence of substructure in the discs (Lambas et al. 1992). We examined whether these deviations from perfectly circular discs might be responsible for rings misaligned with their bars if we were wrongly assuming purely circular discs. We did this by projecting several thousand elliptical discs with random orientations. These discs had a bar also oriented at random and rings with an orientation differing from that of the bar following a normal distribution with a dispersion of the order of 10° . Then, we deprojected the galaxies, but this time we assumed that they were circular. We found that for moderate disc intrinsic ellipticities ($b/a \gtrsim 0.8$), this did not cause a fraction of $\sim 70\%$ rings apparently oriented at random with respect to the bar, as we observe for the late spirals. However, the fraction of rings oriented at random with respect to the bar for galaxies with $1 \leq T \leq 3$ can be explained in this way. This is natural since, as we already argued, at least some ring/bar misalignments in early spirals might be caused by errors in the deprojections.

Therefore our results indicate that at least for late-type galaxies misalignments are not caused by uncertainties in bar and ring properties measured in highly inclined discs or because discs might not exactly be circular, as assumed when calculating the deprojections. Therefore, a significant fraction of inner rings are intrinsically misaligned, especially those in late-type galaxies. A selection of very low-inclination galaxies with such misaligned inner rings is shown in Figure 36.

The existence of misaligned inner features was also shown in simulations by Rautiainen & Salo (2000). In their study, this misalignment appears because a spiral mode with a pattern speed lower than that of the bar dominates the Fourier amplitude spectrum at the radius of the inner ring. This means that our results would be consistent with spiral modes rotating with a pattern speed different from that of the bar and with a significant contribution at the I4R radius for late-type galaxies. Alternatively, this is caused by a rotation of the Lagrangian points from their usual position, in the direction of the bar major axis, by an angle that increases with increasing spiral amplitude (e.g., Athanassoula et al. 2010). A way to explore these possibilities would be to compare the amplitude of the bar and spiral arm torque at the ring radius in our sample galaxies as reported, for instance, by Block et al. (2004) and Salo et al. (2010). The latter authors described that the spiral density amplitude correlates well with the local bar torque as long as it is measured within 1.5 times the bar length. Since bars in late-type galaxies can significantly shorter than their CR radius (see, e.g., Combes & Elmegreen 1993), a correlation between the bar and the spiral torque at the inner ring radius may not be found.

An alternative possibility is that the apparent random orientation between bars and rings is caused by errors in measuring the inner feature position angle. This is because the later a galaxy is, the more ill-defined its rings become. Also, inner pseudorings in late-type galaxies tend to be more spiral-like than those in early-type galaxies, which partly invalidates the approximation made when fitting them with ellipses.

8. Summary and conclusions

We presented ARRAKIS, the atlas of resonant rings as known in the S⁴G, and a catalogue of the ring and pseudoring properties. The preliminary analysis of the data contained in the catalogue (Appendix A) and the atlas (Appendix B) was also presented. In this paper rings and pseudorings have been collectively termed rings.

The most common rings are resonance rings. These rings are thought to be due to gathering of gas, which can later be transformed into stars, at or close to the radii of the resonances caused by non-axisymmetries such as bars, ovals, and strong spiral patterns (e.g., Schwarz 1981, 1984; Sellwood & Wilkinson 1993; Byrd et al. 1994; Rautiainen & Salo 2000). They come in three flavours (outer, inner, and nuclear), depending on their radius relative to that of the bar. Outer features are thought to

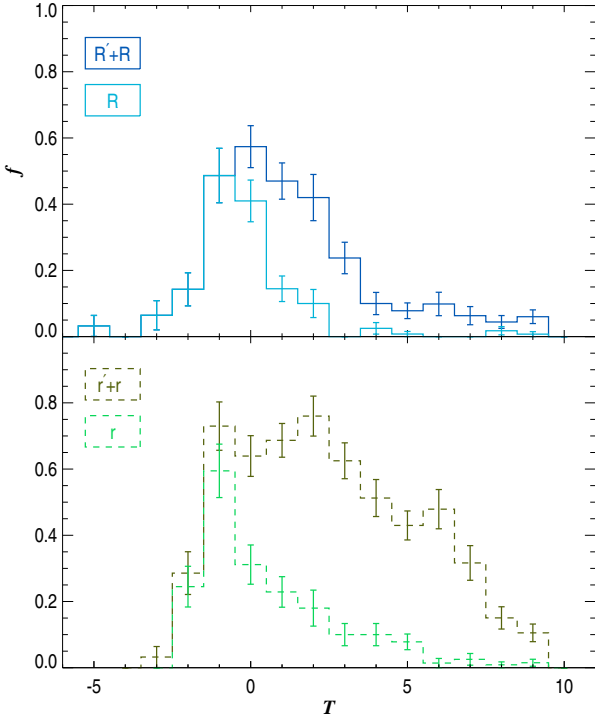


Fig. 37. Fraction of galaxies with outer rings (top panel) and inner rings (bottom panel) for a given stage. The plots only include galaxies with a disc ellipticity $\epsilon_d \leq 0.5$. In each of the panels, both rings as a whole and closed rings are indicated.

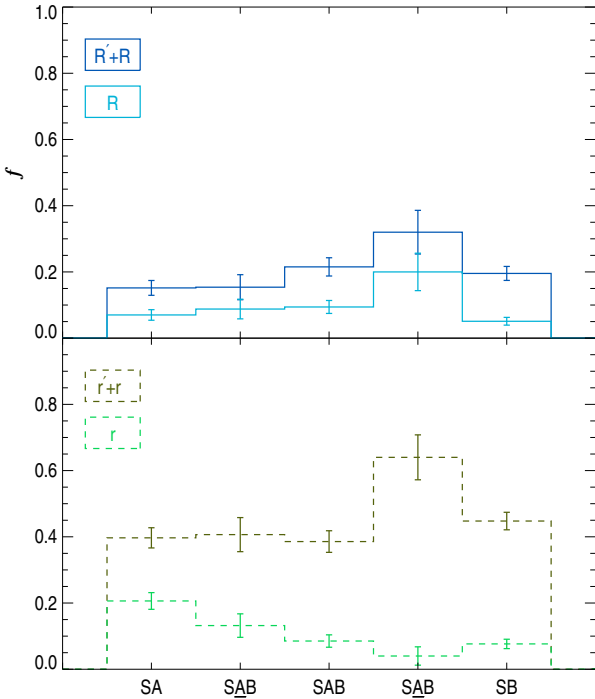


Fig. 38. As in Figure 37, but now with the bar family instead of stage.

be related to the OLR or occasionally to the O4R, inner features to the I4R, and nuclear features to the ILRs. Inner and outer rings might also be based on flux tube manifolds triggered by the bar or oval distortion (Romero-Gómez et al. 2006, 2007; Athanassoula et al. 2009b,a, 2010; Athanassoula 2012b). Either way, rings are tracers of the underlying galactic potential, which makes them important clues for the understanding of the secular evolution of disc galaxies.

The S⁴G is a survey of 2352 galaxies representative of the local Universe observed at 3.6 and 4.5 μm wavelengths. The galaxies in the S⁴G were classified by R. J. Buta, who also identified the rings (Buta et al. in preparation). We studied all the rings in the S⁴G frames, but our focus was on resonance rings in the S⁴G galaxy sample. Because dust obscuration is weak in the mid-infrared, the chances that rings are hidden by dust are much lower than at optical wavelengths. This makes the S⁴G a very good tool for studying rings.

We described the ring shape and orientation by marking their contours and fitting ellipses to them. To do this, we used model-subtracted images of the galaxies produced by the P4 of the S⁴G (Salo et al. in preparation). We obtained intrinsic ring shapes and orientations by deprojecting the fitted ellipses. The deprojection parameters were obtained from the P4 ellipse fits to the outer parts of S⁴G galaxies. Bar orientations and ellipticities (a rough indicator of bar strength) were measured by looking at the ellipse fit corresponding to the radius where the highest ellipticity was found within the bar. They were deprojected in the same way as for rings.

We summarise our findings as follows:

- **Section 6.1 and Figures 18 and 37:** Outer rings are found in $16 \pm 1\%$ of the S⁴G galaxies and are more frequent for stages $-1 \leq T \leq 2$ (over 40% frequency). Outer closed rings account for 100% of outer features with $T \leq -1$. Inner rings are the most frequent resonance feature in the local Universe ($35 \pm 1\%$ frequency in the S⁴G sample). They are typically found in the range $-1 \leq T \leq 6$ (over 40% frequency) and their frequency peaks at stages $-1 \leq T \leq 3$ (over 60% frequency). The inner closed ring distribution is shifted to earlier stages than that of inner features.
- **Sections 6.2 and 7.2 and Figures 19 and 38:** The outer ring frequency increases from $15 \pm 2\%$ to $32 \pm 7\%$ along the family sequence from SA to SAB, and decreases again to $20 \pm 2\%$ for SB galaxies. The inner ring frequency is qualitatively different, since it is roughly constant at $\sim 40\%$ for all families except for a peak at $64 \pm 7\%$ frequency for SAB galaxies. The reason might be that outer rings take a longer time than inner rings to be built in galaxies with weaker non-axisymmetries. We also found that inner closed rings have a preference for unbarred and weakly barred galaxies.
- **Section 7.3:** Barred galaxies have outer rings 1.7 times more often than unbarred ones. Barred galaxies have 1.3 more inner rings than their unbarred counterparts. This indicates that although they are stimulated by bars, rings do not need them to exist. Simulations suggest (e.g., Salo et al. 1999; Rautiainen & Salo 2000) that rings in unbarred galaxies may be related to weak ovals and/or long-lived spiral modes. Alternatively, they may have formed because of bars that have since been destroyed or have dissolved.
- **Sections 6.1 and 7.3:** We confirmed the results of the NIRS0S survey regarding the frequencies of outer and inner rings as a function of the stage and the family for galaxies with stages $-3 \leq T \leq 1$.

- **Section 6.3 and Figures 20, 21, and 22:** The axis ratio distribution of each of the three ring flavours - outer, inner, and nuclear - can be fitted with a Gaussian curve. Their intrinsic axis ratios typically range from $q_{r,0} = 0.6$ to $q_{r,0} = 1.0$. Inner rings are in general more elliptical than their outer counterparts. We found that outer and inner rings become on average more elliptical when the bar strength increases (when the galaxy family changes from SA to SB) and that inner rings are more elliptical in late-stage galaxies than in earlier-stage galaxies.
- **Section 6.4 and Figure 23:** We confirmed that outer rings have two preferred orientations, namely parallel and perpendicular to the bar. Of the outer rings in barred galaxies $35 \pm 18\%$ are parallel to the bar and $65 \pm 39\%$ are oriented perpendicular to it.
- **Sections 6.4 and 7.4 and Figures 23 and 25:** We found that many inner rings have their major axes oriented parallel to the bar, as predicted in simulations and as previously reported from observations. However, we also found that maybe as much as 50% of inner rings have random orientations with respect to the bar. These misaligned inner rings are mostly found in late-type spirals ($T \geq 4$). We speculate that this may be because the Fourier amplitude spectrum at the radius of the I4R is dominated by spiral modes with a pattern speed different from that of the bar late-type galaxies. Alternatively, this can be due to the increased difficulty of measuring inner ring properties when they become ill-defined at late stages.
- **Sections 6.5 and 6.6 and Figures 26, 27, 29, and 30:** The size of a ring relative to that of the galaxy is a much better indicator of its flavour (outer, inner, or nuclear) than its absolute size. The wings of both the absolute and relative size distributions of inner rings are more extended in unbarred galaxies than for those with bars. This may indicate that several outer and nuclear rings have been misclassified as inner features in unbarred galaxies.
- **Section 6.7:** Several of our sample galaxies have both an outer and an inner ring. The distribution of their diameter ratio peaks at $D_{r,0}(O)/D_{r,0}(I) \sim 2$, which agrees with the literature.

8.1. Open questions

We discussed two very interesting questions on rings which still have no clear solution. Why are some rings found in apparently unbarred galaxies? And why do inner rings in late-type galaxies have a higher tendency to be oriented at random with respect to the bar than those in earlier-type galaxies?

As developed in the discussion in Section 7, galaxies with these properties have occasionally been found in simulations. However, to test whether the mechanism creating rings in unbarred galaxies and the one shaping inner rings that are misaligned with the bar is the same in nature and in simulations, one has to study each galaxy at a deeper level of detail than we did here. Indeed, visual identification of the bar and a rough estimate of its orientation may be insufficient and one may need to perform a Fourier analysis to unveil the effects of non-axisymmetries induced by spiral arms or broad weak ovals. Again, the S⁴G is the right tool for this type of research because the mid-infrared is an excellent tracer of the stellar mass and thus of the baryonic matter contribution to the galactic potential.

Acknowledgements. We thank our anonymous referee, who very carefully read this paper. The authors wish to thank the entire S⁴G team for their efforts in this

project. We thank Pertti Rautiainen for useful discussions on the ring formation in his simulations, Simón Díaz-García for helping with fundamental statistical concepts, and Glenn van de Ven for his useful comments.

We acknowledge financial support to the DAGAL network from the People Programme (Marie Curie Actions) of the European Union's Seventh Framework Programme FP7/2007-2013/ under REA grant agreement number PITN-GA-2011-289313. EA and AB acknowledge financial support from the CNES (Centre National d'Études Spatiales - France). KS, J-CM-M, TK, and TM acknowledge support from the National Radio Observatory, which is a facility of the National Radio Astronomy Observatory operated under cooperative agreement by Associated Universities, Inc. SC, HS, EL, MH-H, and JL acknowledge support from the Academy of Finland.

This work is based on observations and archival data made with the Spitzer Space Telescope, which is operated by the Jet Propulsion Laboratory, California Institute of Technology under a contract with NASA. We are grateful to the dedicated staff at the Spitzer Science Center for their help and support in planning and execution of this Exploration Science program. We also gratefully acknowledge support from NASA JPL/Spitzer grant RSA 1374189 provided for the S⁴G project.

This research has made use of SAOImage DS9, developed by Smithsonian Astrophysical Observatory.

This research has made use of the NASA/IPAC Extragalactic Database (NED) which is operated by the Jet Propulsion Laboratory, California Institute of Technology, under contract with the National Aeronautics and Space Administration.

References

- Appleton, P. N. & Struck-Marcell, C. 1996, *Fund. Cosmic Phys.*, 16, 111
- Athanassoula, E. 1996, in *Astronomical Society of the Pacific Conference Series*, Vol. 91, IAU Colloq. 157: Barred Galaxies, ed. R. Buta, D. A. Crocker, & B. G. Elmegreen, 309
- Athanassoula, E. 2012a, arXiv:1211.6752, to be published by Cambridge University Press; *Proceedings of the XXIII Canary Islands Winter School of Astrophysics: 'Secular Evolution of Galaxies'*, edited by J. Falcon-Barroso and J. H. Knapen
- Athanassoula, E. 2012b, *MNRAS*, 426, L46
- Athanassoula, E., Bosma, A., Creze, M., & Schwarz, M. P. 1982, *A&A*, 107, 101
- Athanassoula, E., Machado, R. E. G., & Rodionov, S. A. 2013, *MNRAS*, 429, 1949
- Athanassoula, E., Romero-Gómez, M., Bosma, A., & Masdemont, J. J. 2009a, *MNRAS*, 400, 1706
- Athanassoula, E., Romero-Gómez, M., Bosma, A., & Masdemont, J. J. 2010, *MNRAS*, 407, 1433
- Athanassoula, E., Romero-Gómez, M., & Masdemont, J. J. 2009b, *MNRAS*, 394, 67
- Berentzen, I., Athanassoula, E., Heller, C. H., & Fricke, K. J. 2003, *MNRAS*, 341, 343
- Berentzen, I., Shlosman, I., Martínez-Valpuesta, I., & Heller, C. H. 2007, *ApJ*, 666, 189
- Bettoni, D., Galletta, G., García-Burillo, S., & Rodríguez-Franco, A. 2001, *A&A*, 374, 421
- Block, D. L., Buta, R., Knapen, J. H., et al. 2004, *AJ*, 128, 183
- Block, D. L., Puerari, I., Knapen, J. H., et al. 2001, *A&A*, 375, 761
- Bournaud, F. & Combes, F. 2002, *A&A*, 392, 83
- Bournaud, F., Combes, F., & Semelin, B. 2005, *MNRAS*, 364, L18
- Buta, R. 1986a, *ApJS*, 61, 609
- Buta, R. 1986b, *ApJS*, 61, 631
- Buta, R. 1987, *ApJS*, 64, 383
- Buta, R. 1991, *ApJ*, 370, 130
- Buta, R. 1995, *ApJS*, 96, 39, (CSRG)
- Buta, R. 2002, in *Astronomical Society of the Pacific Conference Series*, Vol. 275, *Disks of Galaxies: Kinematics, Dynamics and Perturbations*, ed. E. Athanassoula, A. Bosma, & R. Mujica, 185–192
- Buta, R. & Combes, F. 1996, *Fund. Cosmic Phys.*, 17, 95
- Buta, R. & Crocker, D. A. 1993, *AJ*, 105, 1344, (BC93)
- Buta, R., Purcell, G. B., & Crocker, D. A. 1995, *AJ*, 110, 1588
- Buta, R. J. 2013, *Galaxy Morphology*, ed. T. D. Oswalt & W. C. Keel, 1
- Buta, R. J., Corwin, H. G., & Odewahn, S. C. 2007, *The de Vaucouleurs Atlas of Galaxies* (Cambridge University Press)
- Buta, R. J., Sheth, K., Regan, M., et al. 2010, *ApJS*, 190, 147
- Byrd, G., Rautiainen, P., Salo, H., Buta, R., & Crocher, D. A. 1994, *AJ*, 108, 476
- Byrd, G. G., Ousley, D., & dalla Piazza, C. 1998, *MNRAS*, 298, 78
- Combes, F. & Elmegreen, B. G. 1993, *A&A*, 271, 391
- Combes, F. & Sanders, R. H. 1981, *A&A*, 96, 164
- Comerón, S. 2013, *A&A*, 555, L4

- Comerón, S., Knapen, J. H., & Beckman, J. E. 2008a, *Journal of Physics Conference Series*, 131, 012046
- Comerón, S., Knapen, J. H., & Beckman, J. E. 2008b, *A&A*, 485, 695
- Comerón, S., Knapen, J. H., Beckman, J. E., et al. 2010, *MNRAS*, 402, 2462, (AINUR)
- Comerón, S., Knapen, J. H., Beckman, J. E., & Shlosman, I. 2008c, *A&A*, 478, 403
- Corsini, E. M., Pizzella, A., Funes, J. G., Vega Beltran, J. C., & Bertola, F. 1998, *A&A*, 337, 80
- Crocker, D. A., Baugus, P. D., & Buta, R. 1996, *ApJS*, 105, 353
- Curtis, H. D. 1918, *Publications of Lick Observatory*, 13, 9
- de Grijs, R. 1998, *MNRAS*, 299, 595
- de Vaucouleurs, G. 1948, *Annales d'Astrophysique*, 11, 247
- de Vaucouleurs, G. 1959, *Handbuch der Physik*, 53, 275
- de Vaucouleurs, G. 1963, *ApJS*, 8, 31
- de Vaucouleurs, G. & Buta, R. 1980, *AJ*, 85, 637, vB80
- de Vaucouleurs, G., de Vaucouleurs, A., Corwin, Jr., H. G., et al. 1991, *Third Reference Catalogue of Bright Galaxies. Volume I: Explanations and references. Volume II: Data for galaxies between 0^h and 12^h . Volume III: Data for galaxies between 12^h and 24^h . (RC3)*
- de Vaucouleurs, G. H., de Vaucouleurs, A., & Shapley, H. 1964, *Reference catalogue of bright galaxies*
- Debattista, V. P., Carollo, C. M., Mayer, L., & Moore, B. 2004, *ApJ*, 604, L93
- Debattista, V. P., Mayer, L., Carollo, C. M., et al. 2006, *ApJ*, 645, 209
- Dreyer, J. L. E. 1888, *MNRAS*, 49, 1
- Dreyer, J. L. E. 1895, *MNRAS*, 51, 185
- Elmegreen, D. M., Elmegreen, B. G., Combes, F., & Bellin, A. D. 1992, *A&A*, 257, 17
- Englmaier, P. & Gerhard, O. 1997, *MNRAS*, 287, 57
- Erwin, P. 2005, *MNRAS*, 364, 283
- Erwin, P. & Sparke, L. S. 1999, *ApJ*, 521, L37
- Erwin, P. & Sparke, L. S. 2002, *AJ*, 124, 65
- Fazio, G. G., Hora, J. L., Allen, L. E., et al. 2004, *ApJS*, 154, 10
- Ferrers, N. M. 1877, *Q. J. Pure Appl. Math.*, 14, 1
- Friedli, D. & Benz, W. 1993, *A&A*, 268, 65
- Gadotti, D. A., Athanassoula, E., Carrasco, L., et al. 2007, *MNRAS*, 381, 943
- Grouchy, R. D., Buta, R. J., Salo, H., & Laurikainen, E. 2010, *AJ*, 139, 2465
- Hubble, E. P. 1926, *ApJ*, 64, 321
- Jaffe, W. 1983, *MNRAS*, 202, 995
- Jardel, J. R., Gebhardt, K., Shen, J., et al. 2011, *ApJ*, 739, 21
- Jore, K. P., Broeils, A. H., & Haynes, M. P. 1996, *AJ*, 112, 438
- Joye, W. A. & Mandel, E. 2003, in *Astronomical Society of the Pacific Conference Series, Vol. 295, Astronomical Data Analysis Software and Systems XII*, ed. H. E. Payne, R. I. Jedrzejewski, & R. N. Hook, 489
- Jungwiert, B. & Palous, J. 1996, *A&A*, 311, 397
- Keeler, J. E. 1908, *Publications of Lick Observatory*, 8, 1
- Kim, W.-T., Seo, W.-Y., Stone, J. M., Yoon, D., & Teuben, P. J. 2012, *ApJ*, 747, 60
- Knapen, J. H. 2005, *A&A*, 429, 141
- Knapen, J. H., Beckman, J. E., Heller, C. H., Shlosman, I., & de Jong, R. S. 1995, *ApJ*, 454, 623
- Knapen, J. H., Pérez-Ramírez, D., & Laine, S. 2002, *MNRAS*, 337, 808
- Knapen, J. H., Whyte, L. F., de Blok, W. J. G., & van der Hulst, J. M. 2004, *A&A*, 423, 481
- Kormendy, J. 1979, *ApJ*, 227, 714
- Kormendy, J. & Kennicutt, Jr., R. C. 2004, *ARA&A*, 42, 603
- Kuijken, K. & Merrifield, M. R. 1995, *ApJ*, 443, L13
- Lambas, D. G., Maddox, S. J., & Loveday, J. 1992, *MNRAS*, 258, 404
- Laurikainen, E., Salo, H., Buta, R., & Knapen, J. H. 2011, *MNRAS*, 418, 1452, (NIRS0S)
- Laurikainen, E., Salo, H., & Rautiainen, P. 2002, *MNRAS*, 331, 880
- Lynden-Bell, D. & Kalnajs, A. J. 1972, *MNRAS*, 157, 1
- Lynds, R. & Toomre, A. 1976, *ApJ*, 209, 382
- Marochnik, L. S., Mishurov, Y. N., & Suchkov, A. A. 1972, *Ap&SS*, 19, 285
- Martin, P. 1995, *AJ*, 109, 2428
- Martinez-Valpuesta, I. & Shlosman, I. 2004, *ApJ*, 613, L29
- Mazzuca, L. M., Sarzi, M., Knapen, J. H., Veilleux, S., & Swaters, R. 2006, *ApJ*, 649, L79
- Parsons, C. 1880, *Scientific Trans. Roy. Dublin Soc.*, II
- Paturel, G., Petit, C., Prugniel, P., et al. 2003, *A&A*, 412, 45
- Peng, C. Y., Ho, L. C., Impey, C. D., & Rix, H.-W. 2002, *AJ*, 124, 266
- Peng, C. Y., Ho, L. C., Impey, C. D., & Rix, H.-W. 2010, *AJ*, 139, 2097
- Perrine, C. D. 1922, *MNRAS*, 82, 486
- Raha, N., Sellwood, J. A., James, R. A., & Kahn, F. D. 1991, *Nature*, 352, 411
- Rautiainen, P. & Salo, H. 2000, *A&A*, 362, 465
- Regan, M. W. & Teuben, P. J. 2004, *ApJ*, 600, 595
- Romero-Gómez, M., Athanassoula, E., Masdemont, J. J., & García-Gómez, C. 2007, *A&A*, 472, 63
- Romero-Gómez, M., Masdemont, J. J., Athanassoula, E., & García-Gómez, C. 2006, *A&A*, 453, 39
- Salo, H., Laurikainen, E., Buta, R., & Knapen, J. H. 2010, *ApJ*, 715, L56
- Salo, H., Rautiainen, P., Buta, R., et al. 1999, *AJ*, 117, 792
- Schommer, R. A. & Sullivan, III, W. T. 1976, *Astrophys. Lett.*, 17, 191
- Schwarz, M. P. 1981, *ApJ*, 247, 77
- Schwarz, M. P. 1984, *MNRAS*, 209, 93
- Schweizer, F., van Gorkom, J. H., & Seitzer, P. 1989, *ApJ*, 338, 770
- Schweizer, F., Whitmore, B. C., & Rubin, V. C. 1983, *AJ*, 88, 909
- Sellwood, J. A. 1981, *A&A*, 99, 362
- Sellwood, J. A. & Wilkinson, A. 1993, *Reports on Progress in Physics*, 56, 173
- Sheth, K., Regan, M., Hinz, J. L., et al. 2010, *PASP*, 122, 1397
- Sheth, K., Regan, M. W., Vogel, S. N., & Teuben, P. J. 2000, *ApJ*, 532, 221
- Shlosman, I. 1999, in *Astronomical Society of the Pacific Conference Series, Vol. 187, The Evolution of Galaxies on Cosmological Timescales*, ed. J. E. Beckman & T. J. Mahoney, 100–114
- Sil'chenko, O. K. & Moiseev, A. V. 2006, *AJ*, 131, 1336
- Sulentic, J. W. & Arp, H. C. 1987, *ApJ*, 319, 687
- Thakar, A. R., Ryden, B. S., Jore, K. P., & Broeils, A. H. 1997, *ApJ*, 479, 702
- Theys, J. C. & Spiegel, E. A. 1977, *ApJ*, 212, 616
- Tody, D. 1986, in *Society of Photo-Optical Instrumentation Engineers (SPIE) Conference Series, Vol. 627, Society of Photo-Optical Instrumentation Engineers (SPIE) Conference Series*, ed. D. L. Crawford, 733
- Tody, D. 1993, in *Astronomical Society of the Pacific Conference Series, Vol. 52, Astronomical Data Analysis Software and Systems II*, ed. R. J. Hanisch, R. J. V. Brissenden, & J. Barnes, 173
- Toomre, A. 1977, in *Evolution of Galaxies and Stellar Populations*, ed. B. M. Tinsley & R. B. G. Larson, D. Campbell, 401
- Treuthardt, P., Salo, H., Rautiainen, P., & Buta, R. 2008, *AJ*, 136, 300
- Tutukov, A. V. & Fedorova, A. V. 2006, *Astronomy Reports*, 50, 785
- van den Bergh, S. 1976, *ApJ*, 206, 883
- van Driel, W., Combes, F., Casoli, F., et al. 1995, *AJ*, 109, 942
- Werner, M. W., Roellig, T. L., Low, F. J., et al. 2004, *ApJS*, 154, 1
- Whitmore, B. C., Lucas, R. A., McElroy, D. B., et al. 1990, *AJ*, 100, 1489

Appendix A: Catalogue

The catalogue contains two tables. One for galaxies included in the S⁴G sample and a second one for galaxies that appear in S⁴G frames, but are not included in the original sample. The information in the tables in the catalogue is organized as follows:

Column 1	Galaxy ID
Column 2	NED redshift-independent distance if available, NED redshift distance corrected for Virgo Cluster, Great Attractor and Shapley Cluster effects with $H_0 = 73 \text{ km s}^{-1} \text{ Mpc}^{-1}$ otherwise
Column 3	Type of feature (ring, pseudoring or bar) described in that row
Column 4	Feature major projected diameter (maximum ellipticity major diameter for bars)
Column 5	Feature minor projected diameter (maximum ellipticity minor diameter for bars)
Column 6	Feature major axis PA
Column 7	Feature major intrinsic diameter (maximum ellipticity major diameter for bars)
Column 8	Feature minor intrinsic diameter (maximum ellipticity minor diameter for bars)
Column 9	Counter-clockwise angular distance between the line of nodes of the galaxy deprojection and the major axis of the feature

Deprojected ring parameters are not given for polar rings.

A.1. (Pseudo)Rings in S⁴G sample galaxies**Table A.1.** Catalogue of the properties of ringed galaxies included in the S⁴G sample

ID	D (Mpc)	Feature	$D_{r,b}$ ($'$)	$d_{r,b}$ ($'$)	$PA_{r,b}$ ($^{\circ}$)	$D_{r,b,0}$ ($'$)	$d_{r,b,0}$ ($'$)	$\theta_{r,b}$ ($^{\circ}$)
(1)	(2)	(3)	(4)	(5)	(6)	(7)	(8)	(9)
ESO 13-16	23.0	rs bar	0.78 0.30	0.66 0.08	161.7 166.0	1.01 0.30	0.78 0.12	92.5 0.5
ESO 26-1	19.2	R' ₂ bar	1.25 0.23	0.92 0.07	37.4 66.9	1.26 0.24	0.97 0.08	22.3 49.8
ESO 54-21	16.5	R'	3.15	1.55	101.6	3.78	2.65	53.9
ESO 119-16	26.6	R'	2.24	0.56	30.3	2.33	1.50	22.4
ESO 202-41	17.0	rs bar	0.85 0.73	0.75 0.22	174.4 166.9	1.13 0.75	0.83 0.32	82.9 19.9
ESO 234-49	37.7	r	0.24	0.12	170.7	0.25	0.12	92.2
ESO 240-11	42.4	rs	1.05	0.11	127.8	1.06	0.70	5.0
ESO 285-48	33.1	rs	0.64	0.30	80.7	0.70	0.64	99.8
ESO 355-26	28.9	r	0.23	0.17	154.7	0.32	0.23	91.0
ESO 358-25	16.3	nr	0.14	0.09	57.4	0.15	0.14	75.4
ESO 362-19	16.5	R'	1.82	0.39	3.9	1.87	1.23	19.0
ESO 399-25	38.0	RL	3.08	1.16	153.0	3.09	1.62	171.3
ESO 402-26	39.6	R' r	1.80 0.61	0.61 0.27	113.0 100.4	1.91 0.83	1.59 0.56	38.9 111.4
ESO 402-30	39.5	rs	0.18	0.07	134.4	0.18	0.12	171.4
ESO 404-12	36.2	bar rs	0.49 0.41	0.17 0.40	131.1 145.6	0.50 0.47	0.19 0.41	15.1 86.3
ESO 407-7	32.8	rl	0.49	0.07	168.7	0.49	0.34	4.8
ESO 407-14	37.4	r	0.41	0.16	40.3	0.41	0.30	0.6
ESO 418-8	20.7	R' bar	0.80 0.13	0.50 0.04	151.7 9.0	0.86 0.17	0.68 0.04	42.7 63.8
ESO 420-9	17.7	rs bar	0.40 0.12	0.36 0.06	76.9 39.8	0.50 0.12	0.38 0.08	81.2 13.0
ESO 422-5	26.3	rs bar	0.47 0.25	0.40 0.13	51.0 79.5	0.58 0.32	0.44 0.14	74.9 69.2
ESO 422-41	10.8	R'	2.26	1.87	91.1	2.39	2.15	55.8
ESO 440-4	49.0	rl	0.98	0.75	82.4	1.80	0.98	87.7
ESO 440-11	27.6	rs bar	0.58 0.29	0.44 0.08	15.9 176.5	0.59 0.30	0.48 0.09	154.5 140.3
ESO 443-69	34.8	rs bar	0.67 0.52	0.59 0.18	172.9 174.0	0.73 0.56	0.61 0.19	67.1 53.2
ESO 443-80	36.8	RG	1.34	0.57	142.5	1.37	0.79	162.1
ESO 479-4	19.4	rs bar	0.84 0.20	0.49 0.06	59.3 37.4	0.92 0.23	0.83 0.09	72.1 143.8
ESO 482-35	27.3	rs bar	0.70 0.69	0.45 0.19	8.3 28.5	0.75 0.80	0.66 0.25	50.4 42.3
ESO 507-65	32.6	R'	0.77	0.24	16.8	0.77	0.56	3.4
ESO 508-7	32.7	rs bar	0.59 0.37	0.39 0.18	111.8 91.2	0.91 0.42	0.48 0.30	72.9 46.4
ESO 508-24	40.0	rs bar	0.60 0.21	0.35 0.11	72.9 57.6	0.60 0.22	0.41 0.12	167.3 149.0
ESO 509-74	35.5	nr	0.14	0.03	136.2	0.14	0.12	151.3
ESO 510-58	30.4	R' bar	0.79 0.35	0.48 0.23	5.9 161.1	0.82 0.38	0.69 0.31	36.4 128.9
ESO 510-59	33.6	rs bar	0.59 0.33	0.51 0.07	127.8 116.2	0.89 0.41	0.54 0.09	82.3 49.8
ESO 532-22	30.4	rs bar	0.51 0.45	0.42 0.13	0.5 17.3	0.71 0.63	0.46 0.13	77.6 70.6
ESO 545-16	18.4	R	1.54	1.39	36.9	1.79	1.54	89.5
ESO 547-5	20.9	rs bar	0.66 0.29	0.42 0.11	52.1 31.8	0.66 0.30	0.57 0.14	7.1 153.4

Table A.1. continued.

ID	D (Mpc)	Feature	$D_{r,b}$ ($'$)	$d_{r,b}$ ($'$)	$PA_{r,b}$ ($^{\circ}$)	$D_{r,b,0}$ ($'$)	$d_{r,b,0}$ ($'$)	$\theta_{r,b}$ ($^{\circ}$)
(1)	(2)	(3)	(4)	(5)	(6)	(7)	(8)	(9)
ESO 548-5	21.9	rs bar	0.73 0.59	0.56 0.29	53.7 29.4	0.73 0.60	0.65 0.34	19.9 159.1
ESO 548-23	21.9	RL	0.66	0.35	24.3	0.68	0.66	70.0
ESO 548-25	22.1	R'L bar	0.90 0.25	0.41 0.13	81.5 172.2	0.92 0.47	0.77 0.13	154.2 88.2
ESO 549-18	26.1	R' ₂ bar	1.34 0.66	0.89 0.22	11.2 16.8	1.51 0.66	1.29 0.36	112.9 175.2
ESO 572-18	23.8	rs bar	0.67 0.27	0.27 0.15	45.4 178.7	0.70 0.43	0.52 0.19	27.4 109.4
ESO 576-1	105.2	r bar	0.33 0.21	0.19 0.14	164.1 32.7	0.39 0.38	0.31 0.15	68.2 79.2
ESO 576-3	34.5	rs	1.04	0.24	93.4	1.05	0.61	169.0
ESO 576-32	24.6	bar rs	0.69 0.67	0.17 0.46	153.2 131.6	0.73 0.68	0.23 0.65	26.7 149.0
ESO 576-50	22.5	rs bar	0.75 0.19	0.39 0.08	166.4 70.0	0.84 0.29	0.56 0.09	137.4 75.6
ESO 580-29	35.4	rs	0.76	0.09	71.6	0.77	0.49	168.2
ESO 580-41	30.0	rs	0.48	0.12	78.6	0.63	0.47	77.1
ESO 581-25	29.9	rs nr	1.03 0.21	0.12 0.05	59.2 57.6	1.03 0.26	0.62 0.20	176.8 108.0
ESO 602-30	33.2	rs bar	0.39 0.11	0.29 0.05	65.6 49.1	0.40 0.11	0.38 0.07	140.9 145.4
IC 51	23.3	PRG	0.50	0.10	113.9	–	–	–
IC 719	29.5	rl	0.28	0.06	51.8	0.28	0.14	4.5
IC 749	17.0	rs bar	0.70 0.35	0.60 0.15	53.1 42.1	0.78 0.39	0.61 0.15	106.4 104.7
IC 863	35.0	R' rs bar	0.51 0.24 0.24	0.30 0.22 0.13	44.1 76.6 102.8	0.51 0.30 0.30	0.40 0.24 0.14	167.6 78.7 65.8
IC 1014	24.2	r bar	0.75 0.37	0.54 0.16	78.2 54.2	0.83 0.43	0.73 0.20	116.6 130.3
IC 1029	53.6	R'	2.30	0.33	147.6	2.34	1.41	167.1
IC 1048	28.8	R'	1.08	0.14	164.6	1.11	0.62	15.7
IC 1055	37.9	R' rs r	1.53 0.90 0.33	0.54 0.28 0.13	5.7 3.2 7.6	1.54 0.91 0.34	1.33 0.69 0.31	6.3 170.7 42.4
IC 1067	27.3	r bar	0.63 0.61	0.51 0.22	114.0 150.0	0.65 0.67	0.63 0.25	106.0 41.4
IC 1158	28.8	rs bar	0.31 0.17	0.17 0.10	141.2 81.8	0.33 0.26	0.29 0.11	39.9 105.7
IC 1210	46.3	r	0.47	0.24	172.9	0.54	0.45	64.6
IC 1265	36.5	r	0.39	0.18	73.1	0.40	0.33	155.2
IC 1438	33.8	R ₁ r'l bar	1.77 0.73 0.70	1.32 0.49 0.34	23.4 127.5 123.4	1.86 0.77 0.74	1.40 0.52 0.36	48.6 133.1 132.3
IC 1596	36.2	rs	0.27	0.17	111.6	0.45	0.27	90.7
IC 1953	22.6	bar rs	0.87 0.77	0.22 0.70	157.8 100.8	1.04 1.07	0.27 0.76	48.6 95.4
IC 1954	14.0	rs bar	0.48 0.13	0.25 0.05	77.3 91.6	0.56 0.17	0.39 0.07	50.6 52.3
IC 1993	13.6	R' bar	1.47 0.54	1.44 0.39	78.5 43.8	1.58 0.56	1.44 0.40	88.8 56.2
IC 2051	24.2	rs bar	0.87 0.75	0.54 0.40	74.0 12.8	0.91 1.16	0.86 0.43	71.7 105.2
IC 2056	20.5	rs	0.27	0.23	114.5	0.31	0.24	94.5
IC 2361	31.9	rs	0.39	0.14	80.4	0.43	0.36	46.0
IC 2764	21.9	R	0.84	0.70	3.3	0.84	0.82	9.6

Table A.1. continued.

ID	D (Mpc)	Feature	$D_{r,b}$ ($'$)	$d_{r,b}$ ($'$)	$PA_{r,b}$ ($^{\circ}$)	$D_{r,b,0}$ ($'$)	$d_{r,b,0}$ ($'$)	$\theta_{r,b}$ ($^{\circ}$)
(1)	(2)	(3)	(4)	(5)	(6)	(7)	(8)	(9)
IC 2969	27.5	r	0.37	0.30	101.5	0.45	0.37	80.4
		R'L	2.76	1.45	119.9	2.77	2.33	8.0
IC 3102	28.9	<u>rs</u>	1.55	0.81	117.6	1.55	1.30	178.8
		bar	0.78	0.38	128.0	0.81	0.59	27.7
IC 3267	13.7	rs	0.61	0.48	120.8	0.61	0.52	174.0
IC 3391	14.1	r	0.23	0.13	50.6	0.24	0.17	150.3
IC 3392	13.7	rs	0.58	0.25	39.3	0.60	0.56	47.4
IC 3806	14.0	r	0.40	0.12	179.6	0.41	0.28	12.0
		R ₁	2.03	1.25	2.2	2.13	1.76	36.1
IC 4214	27.3	bar	0.90	0.42	150.0	1.00	0.57	141.4
		r'l	0.89	0.48	160.9	0.92	0.68	153.7
		nr	0.21	0.13	165.2	0.21	0.19	141.4
IC 4216	42.2	r'l	0.73	0.43	51.4	1.02	0.73	94.3
		<u>rs</u>	0.31	0.24	177.9	0.45	0.31	86.2
IC 4221	41.6	bar	0.24	0.09	148.9	0.30	0.14	132.8
		r	0.57	0.39	152.3	0.60	0.53	49.8
IC 4237	40.1	bar	0.49	0.15	118.0	0.54	0.19	144.5
		<u>rs</u>	0.66	0.64	68.5	0.76	0.65	84.2
IC 4536	33.4	bar	0.45	0.12	169.1	0.46	0.14	154.8
		r	0.45	0.36	163.0	0.59	0.39	72.5
IC 4901	21.9	bar	0.41	0.18	119.0	0.42	0.25	172.7
IC 5039	31.4	<u>rs</u>	0.31	0.17	158.6	0.51	0.31	85.3
IC 5156	37.5	<u>rs</u>	0.61	0.29	179.4	0.72	0.58	66.9
		bar	1.33	0.36	89.7	1.34	0.51	166.6
IC 5240	25.4	r	1.26	0.82	108.7	1.31	1.11	34.7
IC 5264	47.8	R	1.58	0.13	81.0	1.58	0.57	177.5
		RL	4.65	3.31	148.4	4.80	4.33	38.4
IC 5267	26.1	r	2.71	1.95	136.3	2.74	2.61	151.0
IC 5271	23.6	rs	1.07	0.39	138.8	1.07	1.02	22.3
IC 5334	44.5	R'	1.09	0.22	126.1	1.09	0.60	1.9
NGC 24	6.9	rs	0.85	0.22	45.9	0.88	0.81	40.9
NGC 131	19.2	<u>rs</u>	0.83	0.23	64.8	0.83	0.64	10.8
NGC 134	18.9	rs	1.26	0.34	45.5	1.30	1.18	146.8
NGC 148	18.4	r	0.70	0.19	88.9	0.71	0.49	4.3
		<u>rs</u>	1.64	0.64	109.1	1.64	1.25	0.8
NGC 150	21.0	bar	0.62	0.23	51.3	1.08	0.26	105.7
		R' ₂ L	4.08	2.90	170.4	4.56	4.00	70.1
		R' ₁	2.94	2.06	144.8	3.49	2.67	116.9
NGC 210	19.7	r'l	1.47	0.88	169.9	1.51	1.32	30.8
		bar	1.05	0.52	172.0	1.08	0.78	21.4
		nr	0.20	0.14	155.5	0.22	0.19	112.7
NGC 244	11.6	rs	0.18	0.14	26.1	0.18	0.15	138.2
NGC 253	3.1	<u>rs</u>	5.80	1.38	52.4	7.22	5.76	80.7
		R	1.59	1.25	139.5	1.91	1.57	79.9
NGC 254	17.1	bar	0.89	0.44	132.4	0.89	0.66	2.5
		rs	0.74	0.53	62.0	0.81	0.53	71.7
NGC 255	20.0	bar	0.20	0.07	57.4	0.22	0.07	64.9
NGC 274	20.7	R	0.57	0.51	167.4	0.59	0.52	56.4
		R	6.07	4.68	139.9	7.19	5.79	69.9
		R'L	3.00	2.18	117.6	3.26	2.95	111.6
NGC 289	22.8	rs	1.35	1.11	120.4	1.63	1.35	93.4
		bar	0.69	0.26	125.4	0.69	0.38	3.1
		<u>rs</u>	0.66	0.63	43.2	0.97	0.63	91.1
		<u>rs</u>	1.23	0.69	145.3	1.43	1.13	121.6
NGC 470	40.4	bar	0.76	0.34	12.0	1.10	0.45	62.5
NGC 473	29.8	r	0.36	0.23	156.4	0.36	0.34	29.0

Table A.1. continued.

ID	D (Mpc)	Feature	$D_{r,b}$ ($'$)	$d_{r,b}$ ($'$)	$PA_{r,b}$ ($^{\circ}$)	$D_{r,b,0}$ ($'$)	$d_{r,b,0}$ ($'$)	$\theta_{r,b}$ ($^{\circ}$)
(1)	(2)	(3)	(4)	(5)	(6)	(7)	(8)	(9)
NGC 474	30.9	R' bar	2.23 0.81	2.07 0.63	67.2 16.8	2.28 0.84	2.21 0.66	62.5 130.3
NGC 485	35.7	rs	0.76	0.17	2.1	0.77	0.44	172.7
NGC 488	29.3	rl	0.92	0.76	178.1	0.95	0.88	135.4
NGC 489	33.5	R	0.67	0.08	121.3	0.67	0.30	2.3
NGC 493	25.7	rs	0.96	0.24	53.7	1.01	0.77	150.4
NGC 532	29.8	r	1.72	0.35	29.4	1.72	1.24	1.4
NGC 600	22.9	rs bar	1.07 0.23	0.76 0.04	76.0 16.9	1.09 0.24	0.81 0.04	35.4 147.7
NGC 613	25.1	bar rs nr	2.90 2.36 0.15	0.70 1.18 0.08	123.3 124.3 114.9	2.90 2.36 0.15	0.90 1.52 0.11	176.6 177.4 160.9
NGC 615	27.0	R' ₂ rl	2.26 0.69	0.70 0.21	157.8 159.0	2.26 0.69	1.72 0.51	177.3 3.2
NGC 658	36.5	rs	0.60	0.24	18.4	0.62	0.39	157.6
NGC 660	13.5	PRG	5.98	1.33	175.5	–	–	–
NGC 672	8.0	R'	3.51	1.34	69.1	3.51	2.93	1.4
NGC 676	19.5	r	1.53	0.29	174.7	1.56	0.87	15.5
NGC 691	36.0	R rs r	2.74 1.67 1.03	1.93 1.06 0.75	98.8 98.6 89.5	2.79 1.68 1.04	2.55 1.41 1.00	29.0 17.0 151.7
NGC 701	22.1	rs bar	0.59 0.21	0.30 0.06	51.9 63.0	0.64 0.24	0.53 0.10	47.5 37.4
NGC 718	21.4	R' rs bar	1.42 0.66 0.66	1.09 0.56 0.39	24.7 148.5 154.4	1.43 0.75 0.72	1.27 0.58 0.42	24.6 112.3 129.7
NGC 723	19.6	R'	0.45	0.40	151.2	0.45	0.41	179.0
NGC 755	20.2	rs	0.89	0.44	50.0	1.18	0.89	89.5
NGC 779	17.7	rs	0.94	0.30	163.4	0.98	0.85	33.8
NGC 864	17.4	rs bar	1.17 0.87	0.83 0.37	59.2 104.8	1.46 1.27	0.97 0.37	64.8 83.1
NGC 895	29.6	rs bar	0.29 0.14	0.19 0.08	94.6 158.9	0.32 0.17	0.24 0.09	138.9 64.4
NGC 908	17.6	rs	0.99	0.46	66.8	1.08	0.80	140.6
NGC 936	20.7	rs bar	1.55 1.33	1.22 0.69	139.8 81.2	1.71 1.61	1.49 0.77	64.1 120.6
NGC 941	21.2	R' r bar	2.11 0.86 0.33	1.52 0.79 0.17	169.4 113.2 13.7	2.15 1.17 0.37	2.08 0.81 0.21	54.4 95.9 43.4
NGC 986	17.2	R' bar rs nr	3.52 1.62 1.56 0.33	2.59 0.52 1.05 0.10	130.1 57.6 51.5 89.9	3.60 1.73 1.69 0.33	2.81 0.54 1.08 0.11	31.7 126.4 117.2 160.0
NGC 1015	33.1	r bar	0.81 0.73	0.67 0.35	17.7 102.3	0.81 0.85	0.77 0.35	22.7 89.9
NGC 1022	18.5	RL rs bar	2.08 0.94 0.59	1.66 0.87 0.35	143.7 59.0 107.7	2.13 1.00 0.63	1.74 0.88 0.36	138.1 76.3 109.1
NGC 1068	13.5	R nr	5.81 0.56	4.89 0.48	63.5 51.9	5.81 0.56	5.09 0.50	2.5 166.9
NGC 1073	15.2	rs bar	1.64 1.59	1.46 0.43	138.6 61.1	1.90 1.77	1.50 0.46	103.9 55.0
NGC 1079	26.1	rs bar	1.36 1.01	0.75 0.51	86.8 119.5	1.42 1.37	1.18 0.62	32.8 62.7
NGC 1087	17.5	rs bar	0.62 0.50	0.49 0.22	14.1 128.5	0.79 0.71	0.61 0.25	78.2 111.9
NGC 1090	31.7	nr'l	0.26	0.10	93.7	0.27	0.21	155.4

Table A.1. continued.

ID	D (Mpc)	Feature	$D_{r,b}$ ($'$)	$d_{r,b}$ ($'$)	$PA_{r,b}$ ($^{\circ}$)	$D_{r,b,0}$ ($'$)	$d_{r,b,0}$ ($'$)	$\theta_{r,b}$ ($^{\circ}$)
(1)	(2)	(3)	(4)	(5)	(6)	(7)	(8)	(9)
NGC 1097	20.0	R'	7.18	4.92	105.7	8.38	6.31	121.4
		rs	3.44	2.03	136.9	3.60	2.91	33.2
		bar	3.17	1.12	147.0	3.44	1.55	33.3
		nr	0.34	0.29	167.3	0.47	0.31	80.1
NGC 1163	30.9	r	0.55	0.07	142.7	0.55	0.30	178.3
NGC 1179	18.2	rs	1.18	1.10	46.0	1.33	1.18	92.0
		bar	0.44	0.21	154.4	0.53	0.21	101.7
NGC 1187	18.1	rs	1.59	0.76	115.5	1.60	1.02	167.4
		bar	1.31	0.38	131.5	1.32	0.51	12.9
NGC 1232	18.7	rs	0.78	0.51	92.2	0.78	0.59	177.0
		bar	0.78	0.35	88.9	0.78	0.41	173.2
NGC 1249	15.9	rs	1.80	0.65	75.0	1.96	1.42	142.7
NGC 1258	25.8	R'	0.78	0.35	4.5	0.80	0.47	160.0
		bar	0.31	0.21	83.3	0.42	0.21	77.3
NGC 1291	8.6	R	8.47	7.08	69.6	8.51	7.10	53.1
		bar	3.17	1.88	166.3	3.18	1.90	148.2
NGC 1297	23.5	rl	0.76	0.72	174.1	0.78	0.75	121.4
NGC 1300	18.7	R'	5.63	4.90	109.5	5.88	5.62	79.1
		bar	2.82	0.63	102.3	2.82	0.75	175.3
		nrl	0.15	0.14	114.0	0.17	0.15	84.0
NGC 1302	20.0	R	3.19	2.98	17.8	3.20	3.09	13.0
		R	2.19	1.95	60.7	2.24	1.98	57.7
		r	1.02	0.94	4.6	1.02	0.97	167.1
		bar	0.93	0.62	169.4	0.93	0.64	155.7
NGC 1310	19.7	rs	0.34	0.27	93.1	0.36	0.32	42.8
		bar	0.25	0.09	89.0	0.25	0.11	12.6
NGC 1326	17.0	R ₁	2.83	1.87	85.9	2.84	2.34	12.2
		r	1.09	0.89	63.2	1.18	1.04	120.9
		bar	1.07	0.62	18.6	1.29	0.65	109.5
		nr	0.18	0.16	61.9	0.20	0.18	112.1
NGC 1341	16.9	R'	0.70	0.57	96.8	0.73	0.57	80.2
		bar	0.30	0.10	161.9	0.30	0.10	141.9
NGC 1350	20.9	R	5.35	2.60	179.5	5.56	4.75	147.5
		r	2.25	1.15	14.1	2.49	1.97	47.4
		bar	1.86	0.78	36.7	2.56	1.08	58.3
NGC 1353	24.4	rs	1.32	0.38	135.9	1.32	0.91	174.4
NGC 1357	24.7	R'L	2.74	2.20	69.5	2.89	2.64	124.6
		rs	1.05	0.86	69.4	1.12	1.02	119.3
NGC 1365	17.9	R'	10.56	5.03	41.4	11.08	8.15	29.6
		bar	3.04	1.11	84.7	4.58	1.26	68.7
		rs	3.03	2.54	90.4	4.97	2.63	83.2
		nr	0.30	0.18	15.6	0.35	0.26	124.6
NGC 1366	18.1	rl	0.38	0.15	1.9	0.38	0.34	177.5
NGC 1367	23.3	RL	3.91	2.91	137.7	4.26	3.88	75.9
		RL	2.63	1.74	119.5	2.85	2.34	133.0
		rs	1.32	0.94	131.9	1.36	1.32	107.7
		bar	0.75	0.42	107.3	0.85	0.53	132.5
NGC 1385	15.0	rs	0.68	0.60	39.5	0.99	0.63	82.6
		bar	0.20	0.06	78.5	0.31	0.06	87.6
NGC 1386	16.2	R'	1.67	0.58	25.8	1.67	1.42	1.6
		r	0.50	0.20	24.8	0.51	0.49	157.2
NGC 1398	21.0	R	4.64	3.17	87.7	4.70	4.22	156.8
		rs	1.63	1.36	107.3	1.88	1.60	73.9
		bar	1.33	0.83	13.4	1.78	0.84	95.7
NGC 1415	17.7	RL	4.10	1.35	157.4	4.29	3.21	27.0
		r'l	1.60	0.51	145.1	1.72	1.18	147.8
		nr	0.24	0.11	164.0	0.32	0.22	63.4

Table A.1. continued.

ID	D (Mpc)	Feature	$D_{r,b}$ ($'$)	$d_{r,b}$ ($'$)	$PA_{r,b}$ ($^{\circ}$)	$D_{r,b,0}$ ($'$)	$d_{r,b,0}$ ($'$)	$\theta_{r,b}$ ($^{\circ}$)
(1)	(2)	(3)	(4)	(5)	(6)	(7)	(8)	(9)
NGC 1425	20.9	R'	4.34	1.56	132.6	4.35	3.51	6.0
		R'	2.17	0.91	134.6	2.24	2.00	33.1
		rl	0.65	0.30	137.1	0.73	0.61	57.5
NGC 1433	10.0	R' ₁	6.26	4.48	14.3	6.31	5.17	162.3
		r	2.96	2.20	96.4	3.40	2.22	78.3
		bar	2.87	1.00	95.2	3.29	1.01	74.0
		nr	0.26	0.25	151.7	0.30	0.25	97.3
NGC 1436	19.1	R'	1.59	0.99	151.8	1.60	1.40	13.7
		bar	0.66	0.29	125.7	0.72	0.39	143.6
NGC 1438	28.9	r	1.05	0.48	70.7	1.06	1.00	21.1
NGC 1448	17.4	rs	1.36	0.19	42.5	1.36	0.97	177.6
NGC 1452	22.8	RL	2.54	1.43	115.1	2.55	2.38	13.0
		r	1.63	0.91	113.7	1.63	1.53	179.8
		bar	0.91	0.48	31.6	1.52	0.48	93.8
NGC 1483	12.5	R'	0.83	0.55	141.0	0.85	0.66	28.3
		bar	0.60	0.20	2.9	0.70	0.21	63.5
NGC 1493	11.3	rs	1.23	0.99	41.5	1.23	1.01	171.4
		bar	0.89	0.34	78.0	0.90	0.34	29.0
NGC 1512	12.3	RL	5.26	4.21	64.8	5.83	5.16	108.6
		r	2.54	2.01	52.0	2.94	2.36	114.5
		bar	2.45	0.84	44.4	2.72	1.03	139.1
		nr	0.27	0.21	85.8	0.30	0.26	69.3
NGC 1515	16.9	rs	2.25	0.44	17.0	2.26	1.68	174.3
NGC 1532	17.1	rs	2.34	0.46	34.4	2.34	1.45	0.4
NGC 1533	18.4	RL	1.66	1.43	135.7	1.66	1.48	11.5
		bar	0.89	0.56	166.4	0.91	0.58	41.9
NGC 1546	13.4	R'	0.96	0.40	150.8	0.99	0.87	33.8
		r	0.53	0.17	148.0	0.53	0.39	2.9
NGC 1553	15.1	rl	1.18	0.67	150.6	1.18	0.93	174.3
		nr'l	0.30	0.16	153.7	0.30	0.23	1.8
		R' ₁	7.55	6.34	85.3	7.55	7.49	167.7
NGC 1566	11.8	r'l	4.07	3.00	14.1	4.76	3.04	101.6
		bar	3.94	2.35	12.6	4.61	2.38	102.3
		R'	1.74	1.55	150.9	1.89	1.56	99.9
NGC 1640	19.1	bar	1.01	0.38	46.5	1.01	0.41	4.2
		r	0.97	0.74	44.5	0.97	0.81	2.5
NGC 1672	14.5	R'	4.89	3.84	163.7	4.95	4.24	26.0
		bar	2.82	0.89	94.5	3.04	0.92	122.4
		rs	2.43	1.54	91.5	2.65	1.58	116.8
		nr	0.22	0.17	124.3	0.23	0.19	143.2
NGC 1808	11.6	R ₁	6.38	4.62	130.5	6.52	6.18	42.2
		bar	2.55	0.84	144.3	2.67	1.10	26.8
		nr	0.24	0.14	138.8	0.25	0.18	26.1
NGC 2460	31.9	rs	0.37	0.29	21.3	0.45	0.34	110.1
NGC 2550	36.7	R	0.82	0.23	102.0	0.82	0.54	177.6
NGC 2552	11.9	R'	1.88	1.22	53.6	1.96	1.67	35.9
NGC 2591	20.6	rs	1.18	0.16	34.7	1.21	0.86	16.8
NGC 2604	32.3	R' ₁	0.88	0.57	146.2	1.01	0.57	97.1
		bar	0.61	0.12	52.9	0.61	0.14	7.3
		rs	0.55	0.43	123.0	0.63	0.43	81.2
NGC 2608	25.5	rs	1.33	0.60	70.1	1.53	0.74	46.9
		bar	1.04	0.34	83.8	1.27	0.39	57.3
NGC 2633	30.1	rs	0.66	0.32	173.9	0.69	0.49	155.5
		bar	0.60	0.25	171.2	0.63	0.38	154.5
NGC 2648	31.8	r	0.55	0.25	150.1	0.87	0.54	81.7
NGC 2654	26.4	r	1.17	0.17	64.6	1.17	0.63	178.5

Table A.1. continued.

ID	D (Mpc)	Feature	$D_{r,b}$ ($'$)	$d_{r,b}$ ($'$)	$PA_{r,b}$ ($^{\circ}$)	$D_{r,b,0}$ ($'$)	$d_{r,b,0}$ ($'$)	$\theta_{r,b}$ ($^{\circ}$)
(1)	(2)	(3)	(4)	(5)	(6)	(7)	(8)	(9)
NGC 2681	15.3	R	2.35	2.13	105.0	2.35	2.16	165.7
		rs	0.62	0.59	172.5	0.62	0.59	66.1
		bar	0.58	0.42	76.8	0.58	0.42	138.4
NGC 2683	10.2	RL	6.82	0.91	43.8	6.83	3.50	3.8
		rs	3.34	0.39	43.3	3.34	1.48	0.8
NGC 2684	43.4	rs	0.38	0.34	35.7	0.42	0.38	105.4
NGC 2685	15.7	R	4.08	1.80	33.9	4.39	2.65	147.0
		PRG	1.36	0.70	114.0	–	–	–
NGC 2712	31.2	R'	2.73	1.16	178.0	2.74	2.36	170.2
		rs	0.85	0.52	175.3	1.07	0.84	98.5
NGC 2715	20.4	rs	1.09	0.42	23.2	1.16	1.05	53.0
NGC 2726	24.0	rs	0.47	0.13	87.3	0.47	0.34	175.3
NGC 2735	37.5	r	0.45	0.13	102.9	0.51	0.33	37.7
NGC 2743	45.3	rs	0.33	0.25	96.9	0.39	0.32	106.6
		bar	0.25	0.10	123.8	0.26	0.15	31.0
NGC 2748	21.7	PRG	1.32	0.51	134.5	–	–	–
		R'	1.08	0.21	38.2	1.11	0.70	163.5
		r	0.39	0.16	35.3	0.57	0.38	104.5
NGC 2764	37.4	rs	0.50	0.10	20.3	0.51	0.29	172.8
NGC 2770	30.0	rs	1.03	0.33	141.3	1.22	0.96	119.0
NGC 2775	17.0	r	1.42	1.06	157.2	1.44	1.30	160.4
NGC 2780	32.9	R'	0.67	0.49	146.6	0.73	0.65	114.3
		bar	0.41	0.10	115.5	0.49	0.12	129.8
		rs	0.35	0.30	165.4	0.44	0.34	83.8
NGC 2782	37.3	rs	1.01	0.87	81.8	1.10	0.95	117.7
		nr	0.15	0.11	80.8	0.17	0.13	133.6
NGC 2787	10.2	r	1.67	0.82	101.9	1.74	1.42	149.5
		bar	0.93	0.60	147.6	1.41	0.72	71.2
NGC 2793	26.3	RG	0.74	0.64	48.3	0.82	0.67	111.5
NGC 2805	28.0	R	1.60	1.26	152.1	1.69	1.52	51.4
		rs	0.53	0.36	90.5	0.63	0.39	115.5
		bar	0.37	0.25	114.7	0.40	0.30	134.5
NGC 2841	16.8	r	2.01	0.86	149.9	2.01	1.88	4.9
NGC 2844	24.1	r	0.28	0.12	10.3	0.28	0.21	169.3
NGC 2854	42.7	r	0.33	0.15	51.7	0.33	0.29	172.1
		bar	0.32	0.10	58.1	0.33	0.19	14.3
NGC 2859	25.4	R	3.42	2.73	85.5	3.48	3.38	47.9
		rl	1.33	1.16	92.7	1.47	1.31	76.5
		bar	1.13	0.71	161.6	1.41	0.71	83.4
NGC 2882	37.1	rs	0.62	0.30	77.4	0.64	0.60	143.0
NGC 2893	26.8	RL	0.87	0.69	58.4	0.88	0.73	11.6
		bar	0.37	0.22	168.0	0.38	0.22	116.6
NGC 2894	45.4	R	1.52	0.65	26.2	1.52	1.43	164.5
NGC 2903	9.1	R'	10.12	3.62	19.5	10.12	7.44	179.5
		rs	2.55	1.28	7.7	3.03	2.21	124.8
		nr	0.16	0.09	24.2	0.19	0.16	70.2
NGC 2906	33.5	rs	0.61	0.33	85.3	0.61	0.55	23.0
NGC 2962	34.2	R	2.13	1.42	7.5	2.18	2.12	108.1
		bar	0.94	0.43	174.5	0.99	0.62	151.3
		rl	0.93	0.55	2.7	0.95	0.82	155.6
NGC 2964	20.7	rs	1.18	0.58	87.3	1.25	0.92	147.9
		bar	0.63	0.29	164.6	1.00	0.31	77.9
NGC 2966	32.0	R'	2.34	1.69	46.0	2.34	2.09	8.2
		r'l	1.48	0.62	71.5	1.57	0.73	36.6
		bar	1.45	0.42	76.4	1.56	0.48	40.1
NGC 2967	30.9	R'	1.55	1.43	126.4	1.61	1.44	71.6
		rs	0.61	0.47	88.2	0.61	0.49	28.4

Table A.1. continued.

ID	D (Mpc)	Feature	$D_{r,b}$ ($'$)	$d_{r,b}$ ($'$)	$PA_{r,b}$ ($^{\circ}$)	$D_{r,b,0}$ ($'$)	$d_{r,b,0}$ ($'$)	$\theta_{r,b}$ ($^{\circ}$)
(1)	(2)	(3)	(4)	(5)	(6)	(7)	(8)	(9)
NGC 2968	25.9	bar	1.18	0.65	39.9	1.31	0.80	134.9
		rs	1.14	0.75	43.1	1.28	0.93	130.4
NGC 2974	25.3	r	1.55	0.92	38.2	1.60	1.29	154.3
NGC 2985	21.5	R'	3.34	2.13	1.3	3.36	2.69	13.6
		r'l	1.48	1.00	175.3	1.48	1.27	0.7
NGC 3003	21.3	rs	1.44	0.28	72.1	1.68	0.99	139.6
NGC 3020	23.5	rs	0.46	0.24	104.9	0.51	0.44	58.1
NGC 3031	3.7	rs	6.45	3.29	148.7	6.88	5.68	139.9
		r	4.30	2.07	157.4	4.30	3.80	6.8
NGC 3032	22.3	rl	0.61	0.54	90.2	0.68	0.61	98.3
NGC 3041	25.1	rs	1.15	0.81	84.8	1.30	1.14	104.6
NGC 3061	38.2	rs	0.59	0.41	2.2	0.61	0.48	34.8
		bar	0.35	0.15	158.7	0.35	0.18	174.6
NGC 3066	32.4	bar	0.44	0.20	91.6	0.46	0.21	135.1
		rs	0.41	0.37	39.5	0.45	0.37	88.8
NGC 3147	41.5	rs	0.67	0.65	75.3	0.81	0.65	92.0
		bar	0.64	0.51	136.3	0.66	0.59	134.7
NGC 3153	39.6	rs	0.65	0.47	172.0	1.03	0.64	84.9
NGC 3166	22.0	RL	4.11	1.73	84.4	4.17	3.03	15.2
		rl	0.92	0.66	89.8	1.21	0.90	78.8
		bar	0.61	0.51	164.9	1.09	0.51	88.9
NGC 3177	21.1	R'	0.63	0.43	130.8	0.63	0.49	169.7
		rs	0.24	0.17	27.9	0.27	0.17	75.7
NGC 3182	33.9	rl	0.19	0.16	132.4	0.20	0.19	91.8
NGC 3184	12.0	rs	0.95	0.81	142.8	0.99	0.82	96.1
NGC 3185	22.0	RL	2.51	1.65	142.6	2.65	2.41	51.5
		rs	1.27	0.73	130.6	1.29	1.10	156.8
		bar	1.13	0.45	114.6	1.25	0.62	142.6
NGC 3198	14.0	rs	1.85	0.40	40.1	1.99	1.12	27.5
NGC 3248	26.8	RL	1.77	1.10	117.8	1.79	1.77	125.6
NGC 3259	35.7	r'l	0.27	0.15	23.9	0.28	0.26	41.2
NGC 3266	29.7	RL	0.79	0.60	86.2	0.79	0.66	170.9
		bar	0.32	0.23	8.3	0.35	0.24	94.7
NGC 3301	23.3	RL	2.25	0.53	50.5	2.26	1.67	172.6
		r	0.99	0.28	53.7	1.01	0.87	26.3
NGC 3310	18.1	rs	0.30	0.19	130.7	0.31	0.21	139.9
NGC 3319	14.0	R'	5.38	2.94	37.2	5.64	4.96	139.1
		bar	0.48	0.06	39.0	0.48	0.11	172.7
NGC 3321	39.5	rs	0.54	0.34	14.0	0.76	0.50	107.9
NGC 3338	24.6	rs	0.68	0.42	92.5	0.87	0.67	98.7
NGC 3344	6.1	r	1.02	0.87	125.2	1.04	0.95	139.8
		bar	0.84	0.52	4.5	0.89	0.55	49.2
NGC 3346	22.4	rs	0.63	0.43	149.6	0.68	0.47	46.9
		bar	0.50	0.14	93.7	0.52	0.17	152.9
NGC 3351	10.1	R'	4.61	3.34	8.7	4.72	4.60	85.5
		r	2.18	1.75	6.2	2.48	2.18	93.7
		bar	2.01	1.08	112.5	2.81	1.10	98.3
		nr	0.20	0.15	26.1	0.23	0.19	63.4
NGC 3359	17.0	rs	1.44	1.32	127.1	2.31	1.39	94.6
		bar	0.62	0.12	15.7	0.77	0.16	47.3
NGC 3361	29.9	rs	0.30	0.17	171.0	0.47	0.27	72.3
NGC 3368	10.9	RL	5.94	3.57	177.8	6.04	5.31	24.5
		rs	2.42	1.58	156.1	2.73	2.13	127.2
		bar	2.09	1.20	125.0	2.82	1.35	113.2
		nrl	0.22	0.15	169.0	0.24	0.22	112.6

Table A.1. continued.

ID	D (Mpc)	Feature	$D_{r,b}$ ($'$)	$d_{r,b}$ ($'$)	$PA_{r,b}$ ($^{\circ}$)	$D_{r,b,0}$ ($'$)	$d_{r,b,0}$ ($'$)	$\theta_{r,b}$ ($^{\circ}$)
(1)	(2)	(3)	(4)	(5)	(6)	(7)	(8)	(9)
NGC 3380	28.5	RL	1.35	1.29	119.1	1.44	1.29	82.5
		bar	0.66	0.28	19.7	0.67	0.29	149.9
		<u>rs</u>	0.57	0.39	16.7	0.58	0.41	144.3
NGC 3381	28.8	<u>rs</u>	0.61	0.54	61.6	0.65	0.61	81.0
		bar	0.59	0.13	75.6	0.60	0.16	22.3
NGC 3389	21.3	<u>rs</u>	0.49	0.29	103.5	0.68	0.49	95.7
NGC 3403	25.6	<u>rs</u>	0.71	0.28	69.0	0.79	0.63	131.4
NGC 3437	24.8	<u>rs</u>	0.54	0.21	119.1	0.54	0.51	10.5
NGC 3455	29.0	<u>rs</u>	0.36	0.22	63.5	0.41	0.36	85.7
NGC 3471	28.6	R'	1.10	0.65	13.5	1.11	0.97	13.0
		bar	0.09	0.03	32.9	0.10	0.04	35.0
NGC 3485	26.3	bar	0.91	0.25	45.8	0.93	0.26	32.1
		<u>rs</u>	0.70	0.61	58.9	0.72	0.63	57.3
NGC 3486	12.2	bar	0.76	0.33	75.3	0.77	0.44	166.5
		r	0.70	0.62	84.9	0.84	0.70	89.1
NGC 3489	9.6	R	1.53	0.45	73.2	1.54	0.90	6.4
		r	0.71	0.58	39.7	1.25	0.66	97.3
NGC 3495	18.8	R'	3.05	0.58	20.1	3.06	2.18	171.6
		<u>rs</u>	1.01	0.30	20.6	1.12	1.01	99.0
NGC 3504	20.1	R' ₁	2.03	1.89	109.2	2.04	1.93	148.6
		<u>rs</u>	1.18	0.65	154.7	1.18	0.67	24.6
		bar	1.13	0.40	145.8	1.13	0.41	15.1
NGC 3507	15.8	R'	2.34	2.11	75.8	2.44	2.34	101.3
		bar	0.79	0.34	109.3	0.82	0.38	34.6
NGC 3513	13.2	<u>rs</u>	0.82	0.67	64.0	0.83	0.81	135.1
		bar	0.72	0.19	118.3	0.82	0.20	57.0
NGC 3521	12.1	rl	1.97	0.89	156.1	2.16	1.79	131.3
		r	0.83	0.27	160.0	0.83	0.59	170.6
NGC 3547	22.3	<u>rs</u>	0.41	0.17	13.0	0.44	0.32	29.0
		bar	0.25	0.07	174.7	0.26	0.13	154.4
NGC 3556	14.3	<u>rs</u>	3.87	0.86	80.6	3.87	2.94	179.3
		R'	1.96	1.04	118.7	2.00	1.30	159.6
NGC 3583	32.8	bar	0.71	0.29	77.4	0.85	0.31	117.6
		<u>rs</u>	0.69	0.53	77.4	0.84	0.56	108.5
NGC 3593	5.5	r	0.32	0.11	89.7	0.32	0.24	1.7
NGC 3611	33.3	R'	1.96	1.08	27.9	1.96	1.72	172.6
		r	0.17	0.12	17.8	0.20	0.17	113.5
NGC 3614	33.1	r	0.47	0.24	70.9	0.63	0.32	119.9
NGC 3623	12.6	R'	5.85	1.32	172.5	5.90	4.65	166.7
		<u>rs</u>	3.86	0.88	169.5	4.16	2.91	148.0
NGC 3625	32.8	<u>rs</u>	0.37	0.15	155.5	0.40	0.35	52.8
NGC 3626	23.2	RL	2.35	1.55	166.8	2.37	2.22	26.1
		R	1.47	1.07	152.9	1.62	1.41	118.6
		rl	0.69	0.47	160.6	0.70	0.67	139.0
		bar	0.66	0.33	169.8	0.66	0.47	14.8
NGC 3633	41.0	r	0.32	0.10	68.8	0.33	0.27	159.8
NGC 3637	28.2	RL	1.44	1.12	133.7	1.44	1.25	171.9
		rl	0.55	0.52	159.1	0.59	0.55	73.6
		bar	0.49	0.33	35.7	0.55	0.33	80.5
NGC 3642	27.5	rl	0.42	0.40	105.1	0.44	0.42	85.4
NGC 3664	24.4	bar	1.42	0.27	40.1	1.65	0.30	125.5
		<u>rs</u>	1.34	1.26	80.2	1.62	1.34	92.4
NGC 3673	23.3	bar	1.47	0.38	84.3	1.50	0.62	14.1
		<u>rs</u>	1.42	0.74	77.7	1.42	1.22	4.6
NGC 3675	17.2	R'	2.42	0.89	177.7	2.45	2.03	161.5
		R'	1.62	0.54	179.4	1.62	1.25	174.3
NGC 3681	24.2	r	0.60	0.51	159.8	0.63	0.53	55.8
		bar	0.26	0.16	154.8	0.27	0.18	38.6

Table A.1. continued.

ID	D (Mpc)	Feature	$D_{r,b}$ (')	$d_{r,b}$ (')	$PA_{r,b}$ (°)	$D_{r,b,0}$ (')	$d_{r,b,0}$ (')	$\theta_{r,b}$ (°)
(1)	(2)	(3)	(4)	(5)	(6)	(7)	(8)	(9)
NGC 3682	26.7	r	0.20	0.13	98.0	0.21	0.19	41.5
NGC 3683A	41.4	rs	0.46	0.24	67.8	0.47	0.36	8.5
		bar	0.18	0.11	76.7	0.19	0.15	33.5
NGC 3684	22.6	R'	1.52	0.98	114.6	1.56	1.42	147.8
		bar	0.36	0.17	128.5	0.37	0.24	17.3
NGC 3687	27.2	RL	1.43	1.34	164.6	1.49	1.35	108.7
		rs	0.44	0.41	123.7	0.46	0.41	85.5
		bar	0.43	0.21	174.8	0.44	0.22	130.4
NGC 3689	47.4	r	0.24	0.13	94.3	0.24	0.21	15.6
NGC 3691	19.4	r	0.75	0.51	11.4	0.77	0.65	150.9
		bar	0.70	0.17	31.2	0.71	0.22	13.1
NGC 3692	36.8	R'L	1.81	0.40	92.9	1.83	1.59	163.4
		r	0.68	0.15	94.0	0.68	0.61	2.7
NGC 3701	44.8	rs	0.26	0.15	155.7	0.33	0.24	67.8
NGC 3705	18.5	R'	2.53	1.06	119.6	2.54	2.00	4.8
		rs	1.17	0.49	121.8	1.18	0.92	13.3
		bar	0.42	0.37	65.5	0.77	0.38	94.9
NGC 3715	42.9	rs	0.32	0.27	112.0	0.35	0.30	119.6
		bar	0.25	0.18	75.8	0.30	0.18	108.1
NGC 3718	17.0	r	2.91	2.14	154.3	6.29	2.57	98.2
NGC 3726	17.4	r	1.50	0.84	12.1	1.54	1.31	154.0
		bar	1.38	0.30	30.2	1.43	0.47	20.2
NGC 3729	20.2	r	1.25	0.59	160.4	1.28	0.80	158.1
		bar	0.70	0.24	25.3	0.80	0.30	45.5
NGC 3730	26.9	rs	0.21	0.18	94.9	0.21	0.19	32.6
NGC 3735	40.2	rs	0.79	0.15	130.7	0.80	0.64	18.8
NGC 3755	31.7	R'	2.64	0.97	130.3	2.71	2.59	52.2
NGC 3769	15.5	R'	0.98	0.30	145.5	1.07	0.87	136.8
NGC 3780	37.2	rs	0.48	0.27	77.5	0.48	0.35	171.7
NGC 3782	14.6	rs	0.93	0.47	175.2	0.94	0.57	170.3
		bar	0.45	0.12	172.6	0.45	0.14	168.3
NGC 3786	41.6	R	1.77	0.79	75.1	1.79	1.43	17.4
		r	0.85	0.40	69.4	0.85	0.73	171.9
NGC 3788	36.5	r	0.44	0.14	0.3	0.61	0.42	72.2
NGC 3835	41.4	rs	0.51	0.16	58.8	0.51	0.48	9.3
NGC 3870	17.0	rs	0.66	0.55	28.9	0.76	0.66	82.8
		bar	0.32	0.14	29.8	0.32	0.19	12.1
NGC 3876	54.7	RG	0.56	0.39	110.0	0.68	0.55	74.0
NGC 3885	27.8	r	0.66	0.32	126.6	0.78	0.63	65.7
NGC 3887	19.3	RL	3.38	2.33	9.9	3.42	2.74	158.3
		bar	1.13	0.33	1.9	1.16	0.39	155.7
		rs	1.13	0.82	174.0	1.20	0.92	134.8
NGC 3888	39.5	rs	0.42	0.30	129.6	0.43	0.39	41.2
NGC 3892	27.2	RL	2.55	2.20	4.0	2.66	2.20	85.5
		r'l	1.16	0.91	92.6	1.16	0.94	171.5
		bar	1.13	0.60	100.5	1.13	0.63	0.9
NGC 3898	21.9	R	2.38	0.84	104.0	2.40	1.48	170.1
		R	1.80	0.65	106.2	1.81	1.14	175.3
NGC 3900	33.8	r	1.10	0.43	179.7	1.10	0.79	171.7
NGC 3936	22.6	rs	0.42	0.12	64.5	0.77	0.42	89.2
NGC 3941	15.6	R	1.78	0.94	3.9	1.80	1.47	164.0
		bar	0.70	0.39	174.9	0.76	0.57	141.3
NGC 3949	18.3	rs	0.67	0.33	117.3	0.68	0.53	164.6
		bar	0.19	0.10	113.5	0.20	0.17	143.2
NGC 3953	18.4	r	1.60	0.73	6.6	1.68	1.33	147.0
		bar	0.91	0.42	47.3	1.29	0.57	61.4
NGC 3955	20.6	rs	0.66	0.16	173.3	0.71	0.42	30.0

Table A.1. continued.

ID	D (Mpc)	Feature	$D_{r,b}$ ($'$)	$d_{r,b}$ ($'$)	$PA_{r,b}$ ($^{\circ}$)	$D_{r,b,0}$ ($'$)	$d_{r,b,0}$ ($'$)	$\theta_{r,b}$ ($^{\circ}$)
(1)	(2)	(3)	(4)	(5)	(6)	(7)	(8)	(9)
NGC 3956	25.7	rs	0.78	0.21	54.7	0.93	0.57	134.5
NGC 3976	35.5	rs	0.85	0.22	58.6	0.85	0.67	7.8
NGC 3982	22.0	rs	0.47	0.42	64.8	0.51	0.44	69.9
NGC 3985	12.9	rs	0.24	0.20	91.9	0.27	0.23	74.0
		bar	0.15	0.09	139.5	0.19	0.09	73.0
NGC 3992	24.9	rs	2.73	1.69	73.4	2.99	2.70	72.7
		bar	1.80	0.69	38.5	2.32	0.94	126.7
NGC 3998	17.9	r	1.21	1.01	139.1	1.26	1.20	73.9
NGC 4027	25.6	rs	0.65	0.56	102.3	0.79	0.57	98.6
		bar	0.22	0.06	87.0	0.28	0.06	94.9
NGC 4030	24.5	rs	0.43	0.31	34.7	0.44	0.40	21.7
NGC 4037	25.6	bar	1.08	0.40	13.3	1.13	0.44	37.1
		rs	0.91	0.85	105.0	1.05	0.86	100.1
NGC 4041	22.7	rs	0.35	0.30	83.6	0.37	0.31	55.9
		bar	0.20	0.10	74.5	0.21	0.10	37.0
NGC 4045	31.4	R'L	1.91	0.95	89.1	1.91	1.43	3.2
		rs	0.65	0.48	85.2	0.73	0.65	96.8
		bar	0.54	0.33	17.9	0.80	0.34	100.1
NGC 4050	32.5	RL	3.36	2.01	88.8	3.38	3.03	165.9
		rs	2.02	1.33	90.1	2.04	1.99	142.6
		bar	1.81	0.54	77.8	1.89	0.78	157.3
NGC 4051	14.6	bar	2.22	0.59	132.1	2.23	0.68	11.6
		rs	2.07	1.32	115.9	2.07	1.53	170.3
NGC 4062	16.3	rs	0.72	0.37	107.6	0.98	0.69	72.4
NGC 4064	10.6	RL	3.27	1.16	148.2	3.27	2.46	176.9
NGC 4067	41.2	rs	0.38	0.33	45.3	0.44	0.38	89.0
		bar	0.37	0.17	61.7	0.38	0.21	27.4
NGC 4094	19.9	R'	1.74	0.64	55.8	2.03	1.47	130.4
NGC 4100	21.4	R'L	4.65	1.48	166.1	4.80	4.36	36.1
		rs	0.94	0.29	155.0	1.14	0.72	131.7
		nr	0.12	0.05	151.7	0.18	0.10	110.2
NGC 4102	21.0	R'	1.24	0.67	42.8	1.27	1.19	42.1
		bar	0.44	0.27	57.9	0.55	0.38	62.7
NGC 4108	40.2	rs	0.26	0.17	97.0	0.26	0.21	4.2
		bar	0.13	0.08	101.4	0.13	0.09	11.0
NGC 4108B	42.3	rs	0.29	0.22	114.8	0.32	0.24	125.0
NGC 4116	21.2	rs	1.58	1.00	135.4	1.88	1.51	111.8
		bar	1.52	0.43	142.7	1.53	0.76	175.2
NGC 4120	36.5	rs	0.42	0.20	168.9	0.68	0.42	88.6
NGC 4123	21.9	bar	1.75	0.42	106.1	1.84	0.59	155.0
		rs	1.61	1.05	114.4	1.68	1.47	141.1
NGC 4136	9.7	rs	0.68	0.50	92.4	0.74	0.52	57.9
		bar	0.49	0.23	22.9	0.50	0.25	154.3
NGC 4138	15.6	r	0.74	0.40	154.3	0.76	0.68	35.8
NGC 4141	32.5	rs	0.38	0.28	57.2	0.41	0.34	125.9
		bar	0.24	0.11	86.2	0.25	0.15	17.9
NGC 4145	17.9	rs	0.79	0.35	81.1	0.88	0.55	141.6
		bar	0.36	0.16	135.6	0.49	0.20	60.9
NGC 4152	35.3	rs	0.32	0.27	93.5	0.38	0.30	107.1
		bar	0.17	0.11	40.9	0.22	0.11	94.3
NGC 4158	38.9	RL	0.62	0.44	68.5	0.62	0.57	5.0
		r	0.30	0.21	77.4	0.31	0.27	32.4
		bar	0.23	0.13	52.0	0.24	0.17	151.3
NGC 4162	38.1	r	0.37	0.22	166.8	0.37	0.34	161.7
NGC 4178	17.0	R' ₂	3.53	1.07	31.3	3.81	3.51	101.7
NGC 4189	28.1	bar	0.84	0.24	102.5	0.91	0.28	38.7
		rs	0.73	0.58	109.5	0.86	0.64	66.1

Table A.1. continued.

ID	D (Mpc)	Feature	$D_{r,b}$ ($'$)	$d_{r,b}$ ($'$)	$PA_{r,b}$ ($^{\circ}$)	$D_{r,b,0}$ ($'$)	$d_{r,b,0}$ ($'$)	$\theta_{r,b}$ ($^{\circ}$)
(1)	(2)	(3)	(4)	(5)	(6)	(7)	(8)	(9)
NGC 4192	16.0	R'	7.96	1.67	155.5	7.97	5.39	175.6
		rs	4.10	0.81	151.2	4.32	2.47	156.4
NGC 4193	37.4	RL	1.75	0.79	88.3	1.75	1.71	159.0
		rs	0.44	0.28	95.5	0.63	0.43	82.0
NGC 4210	43.2	rs	0.47	0.33	123.0	0.54	0.39	55.8
		bar	0.38	0.16	45.4	0.46	0.17	121.3
NGC 4212	19.0	rs	0.72	0.40	76.5	0.72	0.61	6.2
NGC 4216	17.1	R'	5.84	0.55	20.9	5.85	3.02	3.9
		r	1.86	0.26	19.2	1.89	1.42	165.5
NGC 4220	17.9	r	1.17	0.21	137.8	1.17	0.70	172.7
NGC 4224	41.9	R'	1.44	0.28	57.8	1.45	0.70	9.4
NGC 4234	32.9	bar	0.64	0.11	78.3	0.67	0.13	33.5
		rs	0.54	0.37	71.3	0.56	0.43	37.9
NGC 4237	23.5	R'	1.14	0.71	105.8	1.15	1.14	37.5
NGC 4245	9.7	RL	2.65	1.89	16.6	2.72	2.20	30.5
		bar	1.25	0.61	136.5	1.38	0.66	128.1
		r	1.21	0.90	151.8	1.30	1.01	132.4
		nr	0.16	0.13	176.3	0.16	0.15	168.2
NGC 4250	33.4	R	3.10	2.68	83.8	3.19	2.96	133.1
		rl	1.43	1.01	166.5	1.60	1.02	73.7
		bar	1.43	0.60	165.1	1.60	0.61	69.8
NGC 4256	39.1	R	2.37	0.20	41.6	2.37	1.10	0.3
NGC 4258	7.4	R	16.51	5.47	146.6	23.39	15.26	69.9
		rs	6.33	2.03	155.7	10.90	4.66	66.2
NGC 4260	38.3	rs	1.12	0.62	57.9	1.61	1.12	89.4
NGC 4268	29.6	rs	0.66	0.21	48.6	0.67	0.42	13.6
NGC 4274	16.8	R	5.92	1.50	100.8	5.93	4.41	177.3
		r	2.79	0.91	100.3	2.81	2.66	155.6
		nr	0.26	0.08	102.7	0.26	0.24	29.5
NGC 4286	7.0	RL	0.78	0.55	160.2	0.91	0.77	74.3
NGC 4293	14.3	R	4.20	2.11	64.4	4.51	4.19	86.2
		rs	2.49	0.99	72.8	2.71	1.96	36.5
NGC 4298	15.0	R'	2.13	0.96	138.3	2.20	1.62	22.8
		rs	0.71	0.25	132.5	0.71	0.43	3.4
NGC 4303	16.5	bar	1.86	0.56	2.1	1.95	0.60	42.4
		rs	1.59	1.33	81.0	1.76	1.35	106.8
NGC 4309	13.7	rl	0.99	0.37	90.5	1.00	0.68	172.5
		bar	0.66	0.34	73.9	0.80	0.52	126.3
NGC 4310	9.7	rs	0.43	0.14	157.2	0.43	0.30	177.0
NGC 4313	16.1	R'	1.40	0.20	142.0	1.41	0.87	4.5
NGC 4314	9.7	R' ₁	3.72	3.03	51.2	3.72	3.23	179.4
		bar	2.22	0.80	146.9	2.37	0.80	94.9
		rl	2.07	1.74	155.1	2.20	1.74	99.8
		nr	0.23	0.18	140.0	0.25	0.18	88.7
NGC 4316	28.6	rs	0.95	0.06	111.9	0.95	0.39	2.1
NGC 4319	28.2	R'	2.16	1.69	168.0	2.32	2.00	53.9
		rs	1.12	0.61	134.4	1.16	0.76	154.5
		bar	0.60	0.30	162.8	0.61	0.37	19.2
NGC 4321	15.9	bar	2.22	0.90	107.9	2.52	0.96	122.5
		rs	2.03	1.70	103.0	2.38	1.75	106.3
		nr	0.30	0.24	158.6	0.30	0.29	1.6
NGC 4324	31.6	r	0.72	0.32	54.0	0.75	0.71	119.1
NGC 4336	14.2	r	0.59	0.32	167.0	0.60	0.53	26.8
		bar	0.28	0.18	101.7	0.45	0.19	102.2
NGC 4343	27.7	R'	0.92	0.14	127.5	0.93	0.41	171.3
		r	0.45	0.10	132.9	0.46	0.28	12.6
NGC 4344	14.1	r	0.31	0.27	155.8	0.35	0.27	94.8
NGC 4348	34.5	rs	0.68	0.14	33.8	0.71	0.58	151.3

Table A.1. continued.

ID	D (Mpc)	Feature	$D_{r,b}$ ($'$)	$d_{r,b}$ ($'$)	$PA_{r,b}$ ($^{\circ}$)	$D_{r,b,0}$ ($'$)	$d_{r,b,0}$ ($'$)	$\theta_{r,b}$ ($^{\circ}$)
(1)	(2)	(3)	(4)	(5)	(6)	(7)	(8)	(9)
NGC 4351	18.4	R'	1.25	0.83	76.9	1.38	1.11	51.4
NGC 4355	34.7	R'L	0.97	0.49	60.1	1.01	0.95	129.5
		bar	0.63	0.32	61.6	0.63	0.62	127.3
NGC 4369	21.6	R	1.42	1.30	156.8	1.45	1.31	62.2
		rs	0.28	0.25	105.6	0.28	0.26	5.9
		bar	0.27	0.10	150.5	0.27	0.10	50.2
NGC 4371	16.8	r	2.09	1.04	91.1	2.14	1.97	35.1
		bar	1.13	0.84	158.0	2.13	0.86	84.7
		nr	0.35	0.14	87.3	0.35	0.27	177.0
NGC 4378	27.8	R'	2.93	2.45	178.5	2.99	2.85	43.2
NGC 4380	19.9	R	2.02	1.07	156.5	2.03	1.93	169.8
		r	0.98	0.54	151.8	1.04	0.92	132.5
NGC 4384	36.6	rs	0.30	0.15	75.5	0.30	0.20	168.3
		bar	0.07	0.04	157.9	0.09	0.04	80.3
NGC 4385	33.5	rs	1.03	0.60	84.7	1.10	0.96	46.6
		bar	0.97	0.37	99.4	1.12	0.55	41.7
NGC 4388	21.4	rs	1.39	0.17	89.3	1.40	0.62	172.4
NGC 4389	15.5	rs	1.50	0.75	101.9	1.52	1.16	15.7
		bar	1.38	0.25	104.6	1.40	0.38	13.4
NGC 4394	16.8	R	2.74	2.45	77.5	2.99	2.60	113.0
		bar	1.52	0.65	142.2	1.60	0.72	38.3
		rs	1.50	1.31	129.2	1.58	1.44	58.5
NGC 4402	16.7	R'	1.86	0.20	89.8	1.95	1.28	23.2
NGC 4405	14.1	R	1.05	0.66	24.2	1.05	0.87	13.3
		rs	0.37	0.32	13.8	0.42	0.37	96.4
		bar	0.34	0.14	7.9	0.34	0.18	163.6
NGC 4411A	16.8	rs	0.57	0.43	32.6	0.68	0.43	94.5
		bar	0.16	0.03	109.7	0.16	0.03	173.4
NGC 4412	35.6	rs	0.73	0.56	77.9	0.73	0.58	24.3
		bar	0.54	0.16	119.7	0.56	0.16	63.5
NGC 4413	16.7	R'L	2.81	1.52	68.5	2.81	2.14	178.2
		rs	1.28	0.64	58.6	1.31	0.88	159.1
		bar	0.49	0.24	14.2	0.64	0.26	112.6
NGC 4414	18.3	rl	0.68	0.39	145.2	0.82	0.60	122.0
NGC 4416	13.8	RL	1.08	1.01	98.4	1.17	1.07	82.4
		rs	0.41	0.32	66.6	0.43	0.36	139.6
		bar	0.19	0.06	7.5	0.22	0.06	97.7
NGC 4424	16.0	R'L	3.18	1.53	89.9	3.25	2.70	22.5
		bar	1.62	0.58	97.6	1.73	0.98	29.1
NGC 4430	17.0	rs	0.56	0.51	102.8	0.62	0.54	72.6
		bar	0.50	0.21	118.1	0.55	0.22	50.5
NGC 4448	26.5	R'	2.50	0.74	92.6	2.50	2.28	10.9
		r	1.47	0.49	92.2	1.51	1.47	82.6
NGC 4450	16.5	R'	3.43	2.20	164.1	3.56	3.04	145.7
		rs	1.51	0.96	10.0	1.64	1.28	44.2
		bar	1.46	0.68	7.0	1.52	0.94	25.0
NGC 4451	26.6	r	0.43	0.23	157.4	0.43	0.32	172.6
NGC 4454	35.7	RL	2.00	1.83	105.1	2.09	1.83	83.0
		r	1.09	0.80	34.4	1.10	0.83	10.0
		bar	1.02	0.49	22.0	1.02	0.51	175.8
NGC 4457	17.4	R	4.04	3.76	78.8	4.11	3.98	52.8
		R	2.42	2.24	162.7	2.61	2.24	93.3
		bar	0.97	0.61	65.8	0.97	0.65	179.3
NGC 4460	8.8	r	0.42	0.13	38.9	0.49	0.42	95.4
NGC 4461	16.8	r	1.47	0.54	5.1	1.58	1.34	134.2
NGC 4462	26.2	rs	1.33	0.41	118.6	1.33	0.90	174.8
NGC 4491	3.6	rs	0.89	0.43	151.7	0.94	0.80	38.4
		bar	0.40	0.18	130.3	0.46	0.29	134.4

Table A.1. continued.

ID	D (Mpc)	Feature	$D_{r,b}$ ($'$)	$d_{r,b}$ ($'$)	$PA_{r,b}$ ($^{\circ}$)	$D_{r,b,0}$ ($'$)	$d_{r,b,0}$ ($'$)	$\theta_{r,b}$ ($^{\circ}$)
(1)	(2)	(3)	(4)	(5)	(6)	(7)	(8)	(9)
NGC 4492	16.8	rs	0.48	0.42	55.9	0.50	0.45	55.0
NGC 4496A	15.6	rs	0.99	0.89	70.0	1.02	0.98	70.5
		bar	0.53	0.11	52.6	0.53	0.12	168.7
NGC 4498	15.8	rs	1.24	0.62	129.4	1.29	0.97	153.2
		bar	1.05	0.19	123.5	1.10	0.30	155.6
NGC 4501	19.1	rs	1.55	0.61	137.4	1.59	1.18	159.9
NGC 4504	18.6	rs	0.93	0.71	134.1	1.18	0.92	98.6
		bar	0.36	0.18	149.4	0.37	0.29	25.2
NGC 4519	28.4	rs	0.67	0.54	69.2	0.85	0.54	95.5
		bar	0.49	0.24	69.9	0.62	0.24	99.1
NGC 4522	16.8	R'	2.38	0.56	32.9	2.41	2.12	158.6
		r	1.32	0.36	35.4	1.39	1.28	57.7
		rs	0.74	0.17	35.1	0.75	0.65	14.5
NGC 4525	12.6	R'	1.28	0.56	34.9	1.49	0.87	136.0
		bar	0.46	0.20	80.2	0.58	0.28	53.2
NGC 4527	21.6	R' ₂	4.75	0.95	65.4	4.79	3.41	169.1
		rs	1.56	0.33	68.4	1.58	1.20	12.4
		nr	0.23	0.07	61.7	0.28	0.20	120.4
NGC 4528	17.6	r	0.37	0.19	5.4	0.37	0.32	176.7
		bar	0.17	0.15	63.9	0.28	0.15	85.0
NGC 4531	15.2	rs	0.69	0.46	164.8	0.74	0.64	51.1
NGC 4536	15.3	rs	3.05	0.85	121.1	3.11	1.92	164.8
NGC 4540	16.8	rs	0.69	0.66	111.6	0.72	0.66	72.5
		bar	0.30	0.12	53.6	0.30	0.13	177.4
NGC 4548	16.2	rs	2.04	1.52	85.2	2.56	1.56	103.7
		bar	1.93	0.90	61.3	2.49	0.90	91.5
NGC 4565	12.9	r	3.12	0.22	135.6	3.13	1.33	3.3
NGC 4567	25.6	rs	0.51	0.37	36.6	0.71	0.41	106.7
		bar	0.28	0.21	56.0	0.36	0.25	109.9
NGC 4568	20.9	rs	0.41	0.22	22.4	0.50	0.40	108.9
NGC 4569	12.4	rs	4.01	1.76	17.5	4.73	3.66	121.4
		x ₁ r	2.20	0.38	16.0	2.34	0.87	156.3
NGC 4579	19.6	RL	4.33	3.10	96.7	4.39	4.10	27.5
		R'	3.13	2.20	98.7	3.18	2.90	29.6
		rs	2.22	1.34	66.1	2.44	1.62	135.4
		bar	1.41	0.73	59.2	1.59	0.87	132.3
NGC 4580	20.6	R'	1.86	1.26	161.6	1.88	1.64	20.8
		rs	1.12	0.81	158.3	1.12	1.06	19.4
		rs	0.67	0.40	156.2	0.68	0.52	2.4
NGC 4591	50.5	bar	0.28	0.10	38.7	0.28	0.19	6.2
		rs	0.26	0.15	31.1	0.30	0.26	115.2
NGC 4593	33.9	R'	3.54	2.51	108.2	3.55	3.00	8.0
		rs	2.03	1.30	81.4	2.11	1.50	145.3
		bar	1.75	0.70	57.5	1.95	0.75	126.2
NGC 4594	10.4	R	4.59	0.44	89.0	4.59	1.06	0.4
NGC 4596	16.8	RL	3.40	2.66	140.1	3.63	3.07	49.1
		rs	2.11	1.44	82.3	2.34	1.60	126.7
		bar	1.79	0.85	74.1	2.01	0.92	125.8
NGC 4597	17.0	R'	2.52	1.09	39.6	2.65	2.40	131.3
NGC 4618	7.3	R'	2.26	2.03	33.2	2.78	2.22	81.0
		rs	1.17	0.94	82.2	1.55	0.95	81.4
		bar	0.68	0.25	65.3	0.83	0.27	61.8
NGC 4625	8.2	R'	0.95	0.85	151.3	0.96	0.90	159.8
		rs	0.33	0.28	80.8	0.35	0.28	96.9
		bar	0.27	0.17	23.2	0.28	0.18	46.1
NGC 4628	42.9	R'	1.12	0.19	44.4	1.13	0.66	176.9

Table A.1. continued.

ID	D (Mpc)	Feature	$D_{r,b}$ ($'$)	$d_{r,b}$ ($'$)	$PA_{r,b}$ ($^{\circ}$)	$D_{r,b,0}$ ($'$)	$d_{r,b,0}$ ($'$)	$\theta_{r,b}$ ($^{\circ}$)
(1)	(2)	(3)	(4)	(5)	(6)	(7)	(8)	(9)
NGC 4639	22.4	R'	2.36	1.38	116.4	2.63	1.90	134.2
		rs	0.89	0.79	127.6	1.22	0.89	92.5
		bar	0.84	0.37	169.5	1.03	0.47	53.3
NGC 4641	13.9	rl	0.19	0.17	35.4	0.20	0.18	119.4
NGC 4643	25.7	r	1.82	1.55	54.8	1.95	1.82	95.6
		bar	1.59	0.84	132.3	1.96	0.85	79.5
NGC 4647	18.3	rs	0.27	0.17	12.2	0.35	0.18	74.3
		bar	0.14	0.09	114.1	0.14	0.11	147.0
NGC 4651	26.7	rs	0.80	0.49	79.5	0.85	0.80	74.5
NGC 4654	16.3	rs	1.17	0.73	126.8	1.36	1.14	71.3
		bar	0.84	0.27	120.1	0.84	0.49	178.6
NGC 4658	28.6	bar	0.31	0.08	36.0	0.41	0.11	52.8
		rs	0.30	0.22	40.3	0.46	0.25	75.0
NGC 4659	3.7	R	1.04	0.64	2.8	1.06	0.86	25.0
		bar	0.26	0.22	72.4	0.36	0.22	86.1
NGC 4680	34.6	rs	0.53	0.28	58.1	0.55	0.35	31.3
		bar	0.31	0.12	168.5	0.37	0.13	121.0
NGC 4682	32.0	r	0.22	0.16	82.6	0.32	0.22	90.9
NGC 4689	17.9	R	1.86	1.51	165.3	1.88	1.85	62.0
		rs	0.57	0.44	127.2	0.64	0.48	120.1
NGC 4691	22.5	R'L	2.79	2.15	25.3	2.81	2.59	161.7
		R'	1.58	1.37	73.0	1.82	1.44	70.9
		bar	0.46	0.10	98.2	0.55	0.10	71.7
NGC 4698	23.7	R	7.91	2.73	167.7	7.91	4.85	2.2
		r	2.15	0.71	169.4	2.15	1.25	6.3
		r	1.58	0.50	168.9	1.58	0.89	5.0
NGC 4699	24.7	R'	1.95	1.49	47.9	1.97	1.72	20.3
		bar	0.41	0.22	48.5	0.42	0.26	13.2
NGC 4710	16.8	nr	0.31	0.03	28.6	0.31	0.14	7.1
NGC 4713	16.4	rs	0.44	0.38	65.0	0.61	0.42	98.6
		bar	0.38	0.14	84.9	0.39	0.22	164.6
NGC 4722	67.1	rs	0.65	0.18	30.5	0.65	0.48	167.1
NGC 4725	13.6	bar	4.35	1.37	48.8	4.53	1.93	23.5
		r	4.14	2.34	34.2	4.14	3.42	0.7
NGC 4736	5.1	R	10.58	8.68	134.8	10.94	10.13	47.1
		bar	4.71	3.48	94.4	5.07	3.91	131.4
		rl	4.48	3.47	103.9	4.70	3.99	136.6
		nr'	1.48	1.13	114.0	1.50	1.34	152.9
NGC 4746	33.6	R'	1.45	0.17	119.0	1.45	0.77	176.2
NGC 4750	26.1	R'	1.52	1.33	156.7	1.69	1.51	101.5
		rs	0.55	0.49	146.0	0.63	0.53	103.6
NGC 4771	20.3	r	0.62	0.20	139.8	0.93	0.58	72.3
NGC 4772	30.5	R'	3.85	1.93	147.4	3.86	3.68	19.5
		r	2.36	0.61	145.3	2.36	1.16	178.0
NGC 4779	40.8	bar	0.95	0.29	9.2	1.13	0.31	114.2
		rs	0.79	0.62	14.0	0.94	0.65	107.7
NGC 4791	41.2	rl	0.32	0.18	55.7	0.33	0.25	155.8
		bar	0.21	0.14	90.2	0.23	0.17	55.1
NGC 4793	33.8	rs	0.50	0.31	59.7	0.60	0.47	65.0
NGC 4795	32.9	R'	1.38	1.13	116.5	1.56	1.38	87.1
		bar	0.33	0.23	23.8	0.45	0.23	89.5
NGC 4800	22.5	R'	1.22	0.97	40.5	1.34	1.16	61.5
		rs	0.34	0.24	33.8	0.35	0.31	33.9
NGC 4814	39.3	R'	1.45	0.85	117.8	1.47	1.08	159.3
		rs	0.84	0.58	112.0	0.89	0.72	141.2
NGC 4818	20.1	R	2.43	0.67	1.0	2.48	1.70	164.2

Table A.1. continued.

ID	D (Mpc)	Feature	$D_{r,b}$ ($'$)	$d_{r,b}$ ($'$)	$PA_{r,b}$ ($^{\circ}$)	$D_{r,b,0}$ ($'$)	$d_{r,b,0}$ ($'$)	$\theta_{r,b}$ ($^{\circ}$)
(1)	(2)	(3)	(4)	(5)	(6)	(7)	(8)	(9)
NGC 4826	5.3	R'	7.17	3.10	117.1	7.18	5.59	4.5
		rs	2.73	1.44	117.9	2.75	2.57	22.6
		r	1.43	0.70	112.9	1.44	1.26	162.3
NGC 4845	19.4	R'	4.35	0.87	82.0	4.47	3.30	19.9
		rs	2.09	0.34	76.2	2.17	1.29	159.5
NGC 4856	21.1	RL	2.44	0.65	36.2	2.46	1.79	169.3
NGC 4866	23.8	rl	2.52	0.31	87.0	2.53	1.29	175.4
NGC 4880	15.7	RL	2.05	1.48	148.0	2.13	1.80	143.2
		rl	0.89	0.63	167.8	0.89	0.79	15.3
		bar	0.29	0.18	169.0	0.30	0.22	11.7
NGC 4897	43.1	rs	0.48	0.31	164.9	0.48	0.37	21.2
		bar	0.40	0.20	5.7	0.43	0.23	42.1
NGC 4900	24.7	R'	1.18	0.99	118.9	1.19	1.03	150.6
		bar	0.72	0.23	140.1	0.72	0.24	179.3
NGC 4902	39.2	rs	0.88	0.79	171.9	0.95	0.79	78.0
		bar	0.88	0.36	68.4	0.90	0.38	144.2
NGC 4941	18.2	RL	3.33	2.36	22.5	3.33	3.09	175.5
		rs	1.96	0.96	20.0	1.97	1.25	174.2
NGC 4951	15.1	R'	1.67	0.64	90.8	1.89	1.67	95.8
		rs	0.61	0.25	88.5	0.76	0.60	104.3
NGC 4961	43.1	rs	0.40	0.26	105.3	0.41	0.36	25.1
		bar	0.21	0.11	133.9	0.25	0.14	53.3
NGC 4980	18.2	R'	1.17	0.53	173.5	1.19	1.01	22.8
		bar	0.89	0.41	159.1	0.98	0.72	139.2
NGC 4984	21.3	R'	5.07	2.82	24.7	5.07	4.77	0.5
		R	3.26	1.90	20.1	3.39	3.10	136.6
		bar	0.93	0.65	92.2	1.53	0.67	81.9
NGC 4995	29.1	rs	0.72	0.63	118.6	1.01	0.69	82.4
		bar	0.64	0.31	34.5	0.93	0.33	107.1
NGC 5005	19.9	R' ₂	3.53	1.23	63.2	3.66	3.01	151.8
		rs	1.24	0.42	71.5	1.29	1.02	28.4
NGC 5016	43.3	rs	0.24	0.14	77.5	0.25	0.18	27.1
		bar	0.12	0.09	18.7	0.15	0.10	113.2
NGC 5033	19.6	R'	8.84	4.26	167.0	9.07	7.75	153.3
		rs	0.52	0.19	170.9	0.52	0.35	178.0
NGC 5054	19.2	R'	4.45	2.48	157.6	4.45	4.06	6.7
		nr	0.19	0.11	166.9	0.20	0.16	40.5
NGC 5055	8.3	rs	1.40	0.64	93.8	1.45	1.10	152.6
		rl	0.69	0.31	100.0	0.69	0.57	173.5
NGC 5068	6.1	rs	2.06	1.79	69.2	2.07	1.82	145.0
		bar	0.79	0.21	150.5	0.81	0.22	52.2
NGC 5078	26.9	r	0.71	0.09	146.0	0.71	0.27	177.5
NGC 5079	31.6	R'	0.68	0.42	25.2	0.82	0.68	100.4
		bar	0.36	0.16	157.6	0.61	0.19	108.2
NGC 5085	28.9	rs	0.28	0.19	45.8	0.28	0.21	171.6
NGC 5088	22.6	R	1.43	0.41	177.2	1.44	1.17	164.9
NGC 5101	27.4	R' ₂	5.31	4.61	153.9	5.46	4.84	45.4
		R ₁	4.24	3.37	3.8	4.50	3.42	66.1
		rs	1.70	1.41	122.3	1.70	1.52	175.6
		bar	1.62	0.76	122.0	1.62	0.82	176.7
NGC 5105	35.5	rs	0.54	0.42	134.8	0.57	0.54	93.6
		bar	0.19	0.10	1.4	0.23	0.11	60.4
NGC 5112	21.4	rs	1.37	0.59	118.5	1.37	0.88	177.5
		bar	0.33	0.05	131.5	0.33	0.08	18.1
NGC 5117	39.6	R'	1.08	0.69	160.6	1.31	1.05	73.1
		bar	0.78	0.24	157.5	0.79	0.44	12.0
NGC 5122	41.9	PRG	1.79	0.16	25.6	–	–	–

Table A.1. continued.

ID	D (Mpc)	Feature	$D_{r,b}$ ($'$)	$d_{r,b}$ ($'$)	$PA_{r,b}$ ($^{\circ}$)	$D_{r,b,0}$ ($'$)	$d_{r,b,0}$ ($'$)	$\theta_{r,b}$ ($^{\circ}$)
(1)	(2)	(3)	(4)	(5)	(6)	(7)	(8)	(9)
NGC 5134	11.0	R	3.53	2.99	71.8	3.53	3.09	171.0
		bar	1.55	0.60	154.7	1.60	0.60	76.3
		rs	1.51	0.74	150.2	1.56	0.74	72.1
NGC 5145	39.4	r	0.34	0.18	86.5	0.34	0.23	21.1
NGC 5147	21.6	R'	1.10	0.96	128.3	1.19	1.09	77.2
		bar	0.35	0.18	12.0	0.42	0.18	76.8
NGC 5170	28.8	R'	4.85	0.29	126.0	4.85	1.97	177.9
NGC 5194	7.9	rs	0.84	0.75	87.0	0.97	0.77	73.4
		bar	0.74	0.50	138.4	0.88	0.50	96.3
		nr'	0.44	0.41	79.8	0.50	0.42	77.3
NGC 5195	7.9	r	1.54	1.41	130.5	1.91	1.51	81.7
		bar	1.34	0.84	177.8	1.74	0.85	80.1
NGC 5205	29.3	rs	0.55	0.38	167.0	0.70	0.55	89.5
		bar	0.37	0.19	107.5	0.63	0.21	103.9
NGC 5218	50.8	rs	0.63	0.35	69.3	0.72	0.36	114.2
		bar	0.45	0.17	97.9	0.48	0.19	143.6
NGC 5236	7.0	bar	4.18	1.29	53.7	4.33	1.32	51.5
		nr	0.33	0.20	158.5	0.33	0.21	151.5
NGC 5247	22.2	r	0.30	0.25	5.3	0.34	0.26	108.8
NGC 5248	19.2	R'	5.97	4.36	100.2	5.99	5.55	163.7
		bar	2.81	1.17	125.2	2.94	1.44	29.5
		nr	0.22	0.19	139.5	0.26	0.20	68.9
NGC 5289	38.3	R'	1.31	0.24	97.7	1.32	0.90	168.2
		rl	0.42	0.09	98.8	0.42	0.36	170.8
NGC 5300	20.9	rs	0.55	0.32	133.6	0.61	0.45	135.7
		bar	0.30	0.18	163.9	0.33	0.26	47.7
NGC 5313	37.8	r	0.42	0.24	49.8	0.43	0.40	38.1
NGC 5320	34.4	r'l	0.23	0.15	20.7	0.31	0.23	85.1
NGC 5334	24.7	rs	0.84	0.78	118.3	1.10	0.78	92.7
		bar	0.44	0.15	47.1	0.48	0.17	41.7
		x ₁ l	0.42	0.11	44.7	0.45	0.14	38.1
NGC 5336	39.7	rs	0.23	0.17	44.5	0.28	0.18	109.4
		bar	0.20	0.12	78.9	0.21	0.14	145.5
NGC 5337	52.2	rs	0.41	0.22	18.3	0.48	0.40	104.3
NGC 5338	12.8	rs	0.48	0.30	90.8	0.62	0.48	95.1
NGC 5339	41.7	rs	0.92	0.76	22.2	1.05	0.86	113.3
		bar	0.79	0.23	81.8	0.87	0.27	42.2
NGC 5347	27.3	bar	1.01	0.42	100.9	1.01	0.45	12.8
		rs	1.00	0.73	105.7	1.01	0.78	21.4
NGC 5350	30.6	rs	0.80	0.53	42.6	0.83	0.80	100.6
		bar	0.73	0.29	122.1	1.13	0.29	83.3
NGC 5364	20.2	r	1.15	0.66	40.2	1.16	0.98	16.2
NGC 5371	35.3	rs	0.82	0.62	42.2	0.90	0.71	51.6
		bar	0.70	0.42	99.8	0.88	0.42	86.1
NGC 5375	37.8	R'	2.24	1.82	164.7	2.25	2.09	16.0
		bar	0.91	0.38	168.0	0.91	0.44	10.7
		rs	0.85	0.75	7.0	0.91	0.81	61.4
NGC 5376	44.6	rs	0.57	0.38	57.8	0.66	0.56	106.2
NGC 5377	27.7	R ₁	4.05	2.03	21.4	4.19	3.64	146.7
		bar	3.17	1.11	44.3	3.62	1.81	39.0
NGC 5383	37.8	rs	1.98	1.72	102.4	2.11	1.96	106.2
		bar	1.67	0.61	123.5	1.69	0.73	16.6
		nr	0.29	0.14	79.1	0.31	0.16	139.6
NGC 5426	35.9	rs	0.66	0.31	4.2	0.78	0.53	49.8
		bar	0.17	0.10	177.2	0.20	0.16	69.8
NGC 5427	33.8	r	0.22	0.15	29.3	0.24	0.16	130.2
NGC 5430	41.7	R'	1.59	0.83	12.1	1.63	1.23	22.0
		bar	0.56	0.23	153.6	0.65	0.29	133.2

Table A.1. continued.

ID	D (Mpc)	Feature	$D_{r,b}$ ($'$)	$d_{r,b}$ ($'$)	$PA_{r,b}$ ($^{\circ}$)	$D_{r,b,0}$ ($'$)	$d_{r,b,0}$ ($'$)	$\theta_{r,b}$ ($^{\circ}$)
(1)	(2)	(3)	(4)	(5)	(6)	(7)	(8)	(9)
NGC 5443	31.9	R'L	2.50	0.73	36.9	2.52	1.94	10.8
		rs	1.38	0.36	34.3	1.38	0.96	176.2
NGC 5448	33.7	R ₁	3.34	1.34	115.7	3.62	2.96	43.3
		rs	1.67	0.54	110.2	1.67	1.28	179.9
NGC 5457	6.9	rs	1.81	1.60	178.7	1.88	1.65	124.1
		bar	0.84	0.58	80.4	0.87	0.60	48.7
NGC 5472	45.2	R'	0.59	0.17	35.0	0.59	0.45	172.4
NGC 5492	38.8	rs	0.40	0.09	150.0	0.40	0.33	18.8
NGC 5523	20.0	rs	0.81	0.22	89.8	0.89	0.72	135.6
NGC 5534	31.8	R'L	1.21	0.83	170.3	1.30	0.86	58.7
		rs	0.50	0.37	77.6	0.53	0.39	127.2
		bar	0.50	0.22	74.9	0.53	0.23	130.3
NGC 5566	23.3	R'	5.07	1.47	36.0	5.09	3.99	7.4
		r	1.35	0.74	24.8	2.10	1.28	102.6
		nr'	0.20	0.08	34.1	0.22	0.20	100.3
NGC 5577	21.8	rs	0.40	0.16	62.3	0.60	0.37	72.2
NGC 5584	23.9	rs	0.31	0.27	27.4	0.42	0.29	80.0
		bar	0.27	0.14	35.9	0.36	0.15	70.1
NGC 5587	38.9	r	0.64	0.16	158.2	0.67	0.45	157.0
NGC 5595	36.2	rs	0.36	0.31	53.0	0.51	0.36	87.9
NGC 5600	87.8	bar	0.44	0.20	155.6	0.45	0.21	166.1
		rs	0.44	0.35	144.0	0.45	0.37	147.0
NGC 5602	38.0	RL	1.05	0.54	166.2	1.05	0.97	165.1
NGC 5633	44.5	r	0.46	0.30	10.3	0.46	0.39	157.7
NGC 5636	29.7	r	0.84	0.52	35.3	0.85	0.56	152.1
		bar	0.68	0.23	76.3	0.68	0.26	20.6
NGC 5665	27.6	rs	0.95	0.60	139.8	1.09	0.85	123.9
		bar	0.20	0.09	128.9	0.24	0.12	133.3
NGC 5668	26.9	rs	0.41	0.37	146.7	0.43	0.41	79.8
		bar	0.38	0.25	106.5	0.41	0.27	134.3
NGC 5669	20.2	rs	0.38	0.31	89.1	0.45	0.35	70.5
		bar	0.17	0.04	40.5	0.17	0.05	152.4
NGC 5678	32.9	R'	2.31	1.17	1.3	2.32	2.14	169.1
		rs	1.35	0.57	178.3	1.36	1.03	164.9
NGC 5689	35.6	R'	2.50	0.40	83.9	2.50	1.49	179.1
		rl	1.05	0.25	87.0	1.10	0.88	31.5
NGC 5690	21.3	R'	2.03	0.39	141.6	2.03	1.60	177.2
NGC 5701	26.1	R' ₁	3.21	2.72	77.2	3.24	2.80	32.7
		rl	1.34	1.08	178.3	1.37	1.10	123.6
		bar	1.28	0.74	177.2	1.31	0.75	125.1
NGC 5713	23.8	R'	1.67	1.48	87.2	1.89	1.49	82.1
		rs	0.65	0.49	88.8	0.73	0.49	79.8
		bar	0.39	0.14	95.7	0.44	0.14	83.1
NGC 5719	26.0	R'	1.42	0.35	104.2	1.47	0.97	20.7
		nr	0.17	0.05	100.3	0.17	0.15	7.0
NGC 5728	29.1	R ₁	3.61	2.34	1.3	3.65	3.17	161.9
		bar	1.89	0.57	33.4	2.06	0.72	36.5
		rs	1.81	0.89	33.0	1.99	1.11	40.8
		nr	0.20	0.12	7.9	0.20	0.16	3.1
NGC 5740	28.6	R	2.16	1.17	156.3	2.34	2.04	127.3
		r	0.70	0.41	157.3	0.80	0.68	108.0
		bar	0.53	0.28	127.8	0.78	0.36	115.3
NGC 5744	38.5	rs	0.27	0.18	132.9	0.29	0.23	43.8
NGC 5746	29.0	R'	5.06	0.39	170.7	5.09	2.02	6.8
		r	2.43	0.25	171.4	2.47	1.28	12.4
NGC 5750	33.6	RL	2.70	1.30	66.6	2.80	2.52	39.3
		r	1.56	0.80	63.2	1.61	1.56	81.1
		r	1.13	0.56	63.4	1.14	1.12	44.0

Table A.1. continued.

ID	D (Mpc)	Feature	$D_{r,b}$ ($'$)	$d_{r,b}$ ($'$)	$PA_{r,b}$ ($^{\circ}$)	$D_{r,b,0}$ ($'$)	$d_{r,b,0}$ ($'$)	$\theta_{r,b}$ ($^{\circ}$)
(1)	(2)	(3)	(4)	(5)	(6)	(7)	(8)	(9)
NGC 5756	28.7	R'	2.80	1.02	63.9	2.90	2.37	26.9
		R' ₂	1.35	1.19	50.7	1.46	1.31	67.2
NGC 5757	39.5	rs	0.77	0.53	161.2	0.87	0.56	118.4
		bar	0.66	0.23	164.8	0.73	0.25	127.8
NGC 5768	31.9	rs	0.55	0.50	113.8	0.55	0.54	152.8
		bar	0.36	0.16	149.2	0.37	0.17	31.4
NGC 5770	22.4	r	0.75	0.72	71.4	0.79	0.73	74.8
		bar	0.73	0.41	111.5	0.79	0.42	75.3
NGC 5777	36.3	R	2.08	0.17	142.8	2.08	0.79	177.5
		R	1.36	0.78	28.5	1.59	1.31	111.4
NGC 5781	28.1	rs	0.72	0.43	28.6	0.86	0.70	107.8
		bar	0.25	0.05	30.0	0.25	0.09	169.2
		R' ₁	7.09	1.19	81.6	7.55	3.38	156.3
NGC 5792	25.6	r	2.35	0.69	85.6	2.42	2.02	154.2
		nr	0.18	0.06	84.1	0.20	0.16	139.0
		R'	2.68	1.46	170.1	2.77	2.56	42.5
NGC 5806	25.4	bar	1.25	0.40	176.3	1.30	0.70	22.2
		rs	1.23	0.76	175.7	1.44	1.17	65.5
		nr	0.12	0.07	162.5	0.14	0.12	107.7
NGC 5809	42.8	rs	0.37	0.12	147.2	0.37	0.28	177.6
NGC 5821	53.2	r	0.53	0.31	145.6	0.54	0.52	166.7
		bar	0.17	0.10	144.0	0.18	0.17	114.9
		R'	4.00	3.31	3.8	4.26	3.84	58.6
NGC 5850	23.2	bar	2.09	0.79	116.7	2.42	0.85	120.0
		r	2.09	1.83	122.8	2.47	1.91	105.5
		nr	0.26	0.22	150.6	0.28	0.25	122.3
NGC 5854	28.5	R	1.67	0.39	50.5	1.73	1.15	158.9
		r	0.66	0.18	57.4	0.68	0.53	22.4
NGC 5878	30.5	rs	1.08	0.39	10.3	1.23	0.93	48.0
NGC 5879	16.1	rs	0.58	0.27	5.0	0.71	0.58	85.6
NGC 5892	33.7	rs	0.45	0.39	144.1	0.48	0.41	62.0
		bar	0.16	0.09	157.1	0.17	0.09	56.2
NGC 5899	43.9	rs	0.49	0.32	5.4	0.86	0.47	99.4
NGC 5900	65.9	R'	1.15	0.09	127.7	1.15	0.40	179.3
NGC 5913	32.8	RL	2.29	0.84	159.5	2.30	1.92	170.6
		r	0.98	0.45	163.6	1.05	0.96	59.9
NGC 5915	33.7	r	0.42	0.30	80.8	0.55	0.31	76.9
		bar	1.52	0.44	18.6	1.72	0.47	59.6
NGC 5921	19.9	rs	1.19	0.82	23.7	1.38	0.85	69.3
		rs	0.42	0.26	159.4	0.50	0.41	97.1
NGC 5930	35.0	bar	0.25	0.18	73.2	0.46	0.18	90.3
NGC 5937	45.1	rs	0.22	0.17	40.8	0.30	0.20	77.9
NGC 5953	27.1	r	0.21	0.17	72.9	0.22	0.18	47.3
NGC 5954	32.1	R'	0.70	0.28	178.8	0.71	0.44	167.2
		rs	0.28	0.17	0.2	0.29	0.27	146.5
NGC 5956	33.0	rs	0.27	0.23	15.4	0.28	0.23	103.9
		bar	0.23	0.13	30.7	0.23	0.13	120.4
		R'	2.38	2.08	165.4	2.43	2.25	138.2
NGC 5957	32.0	bar	0.96	0.41	95.1	1.06	0.41	92.0
		rs	0.94	0.92	118.7	1.04	0.93	93.8
		rs	0.38	0.34	176.7	0.39	0.37	125.1
NGC 5958	35.3	bar	0.19	0.09	137.5	0.20	0.10	124.6
		rs	0.65	0.31	109.1	0.65	0.43	5.7
NGC 5962	35.8	bar	0.39	0.19	147.7	0.47	0.22	57.3
		nr	0.13	0.08	81.5	0.15	0.11	130.9
		rs	1.17	0.86	121.3	1.37	1.01	119.5
NGC 5964	26.6	bar	0.60	0.09	147.7	0.60	0.12	176.2

Table A.1. continued.

ID	D (Mpc)	Feature	$D_{r,b}$ ($'$)	$d_{r,b}$ ($'$)	$PA_{r,b}$ ($^{\circ}$)	$D_{r,b,0}$ ($'$)	$d_{r,b,0}$ ($'$)	$\theta_{r,b}$ ($^{\circ}$)
(1)	(2)	(3)	(4)	(5)	(6)	(7)	(8)	(9)
NGC 6012	32.6	R'	2.57	2.32	168.5	2.91	2.44	106.6
		r	1.48	0.94	166.7	1.61	1.03	130.0
		x ₁ r	0.74	0.15	151.7	0.84	0.16	121.7
		bar	0.63	0.17	156.1	0.70	0.19	125.6
NGC 6014	41.3	bar	0.56	0.36	31.2	0.66	0.37	70.2
		rs	0.54	0.52	111.9	0.65	0.53	96.8
NGC 6070	30.6	r	1.08	0.44	60.6	1.09	0.95	7.3
NGC 6155	40.3	R'	1.08	0.70	145.0	1.09	0.93	17.6
		R'	0.52	0.40	147.8	0.55	0.50	57.8
		rs	0.23	0.20	14.6	0.29	0.20	79.1
		bar	0.19	0.10	120.7	0.20	0.13	147.7
NGC 6207	19.2	rs	0.62	0.26	2.6	0.69	0.40	140.8
		bar	0.27	0.12	36.6	0.30	0.19	42.6
NGC 6217	23.9	R'	2.72	2.46	91.1	2.73	2.68	164.8
		rs	1.34	1.00	158.0	1.44	1.02	70.3
		bar	1.23	0.33	149.3	1.30	0.33	58.5
NGC 6267	48.5	rs	0.70	0.53	53.1	0.79	0.68	64.3
		bar	0.57	0.15	157.6	0.77	0.16	108.5
NGC 6278	45.8	r	0.43	0.20	115.9	0.45	0.32	146.5
NGC 6340	22.0	R	1.80	1.52	98.8	2.02	1.54	103.5
NGC 6412	23.5	rs	0.42	0.33	69.7	0.44	0.33	72.4
		bar	0.25	0.14	160.9	0.25	0.15	157.4
NGC 6434	37.6	R	1.25	0.50	92.6	1.27	1.11	161.5
		rs	0.50	0.25	88.2	0.60	0.48	114.8
NGC 6870	55.4	PRG	1.89	1.40	102.0	–	–	–
		rs	1.17	0.39	87.1	1.19	1.01	20.1
		rs	0.78	0.23	85.7	0.78	0.60	6.0
NGC 6887	33.5	rs	0.52	0.19	106.5	0.54	0.51	56.1
NGC 6889	36.8	rs	0.26	0.19	71.7	0.27	0.26	122.7
		bar	0.17	0.10	163.5	0.23	0.10	90.5
NGC 6902	37.5	rs	0.68	0.58	147.8	0.71	0.68	91.6
		bar	0.60	0.34	129.4	0.62	0.41	151.3
NGC 6923	36.6	rl	0.36	0.17	73.4	0.36	0.25	178.9
NGC 6925	30.8	rs	0.97	0.25	6.0	0.97	0.76	172.9
NGC 7051	37.4	R' ₂	1.12	0.97	57.4	1.13	1.04	163.5
		R' ₁	0.76	0.58	179.4	0.81	0.59	108.4
		rs	0.29	0.22	78.4	0.30	0.23	15.7
		bar	0.28	0.14	79.4	0.28	0.15	14.7
NGC 7070	30.3	rs	0.38	0.28	170.4	0.40	0.30	140.8
		bar	0.23	0.12	77.6	0.26	0.12	64.7
NGC 7098	29.1	R	3.63	2.26	80.7	4.13	3.46	62.9
		r'l	1.87	1.07	67.8	1.95	1.78	134.9
		bar	1.38	0.63	50.6	1.63	0.93	133.1
NGC 7107	27.6	R'	1.33	1.06	121.4	1.38	1.18	38.2
		rs	0.82	0.60	120.2	0.84	0.66	30.3
		bar	0.50	0.16	130.4	0.52	0.18	34.1
NGC 7140	37.4	R'	3.72	2.60	176.0	4.13	3.62	113.2
		rs	1.94	1.16	22.0	2.19	1.59	48.6
		bar	1.92	0.48	19.1	2.02	0.71	25.3
NGC 7162	28.4	R'	1.19	0.47	11.4	1.20	1.11	159.9
		rs	0.38	0.22	13.7	0.52	0.38	88.1
NGC 7179	46.8	bar	0.91	0.23	44.7	0.93	0.44	166.6
		r	0.89	0.41	50.4	0.89	0.80	179.3
NGC 7184	33.6	r	1.71	0.42	59.1	1.71	1.64	164.6
NGC 7188	26.0	R'	0.79	0.37	48.6	0.80	0.74	28.3
NGC 7191	37.4	R'	0.83	0.37	133.5	0.90	0.80	122.4
NGC 7205	19.1	rs	0.47	0.25	63.1	0.52	0.46	115.7
NGC 7213	22.0	r	0.88	0.79	5.2	0.90	0.82	42.9

Table A.1. continued.

ID	D (Mpc)	Feature	$D_{r,b}$ ($'$)	$d_{r,b}$ ($'$)	$PA_{r,b}$ ($^{\circ}$)	$D_{r,b,0}$ ($'$)	$d_{r,b,0}$ ($'$)	$\theta_{r,b}$ ($^{\circ}$)
(1)	(2)	(3)	(4)	(5)	(6)	(7)	(8)	(9)
NGC 7218	24.9	rs	0.54	0.37	28.2	0.82	0.53	83.3
NGC 7219	41.2	R'_2	1.36	0.83	33.0	1.39	1.27	31.6
		r	0.33	0.24	50.3	0.41	0.30	67.2
		bar	0.29	0.20	86.7	0.42	0.21	76.9
NGC 7290	46.4	rs	0.36	0.21	156.7	0.38	0.36	105.4
NGC 7314	18.5	rs	1.08	0.32	179.6	1.10	0.80	164.5
NGC 7328	39.7	rs	0.36	0.23	65.3	0.61	0.32	103.5
NGC 7378	30.0	rs	0.64	0.26	0.8	0.65	0.42	10.9
NGC 7416	35.1	R'	2.74	0.43	108.9	2.74	1.65	0.8
		r	1.25	0.29	109.2	1.25	1.10	6.8
NGC 7418	18.1	bar	1.10	0.25	119.5	1.12	0.33	163.5
		rs	1.07	0.71	107.1	1.18	0.87	131.1
NGC 7421	25.4	R'	1.68	1.54	76.7	1.76	1.66	71.8
		rs	0.91	0.74	75.1	0.92	0.83	23.5
		bar	0.73	0.25	93.0	0.76	0.28	32.3
NGC 7424	11.5	rs	1.27	0.90	71.5	1.34	0.94	50.8
		bar	0.36	0.11	133.3	0.39	0.11	102.4
NGC 7437	29.2	rs	0.42	0.32	70.0	0.45	0.34	58.5
		bar	0.24	0.16	13.9	0.24	0.18	164.2
NGC 7463	36.2	rs	0.38	0.18	75.2	0.54	0.31	116.7
NGC 7465	27.2	PRG	0.71	0.09	160.1	–	–	–
NGC 7479	33.9	R'	2.77	2.13	27.6	2.92	2.69	57.2
		bar	1.65	0.41	8.1	1.68	0.53	164.3
NGC 7496	15.0	rs	1.43	1.00	160.2	1.47	1.02	123.7
		bar	1.33	0.31	147.9	1.37	0.32	113.7
NGC 7513	19.4	rs	1.31	0.87	90.2	1.46	1.17	127.5
		bar	1.27	0.34	71.0	1.51	0.43	131.9
NGC 7531	22.9	bar	0.99	0.33	11.7	1.03	0.59	156.3
		r	0.95	0.39	17.1	0.96	0.72	164.7
NGC 7537	37.0	rs	0.24	0.11	76.9	0.34	0.24	90.5
NGC 7552	17.2	R'_1	3.08	2.52	179.1	3.14	2.57	135.0
		rs	1.96	1.23	99.7	2.02	1.24	63.3
		bar	1.20	0.43	91.2	1.23	0.44	54.1
		nr	0.12	0.10	104.7	0.12	0.10	71.4
NGC 7582	20.6	R'_1	4.03	1.77	148.5	4.12	3.75	148.5
		rs	1.97	0.79	154.2	2.00	1.69	20.7
NGC 7590	25.3	rs	0.85	0.31	33.8	0.88	0.82	41.3
NGC 7606	31.6	r	0.85	0.38	140.2	1.02	0.81	113.4
NGC 7689	25.2	bar	0.26	0.10	100.8	0.30	0.13	136.5
		rs	0.26	0.22	134.5	0.33	0.26	85.9
NGC 7690	22.3	r	0.23	0.11	128.1	0.23	0.22	171.0
NGC 7716	33.7	r	0.47	0.34	30.3	0.47	0.40	178.0
		bar	0.13	0.10	54.3	0.14	0.11	39.4
NGC 7723	27.3	rs	0.71	0.55	54.0	0.85	0.69	73.6
		bar	0.64	0.23	68.4	0.73	0.30	42.8
NGC 7724	26.9	R'	0.88	0.54	33.4	0.88	0.78	14.1
		bar	0.36	0.17	62.6	0.42	0.21	49.5
		rs	0.30	0.20	77.1	0.39	0.22	67.8
NGC 7731	36.8	R'_2	1.09	0.85	92.6	1.27	1.03	66.9
		R_1	0.69	0.53	88.9	0.78	0.66	64.4
		bar	0.28	0.15	43.3	0.32	0.19	131.1
		r	0.27	0.22	50.5	0.33	0.26	107.4
NGC 7741	14.3	R'_2	2.76	2.23	168.8	3.21	2.74	79.2
		bar	1.46	0.49	95.9	2.00	0.52	107.0
NGC 7742	22.2	r	0.73	0.68	119.8	0.74	0.70	54.2
		r	0.34	0.32	142.3	0.35	0.32	67.6
NGC 7743	21.4	rs	1.38	1.14	119.4	1.80	1.16	79.6
		bar	1.32	0.63	94.7	1.52	0.73	51.7

Table A.1. continued.

ID	D (Mpc)	Feature	$D_{r,b}$ ($'$)	$d_{r,b}$ ($'$)	$PA_{r,b}$ ($^{\circ}$)	$D_{r,b,0}$ ($'$)	$d_{r,b,0}$ ($'$)	$\theta_{r,b}$ ($^{\circ}$)
(1)	(2)	(3)	(4)	(5)	(6)	(7)	(8)	(9)
NGC 7750	32.1	rs	0.54	0.24	173.5	0.54	0.48	20.7
		rs	0.94	0.77	32.9	1.29	0.93	85.5
NGC 7755	31.5	bar	0.84	0.37	123.6	1.39	0.37	94.2
		nr	0.12	0.09	28.5	0.14	0.12	83.4
NGC 7817	27.0	rs	0.66	0.26	50.8	0.86	0.63	71.7
PGC 2492	21.1	rs	0.75	0.67	168.7	0.97	0.75	88.4
		bar	0.37	0.17	171.5	0.38	0.24	13.4
PGC 3853	12.6	R'	3.93	3.03	100.8	4.12	3.87	117.8
		rs	1.55	1.12	78.9	1.76	1.32	123.5
		bar	0.39	0.19	38.1	0.51	0.19	104.6
PGC 6228	21.6	rs	1.06	0.31	65.9	1.14	0.75	149.4
		R'	1.88	1.67	47.7	2.02	1.72	115.0
PGC 6626	19.8	rs	0.92	0.75	40.4	0.99	0.77	116.4
		bar	0.91	0.46	20.6	1.00	0.47	105.9
PGC 11248	31.4	rs	1.00	0.39	123.6	1.00	0.87	174.5
PGC 12633	36.1	rs	0.66	0.56	99.0	0.66	0.57	42.3
		bar	0.63	0.31	99.4	0.63	0.31	39.7
PGC 12664	34.7	rs	0.72	0.57	130.3	1.02	0.67	102.2
		bar	0.17	0.07	88.1	0.28	0.08	101.6
PGC 12981	22.7	bar	0.56	0.28	91.2	0.57	0.36	166.4
		nr	0.24	0.13	95.3	0.24	0.17	172.0
PGC 13684	15.9	rs	0.59	0.26	167.0	0.59	0.48	2.2
		bar	0.18	0.12	112.7	0.31	0.13	103.0
PGC 13716	27.0	rs	0.48	0.12	138.7	0.48	0.29	4.9
PGC 14037	33.9	rs	0.40	0.25	129.1	0.56	0.39	102.8
PGC 32091	37.9	rs	0.67	0.54	50.9	0.68	0.59	21.5
		bar	0.42	0.22	54.3	0.42	0.25	18.6
PGC 36274	27.3	R'	1.09	0.67	57.4	1.17	0.91	41.1
		bar	0.30	0.19	75.2	0.36	0.23	59.4
PGC 36551	27.1	R'	1.29	0.42	73.4	1.31	1.05	19.2
PGC 36643	27.2	R'	1.58	0.52	139.1	1.93	1.44	60.1
PGC 38250	41.8	rs	0.43	0.38	126.1	0.49	0.42	78.6
		bar	0.38	0.19	65.0	0.43	0.21	125.1
PGC 44735	26.0	rs	0.53	0.32	82.6	0.73	0.45	113.3
		bar	0.25	0.17	56.1	0.44	0.19	102.9
PGC 44952	20.1	r	0.52	0.33	0.0	0.62	0.48	61.9
PGC 47721	94.2	rs	1.47	0.74	117.5	1.49	1.27	162.7
		r	1.12	0.48	117.5	1.12	0.82	169.2
		r	0.70	0.34	116.4	0.71	0.58	161.7
PGC 48179	22.7	rs	1.13	1.01	20.6	1.19	1.03	115.7
		bar	0.88	0.30	0.2	0.94	0.31	109.5
PGC 53093	39.6	R'	1.03	0.59	100.8	1.05	1.00	135.8
		R'	0.66	0.42	95.7	0.75	0.64	115.5
		rs	0.31	0.17	98.1	0.32	0.29	140.2
		bar	0.17	0.08	58.3	0.25	0.10	113.6
PGC 53415	35.6	R	1.86	0.63	47.4	1.86	1.19	0.4
		rs	0.29	0.08	50.1	0.29	0.16	7.1
PGC 54944	29.1	bar	0.60	0.15	35.3	0.62	0.21	22.0
		rs	0.58	0.30	10.8	0.59	0.42	157.9
PGC 66242	40.4	R'	1.45	0.66	39.1	1.49	1.40	140.3
UGC 313	28.4	R' ₁	0.38	0.15	14.9	0.38	0.24	0.1
		bar	0.14	0.04	102.6	0.23	0.04	88.6
UGC 1551	35.6	rs	0.65	0.55	170.7	0.73	0.57	69.0
		bar	0.57	0.19	81.2	0.62	0.21	132.7
UGC 1862	20.4	R'	0.79	0.65	2.4	0.85	0.74	121.5
UGC 4151	35.4	rl	0.12	0.10	36.0	0.13	0.10	73.3
UGC 4306	34.3	r	0.21	0.06	140.2	0.21	0.10	5.7

Table A.1. continued.

ID	D (Mpc)	Feature	$D_{r,b}$ ($'$)	$d_{r,b}$ ($'$)	$PA_{r,b}$ ($^{\circ}$)	$D_{r,b,0}$ ($'$)	$d_{r,b,0}$ ($'$)	$\theta_{r,b}$ ($^{\circ}$)
(1)	(2)	(3)	(4)	(5)	(6)	(7)	(8)	(9)
UGC 4549	22.4	r	0.18	0.16	84.2	0.22	0.16	83.4
UGC 4551	28.4	r	1.00	0.26	113.4	1.01	0.68	6.3
UGC 4559	36.5	r	0.51	0.08	51.1	0.51	0.28	2.1
UGC 4621	35.8	rs bar	0.56 0.48	0.33 0.19	132.1 150.6	0.56 0.53	0.55 0.28	142.6 35.2
UGC 4623	44.5	rs	0.31	0.14	56.6	0.51	0.31	92.9
UGC 4714	22.2	rs bar	0.27 0.21	0.22 0.11	100.3 59.4	0.27 0.24	0.27 0.12	90.0 129.5
UGC 4824	32.3	rs	0.89	0.28	95.4	1.04	0.84	116.8
UGC 4867	38.8	rs bar	0.41 0.14	0.25 0.07	94.8 179.4	0.42 0.23	0.40 0.07	35.6 88.6
UGC 4922	32.6	rs	0.78	0.45	52.6	1.01	0.76	103.4
UGC 4982	41.2	r	0.25	0.12	176.4	0.31	0.24	113.4
UGC 5228	25.8	R _s '	1.81	0.38	123.8	1.81	1.25	0.0
UGC 5354	21.4	R bar	0.98 0.56	0.63 0.23	79.0 71.5	1.11 0.56	0.97 0.41	80.7 165.4
UGC 5393	24.2	R' bar	0.94 0.19	0.63 0.08	122.0 145.7	1.24 0.25	0.93 0.11	83.9 56.0
UGC 5446	36.8	rs	0.28	0.13	47.8	0.56	0.28	93.6
UGC 5633	23.4	rs bar	1.01 0.79	0.69 0.15	160.3 162.9	1.17 0.82	0.94 0.23	116.1 161.6
UGC 5646	23.9	rs	0.49	0.14	169.3	0.53	0.43	40.0
UGC 5676	25.5	RG bar	1.09 0.16	0.50 0.10	22.3 88.6	1.12 0.29	0.89 0.10	24.7 83.2
UGC 5707	30.2	rs bar	0.32 0.18	0.21 0.07	59.8 64.9	0.39 0.21	0.22 0.07	77.8 79.7
UGC 5814	149.7	RL	0.52	0.41	105.2	0.74	0.48	104.1
UGC 5841	29.4	R' bar rs	0.76 0.43 0.38	0.45 0.14 0.21	127.0 136.7 136.1	0.82 0.43 0.40	0.74 0.25 0.35	116.8 11.6 33.1
UGC 6023	32.5	rs bar	0.43 0.38	0.22 0.12	48.0 47.7	0.45 0.38	0.42 0.23	129.8 173.5
UGC 6162	12.3	R'	1.67	0.94	90.6	1.74	1.54	38.9
UGC 6169	27.8	R'	0.59	0.10	178.4	0.61	0.34	162.6
UGC 6309	45.4	rs bar	0.69 0.61	0.50 0.13	104.2 139.7	0.72 0.61	0.57 0.15	144.0 16.7
UGC 6335	45.8	rs bar	0.20 0.14	0.15 0.09	160.4 51.4	0.24 0.15	0.15 0.11	91.1 154.5
UGC 6517	40.9	r	0.32	0.18	21.4	0.35	0.28	131.3
UGC 6983	20.2	r bar	1.04 0.94	0.99 0.28	113.3 89.0	1.51 0.94	1.03 0.42	86.9 3.5
UGC 7184	34.2	rs bar	0.64 0.47	0.28 0.12	147.5 163.5	0.65 0.57	0.54 0.21	25.0 41.5
UGC 7239	24.9	R' bar	1.24 0.36	1.10 0.19	11.1 21.3	1.54 0.45	1.11 0.19	86.1 89.2
UGC 7848	51.7	x ₁ r	0.30	0.14	75.3	0.40	0.24	59.9
UGC 8155	47.0	rs	1.24	0.90	12.8	1.24	1.13	172.4
UGC 8909	29.8	rs bar	0.28 0.17	0.19 0.11	68.5 131.3	0.28 0.20	0.23 0.11	21.2 79.4
UGC 8995	23.6	R'	1.44	0.62	6.7	1.51	1.29	38.0
UGC 9215	24.1	R' rs	1.60 0.94	0.70 0.58	160.5 157.1	1.60 1.31	1.56 0.93	168.4 95.4
UGC 9245	17.0	rs bar	1.21 0.26	0.64 0.03	173.2 9.3	1.21 0.26	0.88 0.04	171.7 16.6
UGC 9291	38.2	rs bar	0.50 0.23	0.32 0.10	110.9 84.7	0.59 0.27	0.49 0.16	71.3 136.4

Table A.1. continued.

ID	D (Mpc)	Feature	$D_{r,b}$ (')	$d_{r,b}$ (')	$PA_{r,b}$ (°)	$D_{r,b,0}$ (')	$d_{r,b,0}$ (')	$\theta_{r,b}$ (°)
(1)	(2)	(3)	(4)	(5)	(6)	(7)	(8)	(9)
UGC 9356	37.6	R'L	1.07	0.45	107.0	1.08	0.86	13.6
		rs	0.59	0.27	99.2	0.61	0.51	152.9
		bar	0.24	0.10	60.8	0.37	0.12	113.4
UGC 9364	36.1	R'	0.91	0.40	17.8	0.92	0.81	164.8
UGC 9389	32.1	rs	1.24	0.34	47.1	1.27	1.21	136.5
UGC 9569	41.9	rs	0.69	0.46	168.1	0.80	0.51	60.3
		bar	0.43	0.17	168.8	0.50	0.19	53.3
UGC 9746	29.5	rs	0.97	0.19	137.8	0.97	0.71	179.3
UGC 9858	36.3	rs	0.46	0.13	67.5	0.62	0.36	123.1
UGC 10054	25.6	rs	1.13	0.56	145.1	1.15	1.04	27.7
		bar	0.60	0.10	154.0	0.64	0.18	23.4
UGC 10791	24.0	rs	0.70	0.53	111.4	0.86	0.68	75.5
		bar	0.29	0.12	155.9	0.42	0.13	70.0
UGC 10854	44.6	rs	0.44	0.24	79.0	0.60	0.41	110.3
UGC 12151	23.8	rs	0.60	0.47	7.5	0.78	0.59	81.3
		bar	0.26	0.07	173.8	0.26	0.12	173.3

A.2. (Pseudo)Rings not in S⁴G sample galaxies**Table A.2.** Catalogue of the properties of ringed galaxies that appear in S⁴G frames, but are not included in the S⁴G sample

ID	D (Mpc)	Feature	$D_{r,b}$ ($'$)	$d_{r,b}$ ($'$)	$PA_{r,b}$ ($^{\circ}$)	$D_{r,b,0}$ ($'$)	$d_{r,b,0}$ ($'$)	$\theta_{r,b}$ ($^{\circ}$)
(1)	(2)	(3)	(4)	(5)	(6)	(7)	(8)	(9)
IC 3062	115.7	rs	0.27	0.21	149.9	0.30	0.23	119.1
NGC 2856	40.9	r	0.37	0.16	144.6	0.43	0.28	47.1
NGC 2950	19.1	RL	1.99	1.50	115.9	2.25	1.96	104.8
		rl	0.97	0.68	122.2	1.00	0.97	93.9
		bar	0.80	0.47	155.7	0.98	0.57	56.5
NGC 4175	42.2	r	0.41	0.11	130.4	0.41	0.32	176.0
		PRG	0.29	0.03	38.7	–	–	–
NGC 4277	13.7	rs	0.57	0.43	117.5	0.59	0.57	87.9
		bar	0.41	0.25	169.7	0.51	0.27	67.0
NGC 4288A	101.9	rl	0.25	0.25	40.7	0.26	0.25	89.7
		bar	0.23	0.17	161.2	0.24	0.17	115.5
NGC 4342	16.8	PRG	0.40	0.04	80.7	–	–	–
PGC 43690	32.8	R' ₁	0.80	0.40	108.9	0.81	0.60	169.2
		bar	0.16	0.13	18.8	0.25	0.13	88.7
PGC 50803	169.4	rs	0.31	0.19	94.4	0.32	0.24	145.7
		bar	0.30	0.10	114.2	0.30	0.14	7.2
PGC 52269	185.2	R	0.35	0.33	130.1	0.36	0.35	71.2
		bar	0.17	0.12	165.4	0.18	0.13	50.3
PGC 59663	–	R'	0.37	0.10	87.0	0.41	0.29	141.9